

Air Force Institute of Technology

**AFIT Scholar**

---

Theses and Dissertations

Student Graduate Works

---

3-2021

## **CubeSat Attitude Determination and Control System (ADACS) Characterization and Testing for Rendezvous and Proximity Operations (RPO)**

Steven T. Bednarski

Follow this and additional works at: <https://scholar.afit.edu/etd>



Part of the [Aerospace Engineering Commons](#)

---

### **Recommended Citation**

Bednarski, Steven T., "CubeSat Attitude Determination and Control System (ADACS) Characterization and Testing for Rendezvous and Proximity Operations (RPO)" (2021). *Theses and Dissertations*. 4970.  
<https://scholar.afit.edu/etd/4970>

This Thesis is brought to you for free and open access by the Student Graduate Works at AFIT Scholar. It has been accepted for inclusion in Theses and Dissertations by an authorized administrator of AFIT Scholar. For more information, please contact [AFIT.ENWL.Repository@us.af.mil](mailto:AFIT.ENWL.Repository@us.af.mil).



**CubeSat Attitude Determination and Control System (ADACS) Characterization  
and Testing for Rendezvous and Proximity Operations (RPO)**

THESIS

Steven T. Bednarski, Captain, USSF

AFIT-ENY-MS-21-M-288

**DEPARTMENT OF THE AIR FORCE  
AIR UNIVERSITY**

**AIR FORCE INSTITUTE OF TECHNOLOGY**

---

---

**Wright-Patterson Air Force Base, Ohio**

**DISTRIBUTION STATEMENT A.**  
APPROVED FOR PUBLIC RELEASE; DISTRIBUTION UNLIMITED.

The views expressed in this thesis are those of the author and do not reflect the official policy or position of the United States Space Force, United States Air Force, Department of Defense, or the United States Government.

This material is declared a work of the U.S. Government and is not subject to copyright protection in the United States.

AFIT-ENY-MS-21-M-288

CUBESAT ATTITUDE DETERMINATION AND CONTROL SYSTEM (ADACS)  
CHARACTERIZATION AND TESTING FOR RENDEZVOUS AND PROXIMITY  
OPERATIONS (RPO)

THESIS

Presented to the Faculty

Department of Aeronautics and Astronautics

Graduate School of Engineering and Management

Air Force Institute of Technology

Air University

Air Education and Training Command

In Partial Fulfillment of the Requirements for the

Degree of Master of Science in Space Systems

Steven T. Bednarski, BS

Captain, USSF

March 2021

**DISTRIBUTION STATEMENT A.**  
APPROVED FOR PUBLIC RELEASE; DISTRIBUTION UNLIMITED.

AFIT-ENY-MS-21-M-288

CUBESAT ATTITUDE DETERMINATION AND CONTROL SYSTEM (ADACS)  
CHARACTERIZATION AND TESTING FOR RENDEZVOUS AND PROXIMITY  
OPERATIONS (RPO)

THESIS

Steven T. Bednarski, BA, BS  
Captain, USSF

Committee Membership:

Dr. Andrew S. Keys, Ph.D.  
Chair

Dr. Richard G. Cobb, Ph.D.  
Member

Dr. Bradley J. Ayres, Ph.D.  
Member

## **Abstract**

This research endeavors to evaluate and characterize the performance of CubeSat specific commercial-off-the-shelf (COTS) Attitude Determination and Control Systems (ADACS) for Mission suitability.

To ensure COTS components are capable of meeting CubeSat mission requirements, deliberate performance testing of critical CubeSat subsystems in flight-like conditions is essential. This effort focuses on testing the MAI-401 ADACS subsystem as configured to support the Grissom-1 CubeSat mission, as mounted to an air bearing, residing within a 3-axis Helmholtz Cage, and subjected to a simulated magnetic environment of various orbital parameters. A literature review of spacecraft components, prior missions, operations, environmental simulators, and attitude determination and control algorithms informs the tests and assessments described herein. A test plan developed as part of this research exercises and characterizes the MAI-401 ADACS unit for the Grissom-1 mission and serves as a comparative framework for testing additional ADACS offerings such as the BCT XACT ADACS unit. Results include a baseline characterization of COTS ADACS, discussion of currently available ADACS and suitable Mission types, and suggestions for enhanced testing.

## **Acknowledgements**

First and foremost, I would like to thank the ENY Department, and specifically my advisor Dr. Keys for the support and guidance to always keep pushing forward towards success. Dr. Keys' patience and ability to accept barriers and call an audible mid-stride allowed this research to still have relevance.

I would like to thank the fine folks out at the Starfire Optical Range for planting the Advanced Academic Degree seed from the very beginning. The support, encouragement, harassment, mentorship, and constant example of what is possible from the team drove this dream to reality.

I would also like to thank the CSRA Staff as without them none of this would be possible. Thanks to Chris Lomanno for spending so much time working the cage, commanding, troubleshooting, and teaching the process to me. Thanks to Sean Miller for making sure my assumptions were valid, to Blake Benton for all the hardware support, and to Cheney Sollenberger and the Software Development team for dropping what you were doing and running down my issues.

Finally, I would like to thank my family for the love, encouragement, support, and ultimately understanding through the program. Thank you especially to my wife for taking on way more than her fair share of responsibilities and for keeping our home and way of life in-tact and thank you to my boys for being a constant source of laughter when it was needed most.

Steven T. Bednarski

## Table of Contents

Abstract .....	iv
Acknowledgements .....	v
I. Introduction .....	1
II. Background .....	7
2.1 CubeSats.....	7
2.2 Mission Sets and History .....	10
2.3 Attitude Determination and Control Systems.....	14
2.3.1 Attitude Determination.....	18
2.3.2 Attitude Determination Algorithms.....	19
2.3.3 Determination Sensors .....	22
2.3.4 Attitude Control .....	26
2.3.5 Control Components.....	28
2.4 Space Environment and Test Apparatus .....	30
2.4.1 Earth's Geomagnetic Sphere.....	31
2.4.2 Helmholtz Coils and Cages.....	33
2.4.3 Air Bearings.....	36
III. Methodology.....	38
3.1 Mission, Justification, and Available Solutions .....	39
3.1.1 Mission.....	42
3.1.2 Justification .....	45
3.1.3 ADACS Solutions .....	46
3.2 Performance Evaluation .....	51
3.2.1 Attitude Determination vs. Control Performance.....	52
3.2.2 Performance Metrics and Figures of Merit.....	53
3.2.3 Data Collection .....	54
3.3 Experimental Setup .....	55
3.3.1 Component Frames of Reference .....	61
3.4 Limitations .....	64
IV. Analysis .....	67
4.1 Magnetic Field Data Analysis.....	68
4.2 PhaseSpace Motion Capture Data Analysis.....	77
4.3 Bias and Gains .....	84
4.4 Conclusion of Test Results .....	94
V. Conclusion .....	98
5.1 Summary .....	98
5.2 Conclusion .....	100
5.3 Recommendations for Future development .....	103



Appendix A. Test Plan .....	108
I. Introduction.....	110
1.1 Purpose .....	110
1.2 Scope .....	110
1.3 Limitations .....	112
1.4 Objectives.....	112
II. Resource Requirements .....	113
2.1 Facilities .....	113
2.2 Personnel .....	114
2.3 Documentation.....	114
2.4 Material/Equipment/Software Requirements.....	115
III. Test Configuration.....	116
IV. Test Procedure .....	122
4.1 Experiment Setup and CubeSat Checkout .....	123
4.2 Detumble Test.....	140
4.3 Pointing Accuracy and Slew Rate .....	141
Appendix B. MATLAB Analysis Code .....	144
Code Setup .....	145
IMPORT DATA Files as Tables.....	145
Cage Data .....	146
ADACS Data.....	146
PhaseSpace Data .....	147
Plotting Magnetic Field Data .....	148
BIAS(offset) and GAINS(scaling) at B-Field Measurement.....	148
Magnetic Rotational Data (change in mag field over time).....	149
Plotting ADACS measured Omega B .....	151
PhaseSpace .....	151
Heading Data from PhaseSpace Data .....	154
PhaseSpace Cartesian to Spherical Coordinate.....	154
PhaseSpace Spherical Coordinate Rotational Velocity.....	155
PhaseSpace Spherical Coordinate Rotational Acceleration.....	156
Cage Data .....	157
3D Visualization .....	157
End of Script .....	158
References .....	159

## **List of Figures**

Figure	Page
Figure 1 – Standard 1U, 3U, and 6U CubeSat Configurations	9
Figure 2 – The Gemini VIII spacecraft approaches the Agena during rendezvous maneuvers.	13
Figure 3 – Earth Centered, Earth Fixed coordinate system.	16
Figure 4 - Primary axis Roll, Pitch, and Yaw	17
Figure 5 – NED coordinate system overlaid on ECEF.	18
Figure 6 – Solar-Cell type Coarse Sun Sensor, top and bottom view	24
Figure 7 – Magnetometer Board	25
Figure 8 – Earth’s Magnetic Field Represented as a Bar Magnet	32
Figure 9 – Earth’s Magnetosphere with Solar Wind [24]	33
Figure 10 - Single Pair of Helmholtz Coils in Square Configuration	34
Figure 11 - X, Y and Z Coil Pairs with B-Field Vector	34
Figure 12 – Square Coil Helmholtz Cage Composite of X, Y, Z Coil Pairs	35
Figure 13 - Air Bearing general operation.	37
Figure 14 - AFIT Air Bearing	38
Figure 15 - AFIT CSRA’s CubeSat Program Breakdown	41
Figure 16 - Adcole Maryland Aerospace’s MAI-401	48
Figure 17 - Blue Canyon Technology’s XACT-15 Attitude Control System	50
Figure 18 - Test Component Coordinate Frame	63
Figure 19 – Magnetic Field Measured Data for simulated 450 KM Orbital Altitude at 50 degrees inclination.	72

Figure 20 – Enlarged View: Magnetic Field Data for simulated 450 KM Orbital Altitude at 50 degrees inclination	73
Figure 21 - Rate of Change on the Measured Magnetic Field	75
Figure 23 – PhaseSpace Raw Distance from Centroid Measurements	78
Figure 24 – PhaseSpace Derived Linear Velocity from Centroid Measurements	79
Figure 25 - PhaseSpace Measured Motion in Spherical Representation	81
Figure 26 – PhaseSpace Derived Rotational Velocity in Spherical Representation	83
Figure 27 – Magnetic Field Data in Test Mode with no current to magnetorquers	87
Figure 28 – MAI-401 Magnetic Field Telemetry Corrected for Bias and Gain	92
Figure 29 – Bias and Gain altered B-Field Data for simulated 450 KM Orbital Altitude at 50 degrees inclination	94

## **List of Tables**

Table	Page
Table 1 - First satellite classification [Sweeting, 1991] from [4]	8
Table 2 – Space Mission Definitions [11]	11
Table 3 – Attitude Determination Algorithm Quick Comparison	22

## List of Equations

Equation		Page
Equation 1 -	Problem 65-1, A Least Squares Estimate of Satellite Attitude [14]	21
Equation 2 -	Newton's 2 <sup>nd</sup> Law of Motion	27
Equation 3 -	Newton's 3 <sup>rd</sup> Law of Motion	27
Equation 4 -	Magnetic field strength calculated between two Helmholtz coils [22]	34
Equation 5 -	Magnetic field strength calculated between two Helmholtz coils [24]	36
Equation 6 -	Rotation about X, $\theta=90$ degrees	69
Equation 7 -	Rotation about Y, $\theta=180$ degrees	69
Equation 8 -	Rotation about X, $\theta= -90$ degrees	70
Equation 9 -	Measured ADACS Coordinate Frame	70
Equation 10 -	Problem setup for determining magnetometer to ADACS frame rotation.	71
Equation 11 -	Proof of rotation from ADACS to Cage Frame	71
Equation 12 -	Time derivative of the magnetic field	74
Equation 13 -	Time derivative of of the change in centroid offset	79
Equation 14 -	Spherical Radius	81
Equation 15 -	Spherical degree of rotational about the Z axis in the XY plane	81
Equation 16 -	Spherical deviation from the XY plane in degrees	81
Equation 17 -	Change in $\theta$ over change in time.	84
Equation 18 -	Change in $\phi$ over change in time.	84

## Acronyms

ADACS	Attitude Determination and Control System
AFIT	Air Force Institute of Technology
AGI	Analytical Graphics Inc.
BCT	Blue Canyon Technologies, Inc.
C&DH	Command and Data Handling System
COG	Center of Gravity
COTS	Commercial-Off-The-Shelf products
CSRA	AFIT's Center for Space Research and Assurance
ECEF	Earth Centered, Earth Fixed coordinate system
EPS	Electrical Power System
MAI	Adcole Maryland Aerospace, Llc
MOI	Moment of Inertia
NASA	National Aeronautics and Space Administration
NED	North, East, Down coordinate system
QUEST	Quaternion Estimator
RPO	Rendezvous and Proximity Operations
SEET	Space Environment Effects Tool
STEM	Science, Technology, Engineering, and Math
STK	Systems Tool Kit
TRIAD	Triaxial Attitude Determination
TT&C	Telemetry, Tracking & Control System

# CUBESAT ATTITUDE DETERMINATION AND CONTROL SYSTEM (ADACS) CHARACTERIZATION AND TESTING FOR RENDEZVOUS AND PROXIMITY OPERATIONS (RPO)

## **I. Introduction**

### *Background*

Orbital spacecraft have garnered much global interest since before the first purpose-built satellite to remain on orbit for an extended period, Sputnik I, was launched in 1957. Since 1957 the desire to field orbital craft for both manned and unmanned operations have continually increased. From the early years filled with dreams of proving reliable orbital flight to the current reliance on space for logistics, navigation, and communications, the Industry as had to rely on continual advances in spacecraft componentry to support the expanding Mission needs. Intertwined with the miniaturization of electronic components, the past two decades have yielded a trend of increasing launches of smaller spacecraft such as those based upon the CubeSat standard. The popularity of the CubeSat standard is accompanied by the influx of commercial CubeSat component suppliers which drive costs to programs down but requiring additional effort to understand the performance and applicability of the new components. Of the new components, the need for reliable and accurate Attitude Determination and Control Systems (ADACS) to control spacecraft pointing has become a priority target for assessment.

## *CubeSat*

CubeSats come in a variety of configurations but the standardized test chassis chosen for this research is commonly referred to as a “6U”. As the name implies, the chassis’ volume can be broken down to six 10cm x 10cm x 10cm units. The chassis is outfitted with most of the components and subsystems required to provide a flight spacecraft, though some are engineering units not qualified for space flight, and others are removed for test setup logistics. Of the subsystems required to support testing of the ADACS are the Electrical Power System (EPS) providing power, the Command & Data Handling System (C&DH) providing the flight software, and the Telemetry, Tracking & Control System (TT&C) through which the communications from the ground software are passed. In addition, a laboratory workstation is required as both the hub of data accumulation for the testbed as well as acting as the ground station for commanding the spacecraft.

## *ADACS*

Discussion of ADACS is primarily split into the two separate but related functions they perform, determination, and control. The determination function is commonly comprised of sensors for understanding the space environment and an algorithm for applying the collected data to deliver an attitude estimate. The control function ingests the attitude estimate as the known as well as a desired pointing into the control algorithm to calculate an attitude adjustment solution. The required commands and values are then passed to the control actuators with and the process repeats in a feedback loop. The performance characteristics of the ADACS while useful as a singular system are much more valuable when combined with the required support systems, chassis, and payloads as the emergent



behaviors of a total system can vary widely from that of the component systems. It stems from this idea the necessity to test ADACS performance in a flight-like configuration and under flight-like conditions originates.

### *Problem Statement*

The Air Force Institute of Technology's (AFIT) Center for Space Research and Assurance (CSRA) operates a CubeSat program intent on providing research opportunities to the student and faculty population as well as expanding the knowledgebase of the DoD with regards to small satellite development, operations, and performance. Essential to the program is the ability to make design decisions based off the expected performance of critical satellite components and their inherent operations in variable configurations, procedures, and environments. Derived from current Mission Statements are required performance points of which a selected ADACS must meet to provide full capability. The belief that ADACS performance must be tested in flight-like conditions is at the basis for accepting the test results. The central requirements that aid in the characterization of the ADACS ability to perform operationally in a flight-like simulation are.

1. Detumble: The ADACS must be able to reduce the rate of rotation in all three primary axes after an induced external perturbation simulating ejection from the dispenser.
2. Pointing Accuracy: The ADACS must be able to accurately calculate, transmit, and hold the pointing of the chassis.

Beyond the requirements derived from the Mission Statements are generalities required to support the test procedures.

1. The ADACS must be able to accept commands from an external wireless source to simulate a ground-to-space data link.
2. The ADACS must be able to deliver telemetry data to aid in test analysis.
3. The ADACS must be able to perform within a magnetic environment estimated to be representative of the magnetic field on orbit.

### *Research Focus*

The ultimate goal of this research is two-fold. First the development a test plan capable of assessing the performance metrics of any CubeSat-specific ADACS unit as mounted to a standardized chassis and subjected to a flight-like test environment was required.

Secondarily, testing of an available ADACS unit to inform both the validity of the test plan itself, as well as informing on the performance of the ADACS unit. Two self-contained ADACS units are examined to inform the test plan, the Adcole Maryland Aerospace, Inc MAI-401, and the Blue Canyon Technologies XACT-15. The MAI-401 was ultimately used as the test case for the initial assessment and subjected estimated magnetic fields ranging from 450 to 600 KM orbital altitude at 50 degrees inclination.

The estimated magnetic fields were generated using Analytical Graphics Inc's Systems Tool Kit (STK) product as applied through AFIT's in-house Helmholtz Cage. The results of the test plan as well as the test itself shall provide not only data on the specific ADACS, but a comparative basis for characterizing all future ADACS options as they

relate to performance and ability to complete Mission specific maneuvers, operations, taskings, and in aiding on-orbit decision making processes.

### *Methodology*

To fully test and characterize ADACS performance in a flight-like scenario a number of apparatus are required to simulate the space environment on Earth. The magnetic field emanating from the Earth grows weaker as the distance from the center of the Earth increases, such that the magnetic field in space is much less than that on Earth.

Employing a 3-axis Helmholtz Cage allows for control of the measured magnetic field within a limited space within the Helmholtz Coil structure enabling the tuning of the magnetic field to that of a specified orbit.

Similar to the magnetic field, the gravitational force as produced by Earth also grows weaker as the distance from the center of the Earth increases. An assumption made is that though the ability to negate the gravitational force is absent, manipulation of the effects of gravity acting on an object such as friction can be significantly decreased. By mounting the test chassis onto an air bearing the force of gravity as applied through friction can be determined as negligible allowing for the realization of a largely unaffected rotational spacecraft.

Simulation of the Sun as required for data collection by the onboard Sun sensors is delivered by an incandescent bulb mounted within the Helmholtz Cage. The assumed energy from the Sun across all spectrums in space is approximately  $1350 \text{ W/m}^2$ . The test

setup included a 200 W incandescent lamp set at 0.2 m from the test platform providing enough light energy to indicate a solar track from the Sun sensors.

The test cases are then run at the varying pre-determined orbital parameters with data captures collected from cage mounted magnetometers, telemetry from the ADACS unit, and chassis motion as viewed from the PhaseSpace Motion Capture system. The test data can then be analyzed for performance of the cage, test setup, ADACS, and saved as a comparative for future ADACS units.

### *Preview*

Chapter I delivers the background required to understand the importance of CubeSats and their components to AFIT and the CSRA, leading to the realization of the required testing of commercially available CubeSat components and the methodology on how to accomplish the testing. Chapter II explores the intricacies of CubeSats, ADACS and their constitutive components, algorithms, and operations, as well as a dive into the space environment and how to provide a relative space environment on Earth. Chapter III outlines the methodology used in developing the test plan to create the framework of details, procedures, and standards required to repeatably test and characterize multiple ADACS offerings. Chapter IV discusses the test data, performance of the test plan itself, and results characterizing the ADACS performance, along with qualifications and recommendations for the test plan and setup moving forward. Finally, Chapter V describes the overall conclusion of the research with a view towards future work and the benefits of continuing this research.

## **II. Background**

Chapter I introduced the growth in popularity as well as the increasing role that CubeSats are taking in space exploration, research, and operations. Additionally, the evolving demands imposed upon Attitude Determination and Control Systems (ADACS) of CubeSat platforms are discussed, describing the need for expanded investigation into the performance of ADACS across varied mission sets. This research with the Air Force Institute of Technology (AFIT) and more specifically AFIT's Center for Space Research and Assurance (CSRA) centers on the creation of a plan to comparatively test and characterize ADACS Commercial-Off-The-Shelf (COTS) capabilities for the benefit of future mission component selection and solutions. The following chapter, Chapter II, begins by providing highlights of CubeSat definitions, developments, properties, and interactions in Section 2.1. Section 2.2 explores the Missions and complexities of CubeSats and their increasing relevance in space. ADACS specific hardware, software, and determination algorithms as well as the history of their advancement are found in Section 2.3, and the space environment and test apparatus required to test and characterize ADACS are available in Section 2.4. The four sections referenced in Chapter II include the pertinent background information and contextual explanations of what is required to form a broad and inclusive understanding of the complexities inherent in test and characterization of Attitude Determination and Control Systems.

### **2.1 CubeSats**

Developed jointly between Jordi Puig-Suari of California Polytechnic State University and Bob Twiggs of Stanford University to satisfy the requirements for usage in the Poly-

Picosatellite Orbital Deployer (P-POD), the CubeSat standard was born [4]. CubeSat's are considered small satellites in generality, but are commonly delineated, as shown in Table 1 [5] by mass.

Table 1 - First satellite classification [Sweeting, 1991] from [4]

Nanosatellite	<10 kg
Microsatellite	10–100 kg
Minisatellite	100–500 kg
Small satellite	500–1000 kg
Large satellite	>1000 kg

Mass, as a simplified measurement for classification provides a reference to magnitude of the spacecraft being developed, while CubeSat structure is the objective of the standardization. A single 10cm x 10cm x 10cm cube weighing approximately 1 to 1.5 kg is one standard unit, or “U” of a CubeSat. By combining “U’s” to generate larger chassis shapes, a program can effectively build out standardized configurations. Figure 1 shows the most popular configurations currently in use today , the 1U, 3U, and 6U form factors, which have gained popularity due to several standardized and commercially available CubeSat deployment systems. The P-POD mentioned above, and Planetary Systems Corporation’s Canisterized Satellite Deployer are such systems. With the risk of developing the method and mechanism of dispensing being transferred to another entity with flight heritage, the spacecraft development team can focus on the satellite development specifically, though confined by the bounds of the standardized dispenser configuration.

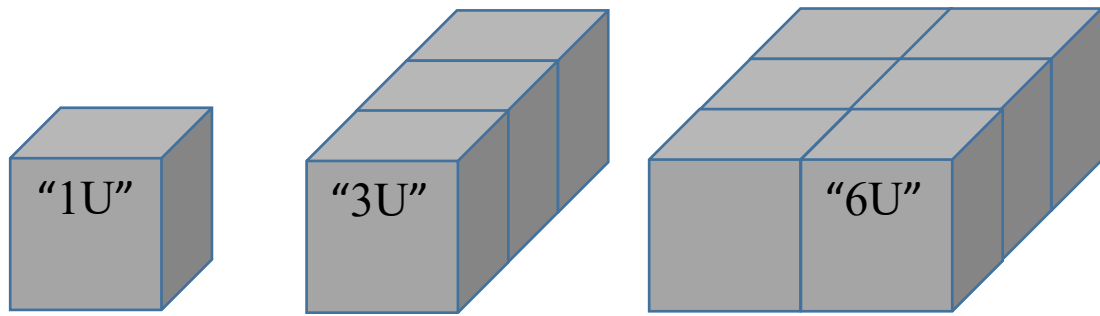


Figure 1 – Standard 1U, 3U, and 6U CubeSat Configurations

With the standardization of the CubeSat structure initially set in 1999 and the release of the CubeSat Design Specification currently on revision 13 [6], multiple commercial entities began developing standardized components specifically intended for use within CubeSats. By adhering to the standardization, a reduction in development effort and re-work inefficiencies could be obtained, which when measured in cost savings can be passed on to the satellite developers. Decreased costs lower the barrier for entry into Space, providing access to a greater pool of organizations to begin developing Space missions with CubeSats as the base platform. The first CubeSat launched in 2003, the 100<sup>th</sup> by 2012 [4], and as of April 2020 an estimated 1210 CubeSats have been launched in total [7].

Prior CubeSat development efforts, as well as those currently in development, span a wide range of owner organizations with a wide array of objectives. Commercial companies such as Planet Labs have developed large constellations leveraging CubeSats such as their PlanetScope constellation [8] for subscription-based services benefitting from public and governmental contracts. Defense organizations such as the United States Air Force’s Air Force Research Laboratory develops CubeSats such as the Very Low

Frequency Propagation Mapper (VPM) [9] for direct Space research enabling increased warfighter support. The National Aeronautics and Space Administration (NASA) leverages programs such as Educational Launch of Nanosatellites (ELaNa) [10] to partner with educational institutions both at the high school and collegiate level to expose and recruit students into Science, Technology, Engineering, and Math (STEM) futures, by providing research topics and funding. CubeSats have become an established portion of the Space portfolio, with a likelihood of increased proliferation.

Though small in physical size, the miniaturization of standardized components has enabled CubeSats to retain many of the same capabilities as larger satellites, while the growth in Commercially available Off the Shelf (COTS) components enabled by the standardization of the CubeSat platform has continued to reduce acquisition costs. From this, the increase in usage of CubeSats as well as an expansion of CubeSat mission sets continues to grow and evolve.

## **2.2 Mission Sets and History**

As space travel, exploration, and technologies become more accessible to the public at-large, the expansion of the possibilities of what can be achieved both in Space as well as from Space will continue to grow. Space-based Worldwide internet can bring connectivity to populations across the globe and to areas where the cost of a terrestrial based system is prohibitive. Space-based communications will allow for seamless scheduling from ships to harbors without the need for repeaters in the loop providing for a streamlining of logistics process. Space-based infra-red (IR) cameras can pinpoint



wildfire hotspots in rugged and mountainous terrain saving time and increasing the safety of wildland firefighters. In each of these cases as well as any number of additional cases, the need for a robust Space platform is increasing along with the potential for new and novel missions. As mission requirements continue to grow more complex and demanding, new space platform architectures with accompanying advancements in subsystem components are the logical solution. However, with the advent of CubeSat standards, these complex and demanding missions may be realized through existing CubeSat architectures. This paper expands upon the knowledge of the current set of offerings available from Commercial-Off-The-Shelf (COTS) Attitude Determination and Control Systems (ADACS) for CubeSat Proximity Operations, and how they can provide an expansion of Rendezvous and Proximity Operations mission capabilities.

To understand past and future missions, it is imperative to have a foundational set of definitions to describe mission aspects. Reeseman and Rogers of The Aerospace Corporation define the major mission operations applicable to this research succinctly in their 2018 article, Table 2 [11].

Table 2 – Space Mission Definitions [11]

Mission	Definition
Rendezvous (R)	Matching the plane, altitude, and phasing of two (or more) satellites.
Proximity Operations (PO)	Two (or more) satellites in roughly the same orbit intentionally perform maneuvers to affect their relative states.
Docking	[A] subset of proximity operations, where one satellite intentionally performs maneuvers to physically contact another satellite.
Cooperative RPO	Information (position, velocity, health/status, etc.) transfer is two-way via crosslinks, ground contact, etc. Example: docking with the ISS.

Non-cooperative RPO	Information transfer between vehicles is one-way only.
---------------------	--

From the beginnings of Space travel, the thought of a spacecraft rendezvous with a target was on the minds of the developers. Beginning in World War II Germany, the German V2 Ballistic Missile, the first craft ever to enter orbit did so in 1944 with the sole purpose to rendezvous with a specified target on Earth. Once space flight was proven achievable by humanity, the doors were blasted wide open, fueled by the Cold War and the Arms Race, a transition to Space became a popular territory for proving National dominance, culminating with the Space Race between Soviet Russia and the United States of America. In 1961 Yuri Gagarin became the first human safely visit and return from Space on the Russian Vostok 1 Mission. In 1962, John F. Kennedy proclaimed to the world that the United States was going to take on the ultimate rendezvous mission of the time, to have a manned spacecraft not only rendezvous with; but also land on the Moon. This feat of engineering would come to fruition on July 20, 1969 when the Apollo 11 mission crewed by Neil Armstrong and Buzz Aldrin achieved their goal.

Along the way to the Moon landing there were multiple steps proving increased capability from both key players. The US's manned Gemini 6 successfully rendezvoused with Gemini 7 as the first spacecraft-to-spacecraft rendezvous in 1965. While in 1966 Neil Armstrong operating Gemini 8 successfully rendezvoused and docked with an Agena rocket body proving manned docking capabilities.

As these manned rendezvous and docking missions became more prevalent, so too did the idea of unmanned or autonomous rendezvous and docking. Up until this point, all

rendezvous missions required a human in the loop. In 1967, the Soviets became the first Nation to achieve autonomous rendezvous and docking of two Cosmos Spacecraft.

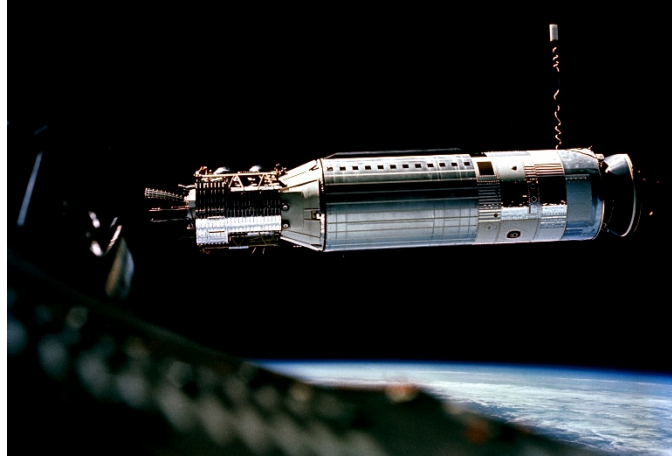


Figure 2 – The Gemini VIII spacecraft approaches the Agena during rendezvous maneuvers.

Credits: NASA/David Scott [12]

The current trend in spacecraft development is to harness the savings of moving to smaller satellites capable of performing the same (or more advanced) missions that were previously accomplished through large-scale and more expensive spacecraft architectures. Many of the mission aspects will stay the same, but with the ability to procure multiple small satellites for the same cost to orbit as one single large satellite, there comes new potential of how to leverage an interaction between satellites. Planet implemented a specific example of a Cooperative Rendezvous and Proximity Operations mission (RPO). It is a constellation of 150+ satellites on multiple differing platforms, including CubeSats, to capture images of the Earth, communicate data including positioning, and cross-link data to larger more capable satellites in the constellation for downlinking [8]. To perform these data linking tasks the componentry of the spacecraft

needs to be extremely precise, and the communication between them must be of very high quality.

Moving a step beyond Cooperative RPO is non-Cooperative RPO. While Cooperative RPO is often performed by transmitting exact attitude, velocity, and rotation data between spacecraft for the utmost in synchronization, non-Cooperative RPO is a one-sided affair. Whether the target spacecraft to be rendezvoused with is defunct, not programmed for rendezvous, or unknowingly being selected, the data flow between the two is non-existent. In this case it is required of the mission spacecraft to not only precisely understand its own orbit, attitude, and rate of motion, but to also be able to assess that of the target spacecraft.

The focus of this paper will investigate non-Cooperative RPO but with a slight skew to the concept. The rendezvous portion of the mission, though extremely important to overall success, will be left out, while the proximity operations portion will be the focus. The specific mission requirements and operational activities pertaining directly to this research will be further discussed in Chapter III.

### **2.3 Attitude Determination and Control Systems**

Attitude Determination and Control Systems are central to mission performance with respect to the knowledge and accuracy of spacecraft pointing. Pointing knowledge is a function of the determination side of the ADACS, with determination overview, determination sensors, and determination algorithms explored in sections 2.3.1, 2.3.2, and

2.3.3 respectively. Pointing accuracy is a function of the controls side of the ADACS with the controls overview and controls sensors explored in sections 2.3.4 and 2.3.5.

Attitude determination and control require quantitative measurements and as such we must first come to an understanding on a common frame of reference from which each component can accurately synchronize. Spacecraft attitude can be described in six variables for six degrees of freedom. Three variables describe the location of the spacecraft within the orbit with respect to an external origin or fixed frame. Earth's approximate center is generally prescribed as the basis for these measurements with the Z axis pointing through the true North Pole, and the X axis pointing through the intersection of the Equator and the Prime Meridian, and Y axis orthogonal to both the Z and X axis. The Y axis is positive in the direction of the right-hand rule for the cross product of Z and X components, shown in Figure 3. This Earth central frame originating from the approximate Earth's core is referred to as Earth-Centered, Earth Fixed (ECEF), where the three variables are measured in latitude, longitude, and distance from the origin at the approximate Earth's core. It is important to remember for future calculation that the rotation of the ECEF frame is referenced to the celestial field and not to the sun, resulting in the need to measurements of time in sidereal time and not solar time [13].

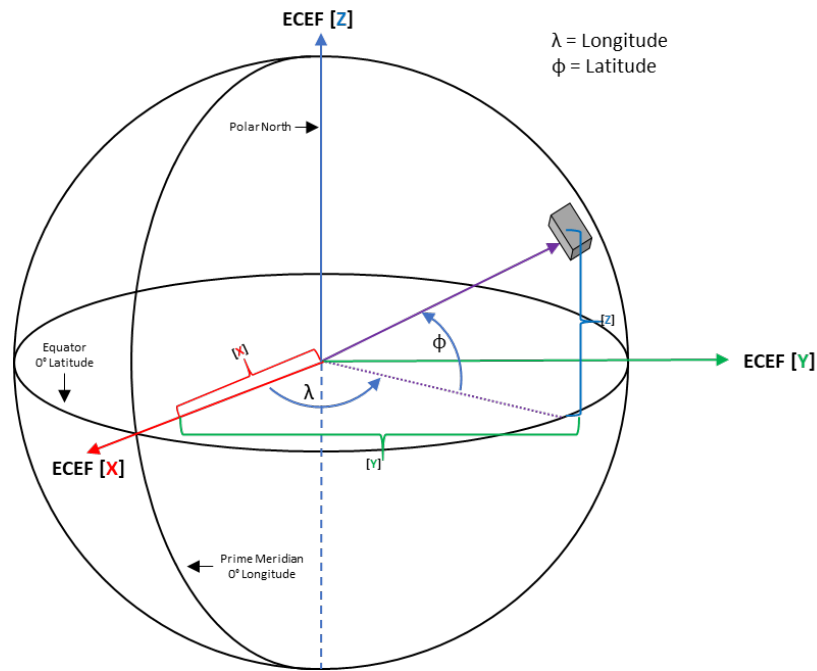


Figure 3 – Earth Centered, Earth Fixed coordinate system.

The three remaining variables describe the spacecraft's own designated body frame. The body frame is developed during the production of the chassis, is generally anchored to a physical part of the chassis and is the basis from which the onboard subsystems derive their position. An example of subsystems utilizing the body frame would be the knowledge that the solar panels are attached to the -Y face, and that aligning the -Y face with the Sun pointing vector would promote optimal charging. From the body frame a coordinate transform can then be applied transforming the orientation into the ECEF coordinate system for relevance to the ground station. These variables are generally referred to as Roll, Pitch, and Yaw (RPY) and the combination of values describe the attitude in rotations about the three-primary axis of the spacecraft. Roll denotes the angular rotation about the X axis, Pitch about the Y axis, and Yaw about the Z axis, depicted in Figure 4.

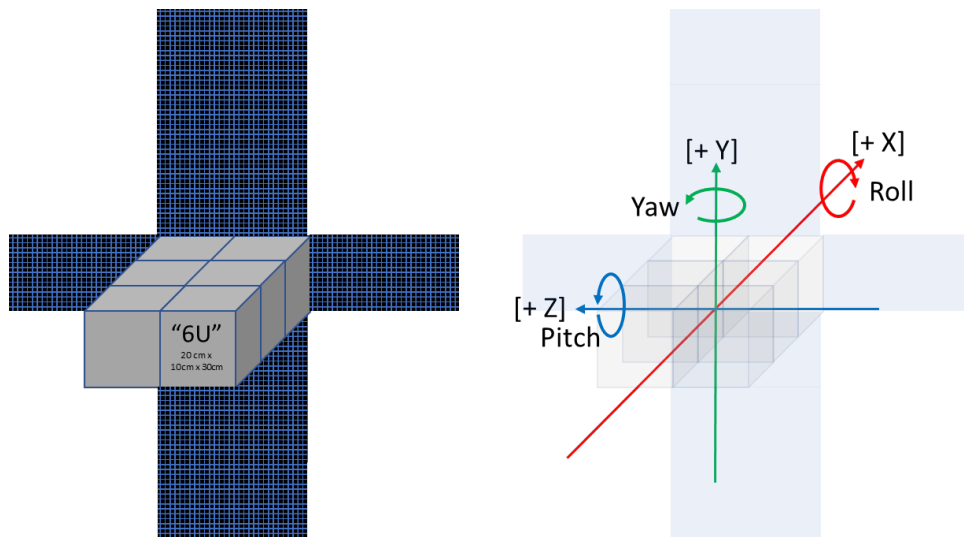


Figure 4 - Primary axis Roll, Pitch, and Yaw

From the initial coordinate frames, additional transforms can then be applied for specific usage such as ground station pointing which may choose a North, East, Down (NED) system measured from any point on Earth, leveraging Earth's magnetic field to align North to polar North, East to polar East, and Down as pointing directly to Earth's center, Figure 5.

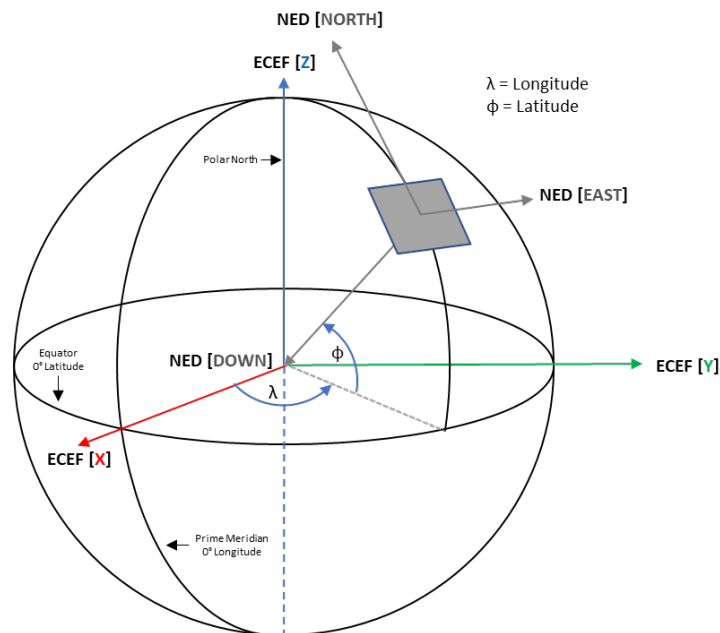


Figure 5 – NED coordinate system overlaid on ECEF.

With the reference frames agreed upon, latitude, longitude, and altitude with respect to the ECEF frame along with the body frame yaw, pitch, and roll transformed into ECFEF, ADACS performance can be discussed. The two primary functions, determination of the attitude of the spacecraft with respect to a specified frame and controlling the attitude or pointing of the spacecraft are central to the discussion of performance. While both functions are significant, attitude knowledge from determination is a required input to the control function.

### **2.3.1 Attitude Determination**

With the movement towards expanded on orbit operations required to satisfy the increasingly more complex mission sets described in section 2.2, systems and sub-systems such as ADACS are pressed to evolve into more complex and capable configurations of hardware and software in order to stay relevant. The push towards on-orbit maneuverability in CubeSats requires that the spacecraft have precise knowledge of orientation in Space, and as such the determination aspect of ADACS has continually progressed.

Attitude determination itself is the mathematical process by which the orientation of the spacecraft is described with respect to a specified reference frame and is often coupled both in ideology and usage with attitude estimation, the estimate of the spacecraft attitude



at a specified time step either at the current time or projected into the future. Though determination and estimation both provide similar data values to the user, the method by which the values are derived varies greatly along with the error and computational difficulty or speed.

Determination algorithms typically ingest vectors delivered from determination sensors to the determination controller. The determination controller then performs the programmed mathematical operations, returning an attitude pointing vector to the spacecraft Command and Data Handling system (C&DH) for further processing, usage, or data transfer. Early determination methods such as Triaxial Attitude Determination (TRIAD) required only two vectors; thus only two distinct sensors were required onboard the spacecraft [14]. As computing performance advanced, the ability to expand determination algorithms for both ground based and onboard determination also advanced allowing for the inclusion of additional sensor inputs, known spacecraft dynamics, prior attitude knowledge, as well as filtering to achieve best estimates. The algorithms such as TRIAD and the more elaborate quaternion-based Quaternion Estimation (QUEST) [15] method are explored in section 2.3.2, while the sensors feeding the algorithms are discussed in section 2.3.3.

### **2.3.2 Attitude Determination Algorithms**

Central to attitude determination is the chosen attitude determination algorithm, the mathematical formulation for ingesting data from environmental and dynamic frame-mounted sensors to produce the most accurate orientation with respect to a specified frame. While there are numerous versions of algorithms that have been studied, they can

be generally deconstructed into three categories, deterministic, optimization, and stochastic solutions [16].

Deterministic solutions are the simplest form of determination which ingest direct sensor observation data in vector form along with reference vectors, and through matrix operations develop a solution to the spacecraft attitude. The earliest contemporary determination algorithms were deterministic, with Harold Black developing the algebraic method in 1964, which described a point to point transformation of attitude [13]. As a linear approximation of a dynamic system the algebraic method did not account for errors present in sensor observations leading to increased error values of the attitude. This algebraic method would be later referred to as Triaxial Attitude Determination (TRIAD) by Malcolm Shuster [15], and is commonly used as a reference for attitude checking of more complex solutions due to its simplicity and computational speed.

In 1965, Grace Wahba essentially kicked off the transition to optimal solutions for spacecraft attitude when she introduced Problem 65-1 “A Least Squares Estimate of Satellite Attitude” in the Society for Industrial and Applied Mathematics (SIAM) Review [1]. Wahba posed that a least squares estimate minimizing the sum of the squares of the residuals of the rotational matrix from satellite fixed frame to known frame, would provide the best solution to satellite attitude while allowing for the inclusion of more than two sensor inputs, thereby obtaining the best least squares estimate from the combined group of inputs [1]. Though this problem introduced by Wahba garnered much attention,

the solution required solving for the eigenvalue's of the 4x4 matrix which was impractical at the time due to the limitations of the computing technology available [13].

*Given two sets of  $n$  points  $\{v_1, v_2, \dots, v_n\}$ , and  $\{v_1^*, v_2^*, \dots, v_n^*\}$ , where  $n \geq 2$ , find the rotation Matrix  $M$  (i.e., the orthogonal matrix with determinant +1) which brings the first set into the best least squared coincidence with the second. That is, find  $M$  which minimizes; [1]*

$$\sum_{j=1}^n \|v_j^* - Mv_j\|^2 \quad (1)$$

Malcolm Shuster realized the potential of further developing Wahba's problem as it was expanded by Paul Davenport with the inclusion of a quaternion based solution based on a la Grange multiplier [17] simplifying the loss function into a direct eigenvalue equation. From the eigenvalue equation, Shuster developed an approximation scheme named the Quaternion Estimation (QUEST) algorithm [15], allowing for the calculation of the optimal quaternion without needing to execute the entire set of eigenvalue equations. The QUEST algorithm has shown itself to be of high accuracy and low computational expense and has become a staple attitude determination algorithm for COTS ADACS.

With the continual advance in computing from the mid-1960's through today, the on-board computational power of satellites has grown exponentially along with drastic reduction in size and mass of the flight computers themselves. This advance in technology expanded the operational potential of onboard computing and data storage, thus providing a unique opportunity to include both spacecraft dynamic modeling as well as past attitude measurements combined through Kalman Filtering to achieve higher fidelity spacecraft attitude estimates. The Kalman Filter is based upon a dynamic model of the spacecraft, and with data sourced from both prior estimates of attitude as well as

incoming data time-synced from onboard sensors, derives the next best estimate or “propagated estimate” of spacecraft attitude at a specified time step [18]. Kalman Filtering has been shown to be non-discretionary as to types of sensors providing data, specifically mentioning sun sensors, magnetometers, star sensors, and gyroscopes, while computing attitude accuracies as fine as the sensors themselves are capable of [19].

Table 3 – Attitude Determination Algorithm Quick Comparison

Algorithm	Vector/Quaternion	# Input Values	Methodology
Algebraic/TRIAD	Vector	2	Deterministic
QUEST	Quaternion	> 2	Optimization
Kalman Filtering	Quaternion	> 2	Stochastic

With the large pool of options in attitude sensors, attitude determination algorithms, and the combination of the two, it behooves the developers of ADACS to provide multiple options to the consumer as the performance requirement can vary greatly by mission. Most commonly available COTS ADACS intended for use in CubeSat applications such as the solutions offered by Adcole Maryland Aerospace (MAI) [20] and Blue Canyon Technologies (BCT) [21] provide commanding to choose both sensor inputs modes as well as determination algorithm modes allowing for configuration control based on mission specifications. Ultimately, by leaving the choice to the consumer, the operational performance can be tuned to suit the accuracy required for the sensors chosen.

### 2.3.3 Determination Sensors

The accuracy of a spacecraft’s attitude solution is a by-product of both the fidelity of the determination algorithm and the accuracy of the sensors that provide measurement data.

As determination algorithms progressed in ability and complexity, covered in Section 2.3.2, so too did the ability to ingest more data in the form of additional sensor inputs. The option of adding more sensors brought with it a growth in sensor development. The proliferation and miniaturization of onboard computing permitted the development of smaller and more complex attitude sensors, which when combined with the more robust algorithms, allows the ADACS to increase the accuracy of the determination solution. This section gives an overview of the most common ADACS determination sensors.

### *Sun Sensor*

The Sun Sensors generally found on CubeSats are in most cases more precisely Coarse Sun Sensors (CSS). Coarse Sun Sensors are essentially photoelectric cells, which transform photon energy impinging on the sensor into electrical current, which is then be measured and transformed into a digital signal. The digital signal from a single CSS is mapped to the known spacecraft frame location where the sensor resides and transmits the intensity of the incoming light sensed on that plane. By combining multiple CSS's on differing planes in the positive and negative X, Y, and Z axis, a 3-dimensional measurement of the sun pointing vector can be established and fed into the ADACS.

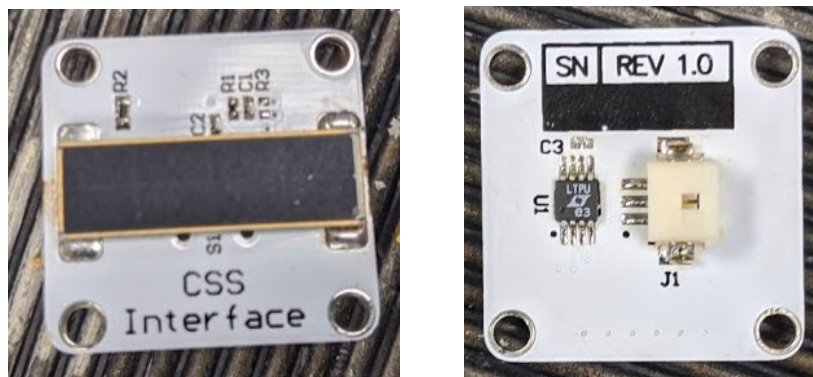


Figure 6 – Solar-Cell type Coarse Sun Sensor, top and bottom view

### *Magnetometer*

Spacecraft magnetometers are sensing instruments designed to measure magnetic fields. They are generally a simple series of wound coils that sense the change in current along the coil due to the change in the ambient magnetic field. Magnetometers provide two separate but linked types of data to an ADACS. The first being a general measurement of the ambient magnetic field with respect to the magnetometer's frame of reference. This measurement plus the known values of Earth's magnetic sphere as well as any known magnetic fields attributed to the spacecraft itself can provide a pointing vector. In addition to a pointing vector, the measurement of both the change in value of the field as well as the rate of change of the field informs the ADACS on the degree of rotation and rate of rotation of the spacecraft. Multiple axis magnetometers are available, but the simplest ADACS systems use single unidirectional magnetometers on each primary axis.

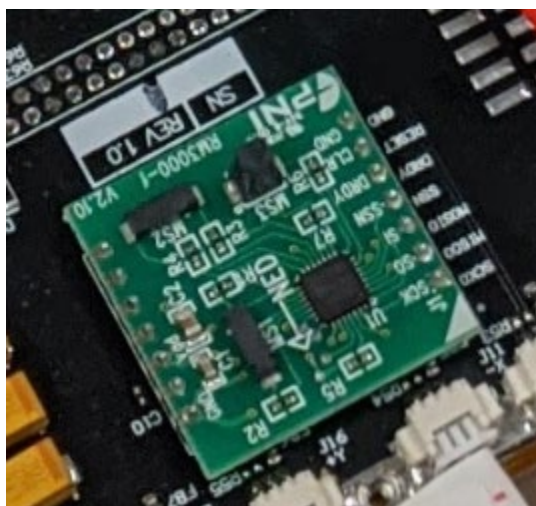


Figure 7 – Magnetometer Board

### *Gyroscopes*

Spacecraft gyroscopes are a common and effective sensor for measuring angular rate of change of a spacecraft. The method on which the gyroscope is based ranges from physical spinning plates to optical sensing systems, and from single axis to multiple axes. In each variation, the change in velocity of the spinning mass in a physical system or the time of travel for a photon in a known path for the optical system, the change be measured with respect to time to provide a rate of change of the of the spacecraft in that axis of rotation. With a single axis gyroscope mounted on each primary axis, the total rotation rate of the spacecraft can be determined.

### *Star Trackers*

Star trackers or star cameras as they are occasionally referred to, are optical sensors that provide both rate of change as well as a directional pointing vector to the ADACS. The technological advances in the past few decades have paved the way for the current

offerings in star trackers to be based off a-priori star fields loaded into the star tracker. For a directional sensor, the star tracker collects imaging data from the celestial field onto an imaging plane, and with a comparative algorithm computes the pointing vector with respect to the known star field. As a rotational sensor, once an initial capture of the star field has been observed, the star tracker can then begin to compute the rotation rate of its body frame around the observed star field pattern. Star trackers are in most cases the most precise input sensor providing data to the ADACS.

There are numerous other sensors available to the spacecraft developer such as Earth Horizon Sensors (EHS) and Fine Sun Sensors (FSS), but the most commonly available sensors for ease of use and capability are explained. One note for clarity, the precise orientation and knowledge of orientation of the sensor is imperative to producing an accurate determination solution. If the angular orientation of any sensor is off the prescribed axis by any degree, the error of the attitude solution will suffer.

#### **2.3.4 Attitude Control**

The Control Function second primary function of the Attitude Determination and Control System. Control generally refers to the ability to maneuver or re-orient the spacecraft to a specified location within a specified reference frame. In the case of an ADACS at the CubeSat level maneuvering can be omitted from the ADACS functionality while the orienting portion remains. To fully orient a spacecraft there are specific variables that need to be known to satisfy the force or torque equations. Current attitude knowledge and rates of rotation of the spacecraft are required from the ADACS determination function. The specific Spacecraft mass, Center of Gravity (COG), and Moment of Inertia



(MOI) are typically stored value in the flight software, can updated as fuel is depleted, and are required to perform the control force calculations about the spacecraft's body frame. Lastly, the frame of reference in which both the target attitude is being commanded required is required in the case of needing to perform another coordinate transform.

With the above variables, and by adapting and applying Newton's 2<sup>nd</sup> and 3<sup>rd</sup> Laws of motion, the ability to compute the reactions necessary to physically re-orient the spacecraft through the onboard control components is achievable. Newton's 2<sup>nd</sup> Law: Force is equal to the change in momentum per the change in time, or more commonly for a constant mass, Force is equal to the mass multiplied by the acceleration, explains the physical phenomena behind the mechanism of a thruster, Equation 2. Newton's 3<sup>rd</sup> Law: For every action (Force), there is an equal and opposite reaction (Force,) provides the physical law behind the mechanism of Reaction Wheels and Magnetorquers, Equation 3. The control components described are further discussed in Section 2.3.5.

$$F = m \left( \frac{dv}{dt} \right) = ma \quad (2)$$

$$F_a = -F_b \quad (3)$$

Controlling the spacecraft attitude can quickly become very complex as there exist a multitude of potential errors and coordinate transforms between components. Each sensor and control component have an intrinsic reference frame. Variations in mounting locations and orientation both within the ADACS unit or within the chassis require

mapping to a known frame of reference. Perturbations in space pose another large error value as each potential perturbation becomes additive. Such perturbations can include 3<sup>rd</sup> body gravitational pull, atmospheric drag in Low Earth Orbits (LEO), magnetic deviations due to the precession of the Earth, Solar wind, and others. Small deviations in pointing accuracy when compounded over the extreme distances covered in space missions can lead to excessive deviations in physical distance, thereby providing a critical need for development of precise and accurate componentry for spacecraft control.

### **2.3.5 Control Components**

The control force or torque value computed in the control function provides the quantitative value required to alter the spacecraft orientation. This quantitative value is dependent both on the physical properties permissible by the control mechanisms, such as the physical weight and maximum rate of rotation of the reaction wheels. The location of the mechanism within the frame and with respect to the MOI are required for moment arms and torque applications. In certain cases, such as thrusters, the physical pointing of the mechanism is also factored.

These dependencies combined can influence the magnitude of Force of Torque value required to alter the attitude of the spacecraft, leading to the topic of efficiencies. Though not discussed in this research, the study of optimization of spacecraft control is a burgeoning field feeding into the continual enhancement of ADACS performance. Novel optimization methods currently under investigation range from in depth research on machine learning [22] as well as continued research into applying stochastic optimization algorithms to control problems [23]. Common control components utilized in

commercially available ADACS are reaction wheels and magnetorquers. While thrusters are commonly used on larger spacecraft for attitude adjustments and station keeping, only recently have they gained traction in the CubeSat form factor, and even so the minimal amount of fuel capacity onboard makes them a poor choice for attitude control.

### *Reaction Wheels*

Reaction wheels operate when electrical motors rotate a weighted wheel within the spacecraft chassis creating a stored momentum value. When a brake is applied to the wheel the momentum is transferred into the body of the spacecraft thus imparting a torque to rotate the spacecraft. Common practice is to align a single reaction wheel on each of the three primary axes thereby allowing for control in all three planes of motion. Alternatively, if the spacecraft is rotating and needs to be slowed the wheel can be commanded to spin in the opposite direction, and when the braking action is applied the torque from the spacecraft body is negated by the opposing torque from the reaction wheel slowing the rate of rotation of the spacecraft. The variation of the rate of rotation of the reaction wheel up to a maximum value can be infinitely controllable, and as such the level of applied torques from the wheels to the spacecraft can be finely tuned. A weakness of reaction wheels is that they have an upper limit of rotation rate and can become saturated requiring additional control componentry to support momentum shedding or dumping maneuvers.

### *Magnetorquers*

Magnetorquers or magnetic torque rods operate on the principle of magnetic dipole moments. The mechanism for control begins when a current is imparted through a magnetic coil mounted to the spacecraft generating a magnetic field onboard the spacecraft. When the generated magnetic field interacts with Earth's ambient magnetic field, a force is created acting about the spacecrafts COG, providing the torque necessary to rotate the spacecraft. As with reaction wheels, magnetorquers shall be mounted in each primary axis allowing for control of the spacecraft in three planes of motion. The current applied to the coils can be varied to create differing strengths of generated magnetic field, thus tuning the torque to required levels. By reversing the current flow through the coils, the dipole of the generated field can be reversed, imparting torques in both the positive and negative direction on the specified axis. Magnetorquers can be very low power draw components but may take extended amounts of time to impart a substantial torque on the spacecraft.

## **2.4 Space Environment and Test Apparatus**

Testing the Attitude Determination and Control Systems is a crucial step to understanding both the performance of the ADACS alone, as well as the overall performance of the spacecraft during orbital flight and commanded control measures. Performance of ADACS can be broken down into the investigation of the two essential functions inherent in the ADACS, attitude determination and attitude control. Attitude determination relies on the accuracy of pointing knowledge, knowing the exact orientation of the spacecraft with respect to a known frame of reference. Attitude control relies on pointing

knowledge for functionality, but control performance is specifically evaluated in pointing accuracy, or how close to the commanded pointing location the spacecraft can be oriented. To test both functions, the test setup needs to account for the differences in the environment that will affect ADACS performance between Space where the spacecraft will be required to perform, and Earth where the testing will need to occur. The environment in Space differs from that on Earth in two main dimensions that will need to be addressed, the first being the magnetic field, and the second being the gravitational pull. Exploring the workings of Earth's geomagnetic sphere and its impact on ADACS system in section 2.4.1, Helmholtz Coils and Cages as the test apparatus required to negate the impact of the geomagnetic field in section 2.4.2, and the implementation of an air bearing to simulate Space's micro-gravity environment on Earth in section 2.4.3 are required to understand the bounds of the testing environment.

#### **2.4.1 Earth's Geomagnetic Sphere**

Space provides a challenging environment in which to operate on many levels. One such challenge is the ability to apply a force onto an object from a spacecraft to impart a reaction force on the spacecraft itself. Terrestrially, by applying a force upon an essentially stationary object such as the Earth, the resultant opposing force will in turn affect the object. In Space, the availability of target objects on which a force may be applied are very limited. One consistent object, or field in this case is Earth's magnetic field.

Earth's core is comprised of a dense molten liquid separated from the less dense mantle which rotate at differing velocities. This combined with conductive currents caused by

heat transferring from the molten core and escaping outwards in what is referred to as the Geo-dynamo create a magnetic field about the earth. Measurements of the magnetic field are plentiful and the data of field strength at specified intervals published regularly. Earth can be outwardly represented as a magnetic dipole with the South end of the magnet facing Earth's geographic North, and the North end of the magnet facing geographic South. The magnetic dipole of the Earth is roughly eleven degrees off the rotational axis of the Earth. As the distance from the Earth increases, the magnitude of the magnetic field decreases such that the magnetic field can be useful to satellites in Low Earth Orbit (LEO) but becomes much less effective as spacecraft altitudes increase into the Medium Earth Orbit (MEO) regimes.

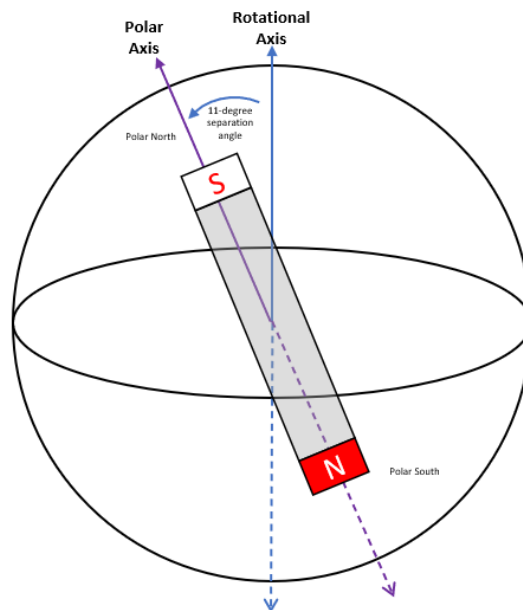


Figure 8 – Earth's Magnetic Field Represented as a Bar Magnet

Earth's geomagnetic field is not symmetrical due to two main factors, the first being the inconsistency in the densities of the Earth, and the second and most influential factor is solar wind. Charged particles released from the Sun interact with the magnetic field creating a compressing effect of the field on the Sun facing side, and an elongation effect on the side opposing the Sun. It is due to these two factors that the knowledge of the spacecraft's position within the orbit is required to accurately compute both attitude determination and control values from magnetic measurements.

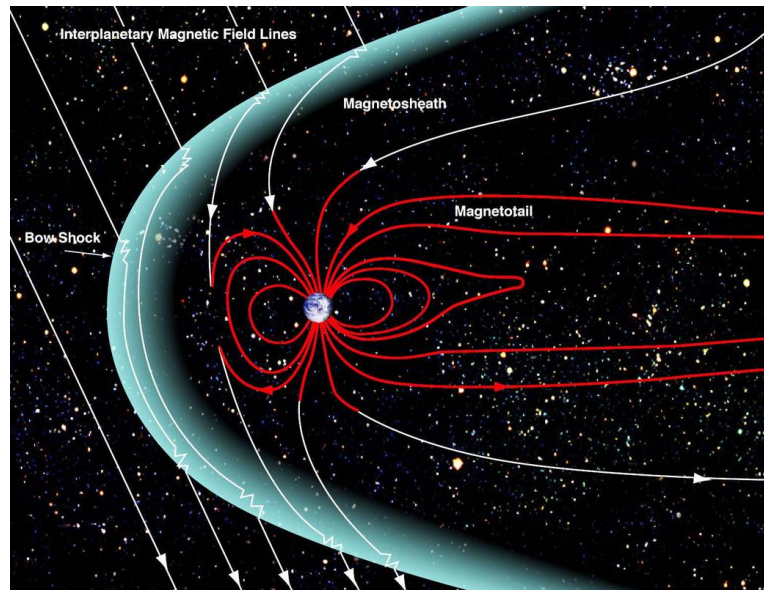


Figure 9 – Earth's Magnetosphere with Solar Wind [24]

#### 2.4.2 Helmholtz Coils and Cages

To effectively simulate the magnetic field strengths and vectors of an orbital position on Earth, the electrical field on Earth at the testing location must be altered. By running a current through a large coil, a magnetic field is generated. When placing two large coils within a specified radius of each other, the mostly uniform magnetic field strength at the

midpoint between the coils can be calculated.  $B$  is the field strength,  $N$  is the number of wraps or wire,  $I$  is the current, and  $\mu_0$  is the permeability of free space (magnetic) constant ( $1.25663706 \times 10^{-6} \text{ m kg s}^{-2} \text{ A}^{-2}$ ) [2].

$$B = \frac{8}{5\sqrt{5}} \frac{N I \mu_0}{r} \quad (4)$$

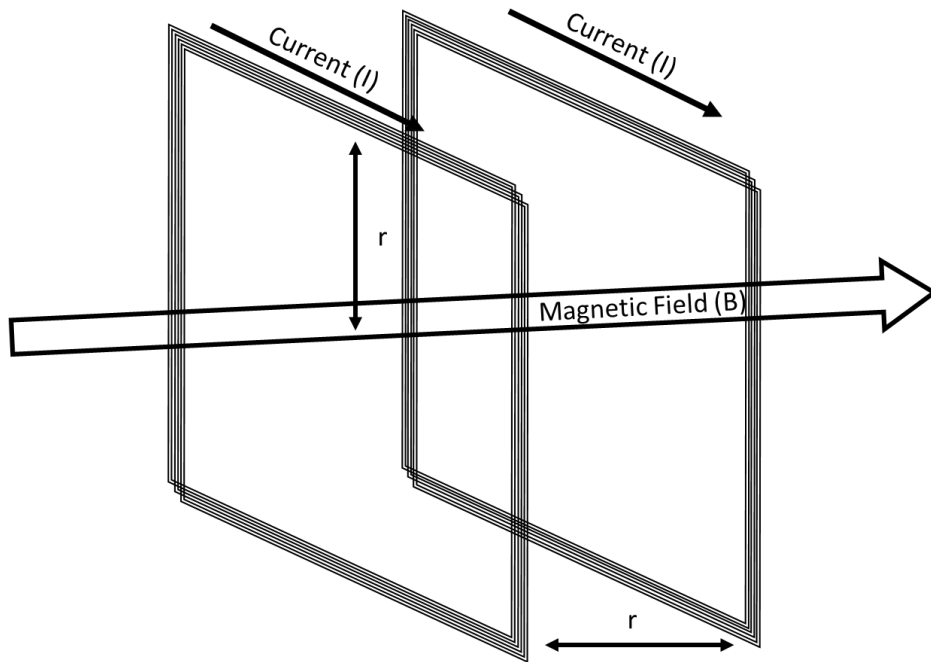


Figure 10 - Single Pair of Helmholtz Coils in Square Configuration

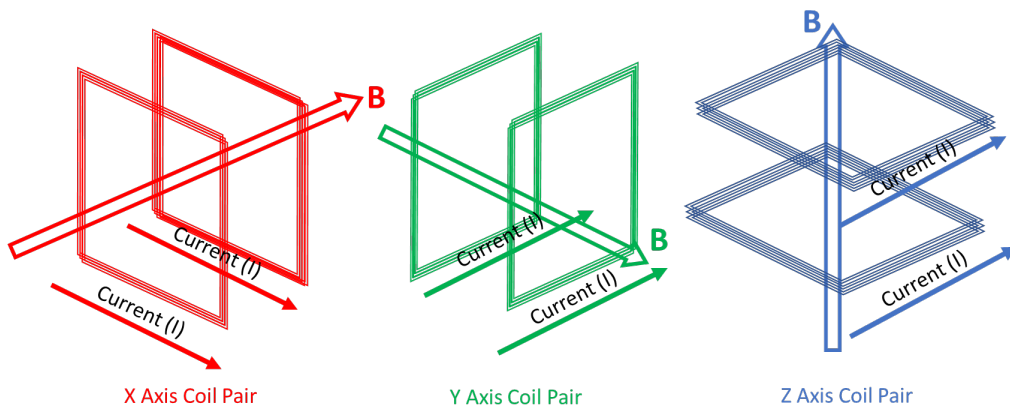


Figure 11 - X, Y and Z Coil Pairs with B-Field Vector



By altering the current through the system of coils the strength of the field between the coils will change. By reversing the flow of current the directionality of the field will change. A single pair of Helmholtz coils when placed one radius apart will create a measurable zone of uniformity between the coils in the direction of the generated magnetic field vector. Combining three pairs of magnetic coils in three axes oriented around a central point will create a box of uniform magnetic field known as a Helmholtz Cage. From this magnetic box, each axis field can be precisely controlled to simulate the space environment at the specified orbital location and time.

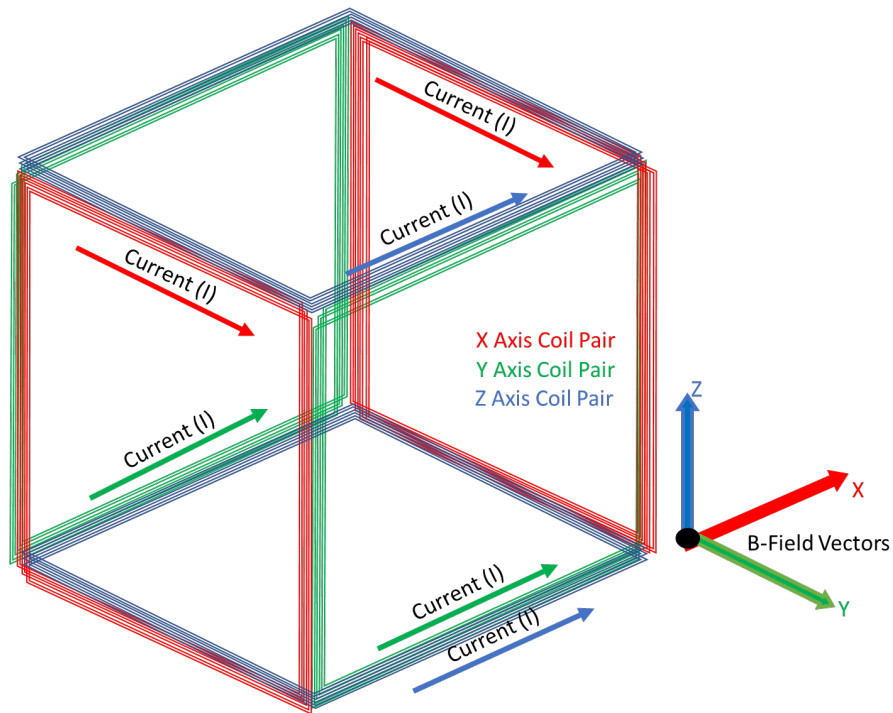


Figure 12 – Square Coil Helmholtz Cage Composite of X, Y, Z Coil Pairs

The Helmholtz Cage at AFIT as developed by Brewer in her 2012 Thesis substituted ring coils for square coils, and as such the coil spacing and the formula for the uniform magnetic field between the square coils is altered. The alteration requires that the square

coils be spaced 0.5445 times the coil height apart as opposed to the rings' one radius spacing, and in the altered equation an additional variable of  $\gamma$  is required.  $\gamma$  is the ratio of the height of the coil over the separation distance. This square coil design has been used to develop Helmholtz cages at both Carthage College, Kenosh WI [2] and Massachusetts Institute of Technology, Cambridge MA [25], though MIT chose to use the Merritt 4-Coil Design to provide a more uniform magnetic field.

$$B = \left( \frac{2NI\mu_0}{\pi r} \right) \left( \frac{2}{(1 + \gamma^2)(\sqrt{2 + \gamma^2})} \right), \quad \gamma = \frac{H}{r} \quad (5)$$

### 2.4.3 Air Bearings

For a space system to be properly characterized on Earth it must be tested in a relative environment to Space, specifically the environment on Earth needs to mimic the microgravity and minimally torqued nature of Space. With the Helmholtz cage mostly negating any induced magnetic torques, the remaining torques are largely friction induced. A reduction of friction surfaces within the experimental setup will play a large role in the fidelity of the test results as well as the ability to take precision measurements. Methods to reduce the friction supplanted into the tests include magnetic levitation systems, gravity offload systems, and air bearings [26]. Air Bearings create a very low friction environment between two surfaces and can be developed in several shapes and orientations allowing for large degrees of movement in both the planar and rotational aspects. The downside to an air bearing is that it must be attached at some point to a test apparatus and as such the bearing will be encumbered along some plane of motion.

Generally, an air bearing will allow for full rotational freedom along one plane of rotation, while the two remaining planes of rotation will be hindered the apparatus itself.

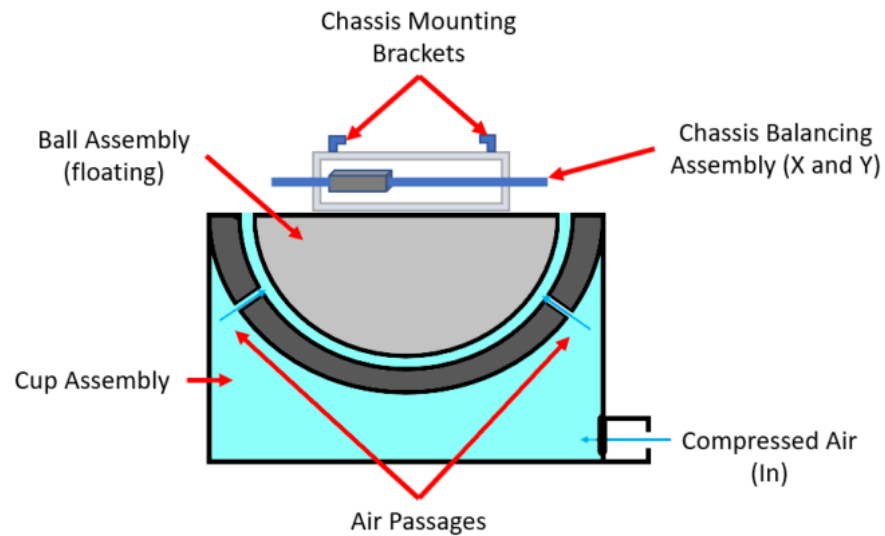


Figure 13 - Air Bearing general operation.

Air bearings, such as the apparatus at AFIT are commonly a cup and ball style.

Compressed air is fed through the cup portion, while a finely machined ball or half sphere sits into the cup. The air being forced through the cup creates an air cushion so that the ball is essentially floating. The test article, or spacecraft in this case is attached to the ball and balanced as precisely as possible. If the machining of the cup, air nozzles, and ball are precise enough the system will be in equilibrium. If the machining is not perfect there will be additional torques produced that will affect the performance of the system and introduce bias into the measurements. Though not a perfect representation of the space environment, the performance aspects of the air bearing system does provide a solid understanding and test scenario for ADACS performance.

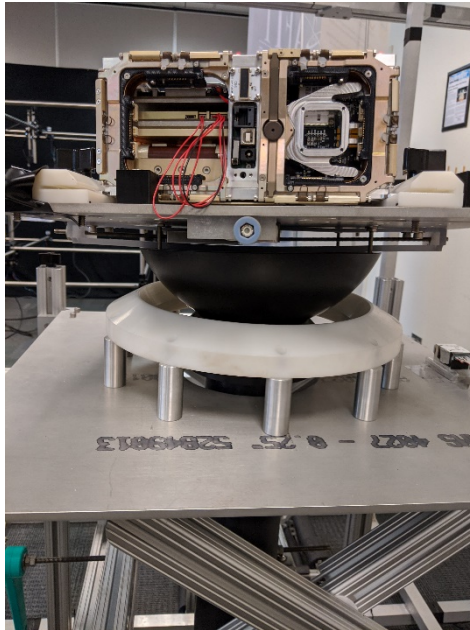


Figure 14 - AFIT Air Bearing

### III. Methodology

The benefits of characterizing and understanding the currently available COTS ADACS offerings provide clarity to the component selection process and aid in streamlining the required design effort for current and future CubeSat missions. Armed with a broad and inclusive understanding of the fundamental components and functionality of ADACS systems achieved through the literature review in Chapter II, the methodology of the characterization process can be developed. Chapter III outlines the effort to produce a standardized characterization method to which ADACS offerings may be subjected, through a deliberate set of test procedures. The focus on standardization provides a fair evaluation procedure allowing the capability of each platform to be quantified against other units. Additionally, specific mission requirements can be tested to classify suitability of each offering to specific mission sets.

The addition of specific Mission knowledge enhances performance assessment metrics by providing an additional tool with which the design team can leverage to reduce resource demand for component selection. Reduced resource demand allows for increased focus on development of command, telemetry, and mission build-out for the chosen hardware. The Mission focus, justification for characterization, and available ADACS solutions for this research are discussed in Section 3.1. Details of the performance evaluation criteria as well as performance metrics and figures of merit are discussed in Section 3.2. The experimental setup including limitations are discussed in Section 3.3. Data collection and data analysis are discussed in Section 3.4. The methodology outlined in Chapter III shall deliver a standardized assessment to increase the understanding of current COTS ADACS offerings, and by extension, shall provide the means for characterization of any new potential offerings on the market in the future with a platform to baseline capabilities against.

### **3.1 Mission, Justification, and Available Solutions**

With the increased accessibility of Space brought forth by the standardization of CubeSat form factors, the expansion of who has access to Space and the breadth of mission objective has continued to increase. Of the many beneficiaries, academia has perhaps seen the greatest advantage. Academic institutions have gained access to low-cost spacecraft components which excite potential STEM students and can bring in additional research funding for specific research areas. With this arrangement, the institution itself, the research partners, and the STEM students in both the undergraduate and graduate

level programs can all benefit and progress in their respective fields. The institution gains funding, research focus, and visibility to outside organizations for further funding, as well as an increase in both the reputation and quality of the educational program which attracts potential students. Research partners benefit from a favorable cost to performance ratio, leveraging the institution's collective knowledge base, research equipment, and low cost of labor from faculty, staff, and students to undertake research across a broad range of topics within a specified domain. Students benefit tremendously with potential knowledge gain in a multitude of space research areas from a hands-on environment of design, engineering, and research performed on and with the spacecraft.

The Air Force Institute of Technology (AFIT), an academic institution falling under the Department of Defense (DoD), is one of the institutions that has continued to benefit from the rise of CubeSat missions. AFIT's Center for Space Research and Assurance (CSRA) is an extra-Departmental entity with a broad scope of activities centering within the space domain, providing support to, and leveraging output from the AFIT students and staff. CSRA is the program owner for the AFIT CubeSat Program. Under the CubeSat Program lies a handful of CubeSat Projects all based on the various standardized CubeSat form factors. Specific Missions fall under each Project, and these Missions comprise the level where the bulk of the work takes place. Creating this structure where the Mission is owned by a non-Departmental entity allows for the CSRA to support and harness input from students and faculty across multiple departments in space related research endeavors.

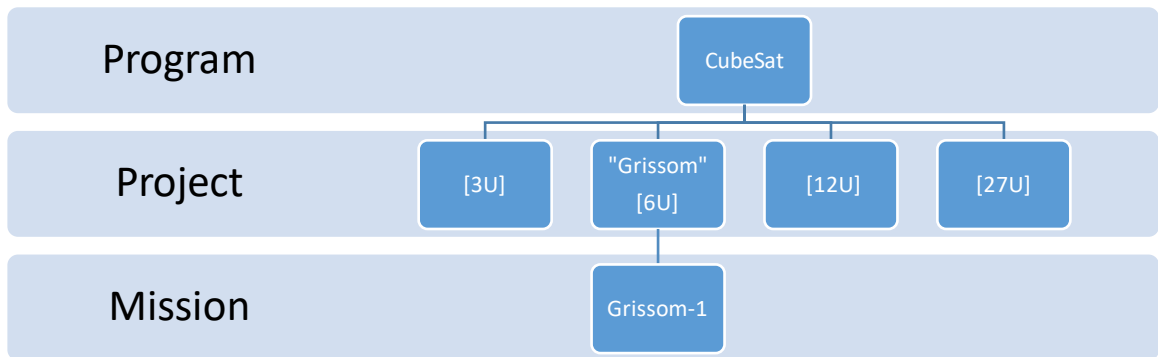


Figure 15 - AFIT CSRA's CubeSat Program Breakdown

CSRA is inherently tied to the Department of Aeronautics and Astronautics with common focus and shared staff where students often perform space-specialty research such as orbital determination optimization and spacecraft design. The non-Space Departments also provide a wealth of knowledge base, focus, and direction to the CSRA Missions. The Department of Electrical and Computer Engineering often supports CSRA Missions with guidance, hardware, and software solutions to a multitude of issues, while providing a requirement for space access for flight-testing of sensors and payloads. The Department of Engineering Physics and more specifically the research areas of Remote Sensing and Space Weather often provide requirements to CSRA for on-orbit access for a multitude of sensors and payloads spanning a variety of topics sourced either in-house, or from their own respective partners. Students from the Department of Systems Engineering and Management are often integrated into each Mission and provide support in Systems Engineering and Program Management roles including developing modeling solutions and simulations for each Mission. It is this inclusive structure that both allows for the integration of aspects from the full complement of AFIT Departments, while also

providing the requirement for continued operation, research, and support to the CubeSat program.

### **3.1.1 Mission**

Understanding the over-arching goals and priorities of the institution, departments, and the flow of funding and decision-making of each Mission is beneficial to forming baseline assumptions that will inform research decisions. In the case of this research and the CubeSat form factors that CSRA are developing, the highest priority and demand falls on that of the Grissom Project. The Grissom Project is based on a highly configurable 6U CubeSat chassis referred to as the “Grissom Bus.” The Grissom Bus while conforming to the standardized 6U form factor utilizes a modular design permitting a large variation of mission profiles, objectives, and operational characteristics as well as delivering a platform to host the addition of payloads. The Grissom-1 project will be the basis of this research, but the knowledge gained in both the operational characteristics of the ADACS within the flight-like configuration as well as the performance of the test plan shall be applicable to all related and future AFIT CubeSat missions.

#### *Grissom-1*

Grissom-1 is the first in the line of AFIT CubeSats based off the Grissom Bus. The objective of the mission is two-fold, first to gain flight heritage for the bus, flight software, and development team, and secondarily to support the added payloads. Grissom-1 is considered a basic 6U offering, developed with only the subsystems necessary to perform a simple mission. The subsystems included with the chassis structure are the Electrical Power System (EPS), Command & Data Handling (C&DH),



Tracking, Telemetry & Control (TT&C), Attitude Determination and Control (ADACS), and Thermal Control (Thermal) which collectively occupy about 3U worth of spacecraft volume. The remaining volume provides the volume necessary for the addition of payloads, which for Grissom-1 are the Extremely Low-Resource Optical Identifier (ELROI) payload provided by Los Alamos National Labs, and the NanoSatellite Tracking Experiment (NTE) developed by the Naval Intelligence Warfare Center.

ELROI delivers with it a list of spacecraft requirements one of which is pertinent to this research. ELROI requires that the spacecraft shall provide Nadir pointing of the payload over a specified latitude and longitude for operational testing. Similar to ELROI, NTE includes the requirement for Nadir pointing over a specified range of latitude and longitude values to complete its mission. The objective and threshold values of the Nadir pointing requirement are not implicitly defined in either case, driving the need for data in the relative sense. Thus, if the spacecraft is commanded to a specific pointing, what is the accuracy or error in pointing that the ADACS can deliver in each axis.

While the objective and threshold values are not known at the current time, it is reasonably assumed that the beam pattern of the payload in either mission mode or while downlinking data is likely driving the requirement. It can also be reasonably assumed that ADACS with increased accuracy can support payloads with finer pointing requirements. From these assumptions, the requirement for ADACS Pointing Accuracy can be derived and will assist in defining the total performance of the ADACS.

### *Future Missions*

With AFIT operating as a research hub of new and novel concepts and pushing the bounds of current practices, the assumption that more complex mission profiles will eventually be the norm for the work within the CSRA is valid. Flight heritage for the chassis, components, and development team open the possibilities of new funding and new research opportunities. Currently, research into CubeSat specific propulsion systems has been investigated along with the potential missions that the addition of propulsion could support. With respect to ADACS, current COTS propulsion units are rarely outfitted with steerable nozzles leaving the ADACS to alter attitude to provide the proper alignment with the required thrust vector. Definitive objective and threshold values for pointing accuracy for thruster operation have not yet been specified, though as the attitude angles diverge from the required pointing vector, the efficiency of the thruster will decline. On a CubeSat the volume of propellant is extremely limited and thruster efficiency will be heavily weighted for design decision making.

In Grissom-1 and with future CSRA CubeSat missions, the spacecraft will likely be ejected from a CubeSat canister mounted to the host vehicle as the method in which orbital access is provided. The standardized ejection canisters often impart relatively small external torques to the spacecraft at time of release due to the launch mechanism friction, which may also be combined with tip-off rated imparted from the host spacecraft. These external torques leave the spacecraft in an uncontrolled and potentially unstable motion described as a tumble. The first step in spacecraft control once the onboard Command and Data Handling system is booted and initialization has occurred is

the ADACS will be required to perform a detumble process to retake control of spacecraft. Detumble is most often linked directly with a Safe Mode where the spacecraft will autonomously compensate for the external torques imparted on the spacecraft. In most cases, the rotation will be damped down to a threshold limit where the next series of autonomous steps can take place. Once satisfactorily detumbled, the spacecraft can then begin the process of sun searching and finally altering attitude to position the solar panels in the sun pointing direction for charging. An uncontrolled spacecraft is both unproductive to the Mission as well as a danger to any co-orbital spacecraft, thus the detumble is deemed a significant requirement.

The total set of requirements both explicit and derived from the bus, hardware, mission objectives, payloads, and physical phenomena are then transferred to the Grissom Bus as operational and performance requirements.

### **3.1.2 Justification**

AFIT is a research institution with challenging requirements. Not only must AFIT satisfy the requirements and standards set forth by academic regulatory and accreditation agencies, but also adhere to regulations passed down through military guidance and objectives. Where private or state-run institutions have the luxury to adjust to their own vision at their own pace, AFIT must conform to the standards and time scales implored by the Major Command (MAJCOM) as well as the funding agencies. This hurdle forces AFIT to look towards research focus areas that are not just relevant today, but those

which the DoD assess will provide increased capabilities to the warfighter in the future. It is safe to say that Space is now a higher priority than ever before in the DoD, and that AFIT and the CSRA understand the complexities and trends of the space acquisitions and are steering student programs as well as expending resources on space topics.

Getting out in front of the curve with research focus areas such as those specific to CubeSats, AFIT has positioned itself as a leader in the space-related education theme and as a support system to the greater DoD. In addition to providing programs of study, investments into CubeSat development processes as well as laboratory and testing facilities enable both students and operational missions. The combination of access to spacecraft components, lab space, and testing equipment attracts students to take on challenging research topics, ushering a growth of knowledge across the space domain for the students and the community in which they will then be employed. AFIT programs and research topics have benefits reaching beyond the institutional walls, with the goal of supporting critical decision points in future operational DoD Missions. Research topics such as CubeSat ADACS performance are examples of this type of research that support current and future needs.

### **3.1.3 ADACS Solutions**

The key driver for this thesis is the Attitude Determination and Control System performance of the Grissom bus for the Grissom-1 mission, as well as accounting for provisions for future CubeSat missions. The assumption is that all known missions are built upon the Grissom bus, and the configuration of each mission impacts a variety of ADACS performance parameters. The Missions themselves may require differing on-

orbit activities, which lead to the inclusion of a thruster system and investigation into the performance with increased complexity of maneuvers. The potential of adding thrusters and the increased complexity which follows led to the decision of obtaining an alternate ADACS than the model chosen for Grissom-1. The assumption of the thruster system being statically positioned requires a central location within the chassis to limit rotational torques occurring when the thrusters are activated and not aligned with the Center of Gravity (COG). This leads to the decision of mounting the thruster system in the middle cube of the 3U volume on one side of the chassis. The combination of the thruster system and a generic payload would likely add a significant amount of mass to the chassis. The added masses coupled with their specific location within the chassis leads to a center of gravity (COG) and Moment of Inertia (MOI) that can be effectively much different as each mission evolves. In each case, the ADACS solution chosen along with the full mission loading must be carefully understood before a true flight test and comparison can be performed.

#### *MAI-401*

The ADACS solution chosen to support the Grissom-1 Mission is an Adcole Maryland Aerospace, LLC (MAI) MAI-401 Mini ADACS [20]. The MAI-401 is a self-contained ADACS solution configured and marketed towards the Nanosat and more specifically CubeSat market. The MAI-401 requires less than a full “U” in volume and provides both determination and control in three axes. Attitude determination is supported by six Coarse Sun Sensors (CSS) inputs, a 3-axis accelerometer, a 3-axis magnetometer, and a star tracker. Attitude control relies on three reaction wheels and three electromagnets

each supporting 1 rotational axis. The attitude sensors along with the control components are enabled by the ADACS computer. Communicating with and receiving telemetry from the ADACS computer is performed through the Command & Data Handling System (C&DH) linked to the ground station software.



Figure 16 - Adcole Maryland Aerospace's MAI-401

Operationally there are a multitude of commands, modes, and settings that can be applied to the MAI-401, all of which alter its performance. To reduce complexity and biasing towards specific tests, the operation structure will be simplified to performing the nominal tasks and actions associated with general on-orbit operation. General on-orbit operation begins with the CubeSat deployment from the canister, release of the stowed solar panels, and initializing the power-up sequence. With power initially removed from the ADACS during launch, the Electrical Power System (EPS) will initialize the ADACS through the power-up sequence. The MAI-401 is preset to initialize in Acquisition Mode, which is one of thirteen ACS modes available to the ADACS. Acquisition mode is also known as the rate null mode within MAI documentation, in which the ADACS attempts to reduce the spacecraft rotational rate to 0 deg/second in each axis as measured

by the magnetometer. This rate nulling process is referred to as a detumble process or action for this research.

A consideration worth mentioning is that though the rate nulling process will decrease the initial spacecraft momentum post-ejection, the separation of autonomous acts built into the ADACS software is not readily apparent. It is possible that without the inclusion of a sun simulator in the testbed, that the ADACS will detumble and then continue attempting to find the sun in the sun acquisition process. Without a sun to find, as possible in an eclipse scenario, the ADACS will follow a constant motion process until the sun is found. The pre-set rate of rotation maintained within Acquisition Mode is roughly two times the orbit rate (average inertial rate of magnetic field) [20]. With this knowledge there is potential that the ADACS will detumble to a momentary stable state and then begin rotating again at a controlled state.

### *BCT XACT-15*

The increased complexity inherent with the addition of a thruster system drove the CSRA CubeSat development team to obtain a Blue Canyon Technology's (BCT) XACT-15 ADACS [21] for their research efforts. The XACT-15 is like the MAI-401 in that it is a self-contained spacecraft attitude determination and control system marketed towards small satellites and is touted as a "0.5U micro-package," leading one to believe that it is intended for use in CubeSat configurations. Attitude determination input arrives from a star tracker, an inertial measurement unit (IMU), a magnetometer, and a Coarse Sun Sensor assembly. The verbiage of an IMU does not necessarily denote what sensors are

housed within the unit, but since magnetometers are specifically referenced outside, the internal components are likely accelerometers or gyroscopes. Three-axis attitude control is driven by reaction wheels and torque rods. Commanding the ADACS and retrieving telemetry is handled through the C&DH interface, which translates commands from the ground station software.

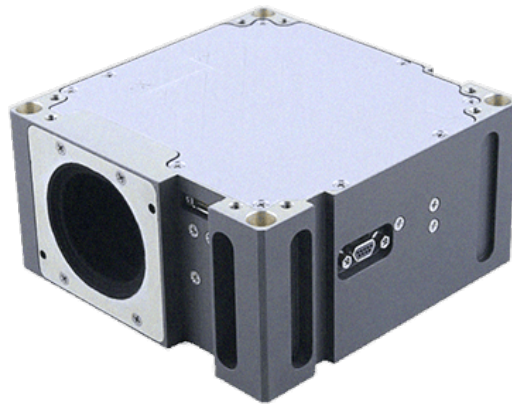


Figure 17 - Blue Canyon Technology's XACT-15 Attitude Control System

Operationally the XACT-15 User Guide describes behavior much like the MAI-401 referenced above. The XACT-15 will be unpowered during launch and will be initialized post-ejection from the canister when the separation switch and solar panel deployment switches have been released. Once the EPS has initialized the C&DH and sent power to the XACT-15, the XACT will boot into Sun Point Mode. Sun Point mode is the base level mode for the XACT and serves as both a place-holder state as well as a safe-state mode for the ADACS. Sun Point Mode autonomously begins to shed momentum induced from both ejection and tip-off which is the Detumble process for this ADACS. To alleviate momentum, magnetic torque rods are employed with the reaction wheels locked out by the ADACS software. Once a pre-set floor threshold of momentum is



reached, detumble is considered complete. With detumble complete the XACT-15 autonomously begins its sun search in attempt to begin sun pointing. As with the MAI-401, though the ability to detumble is not specifically affected by the CSS's, due to the autonomous nature of the sun search following detumble it is required that a sun simulator be provided in the setup to reach a steady state after detumble.

### **3.2 Performance Evaluation**

From an overview standpoint the MAI-401 and the BCT XACT-15 are similar in many aspects from component makeup, performance specifications, and operational ability. When investigating deeper into the User Manual for each unit, it becomes evident that the offerings begin to differ in several areas including sensor utilization and attitude determination algorithms. While the design and internal operation of the ADACS becomes difficult to gather information on (proprietary information) as well as test, the external performance of the ADACS becomes the key to the performance evaluation. With the knowledge of requirements from the Mission, Bus, and available hardware, the ability to derive the bounds and processes of the testing procedure became more evident. The known ADACS offerings allow for the simplification of operation into a finite number of states and modes that can be considered similar enough to warrant a comparative. To create a narrative reporting performance of the ADACS within the available test setup it is critical to provide a clear understanding of how the evaluation of the performance will be undertaken. Section 3.2.1 outlines the preference of testing control performance over attitude determination, while Section 3.2.2 describes the

performance metrics and figures of merit for the comparison that can be compiled from the test procedure.

### **3.2.1 Attitude Determination vs. Control Performance**

The development of a test plan for the comparison of opposing products intended to return the same result creates a set of difficulties that can rarely be fully solved without performing the testing within representative environmental conditions. Testing of ADACS falls within this set of products. The differences in ADACS can be vast among each critical function, both determination and control. Determination can differ in number, type, and quality of sensors delivering data, as well as a wide swath of applicable determination algorithms described in Section 2.3.2 that ingest sensor data and provide determination solutions. In addition, the determination algorithm can have the ability to assess a-priori data such as that in a Kalman filter application and weighting past solutions. Control is complicated with its own set of potential differences. Control actuators vary by size, type, and performance, while acting upon a spacecraft that can vary in total mass, center of gravity (COG) and moment of inertia (MOI). Furthermore, control ingests the determination solutions into the control algorithm driving increased divergence in system operation.

Though each component of the ADACS system can be tested separately for accuracy, precision, and behavioral characteristics, it is the performance and function of the system as a whole that is the focus of this work. The idea of emergent properties emanating from

a buildup of a total system gives the system its final usable characteristics, in both positive and negative aspects. In the case of the ADACS, the nature of the control function, requiring input of the attitude solution as well as the control solution for computation, allows for the operational characteristics of the ADACS system as a whole to be tested solely while testing control performance. By focusing the test scenarios on the control performance, the full complement of attitude determination and control performance can be accurately established.

### **3.2.2 Performance Metrics and Figures of Merit**

The attitude of a spacecraft as referenced in Section 2.3 can be described as rotations about the X, Y, and Z axes with respect to a known reference frame. Attitude will be derived from two distinct sources linked by common reference frames, including the raw telemetry as measured from the ADACS, and the chassis motion data as measured from the PhaseSpace Motion Capture camera system. Direct measurements from the separate sources with respect to each axis within the known frame can be used to understand the accuracy and precision of the control function. Both data sets require coordinate transforms to reach a common reference frame, and both require data manipulation to allow for comparative data analysis. Performance of the ADACS overall satisfying the pointing accuracy requirements can thus be made.

From the direct measurements of each source, a time derivative of the data can also be achieved, resulting in the time-rate of change value with respect to each variable in each primary axis. From the time derivative an assessment on the rate of change of the system can be made, providing insight into the rotational rate of change of the test platform.

With the understanding of the motion of the test setup is limited to axial rotation about the X, Y, and Z (also referenced as yaw, pitch, roll), or any combination of the three in both the positive and negative directions when referenced with the right-hand rule, an assessment of the performance of the ADACS with respect to the detumble requirement may be made. In both cases, that of raw measured data as well as time-derivative data, plots of the resultant data series will be beneficial in understanding not only trend of each data set, but the quality of the test setup and test plan as well.

### **3.2.3 Data Collection**

From the test setup the three important data sets can be obtained.

- (1) Telemetry data from the ADACS
- (2) Helmholtz Cage Data from the MATLAB script operating the Helmholtz Cage.
- (3) Rotational Data from the PhaseSpace Cameras System

Data is easily mined from the laboratory desktop workstation that operates the simulations, allowing for ease of access to all data and continued visibility of the both the physical test as well as the data output flow. The data files are saved to the appropriate test folders for future analysis. While the ability to immediately analyze the data would be beneficial for understanding any anomalies or unexpected trends in the data output while testing, the decision to progress through all test scenarios while the test configuration was set and performing properly is the preferred course of action. The potential for changes to the system with regards to the positioning of the truth magnetometer or the balance of the spacecraft on the air bearing due to raising and lowering the air bearing setup has the potential to alter visible trends in the small number

of tests. Once all test scenarios are run, the data is then compiled to be analyzed.

Analysis of the test data is performed within MATLAB, using the ability to draw on multiple data types, specifically .txt and .csv files for analysis in one location.

### **3.3 Experimental Setup**

From the early stages of forming the base level questions of this research topic through the literary review summarized in Chapter II and expanding through the development of the methodology and test plan outlined earlier in Chapter III, the formulation of how to test an ADACS in a flight-like environment was the focus. The result of a decision made at the cross-roads of what is ideal and what is available led to a compromise of the test setup and test operation. Though not the ideal solution, the accepted test plan provides a reasonable resolution to testing an ADACS unit purpose-built for space operation in a terrestrial setting. While each component of a spacecraft must undergo rigorous testing proving flightworthiness in areas such as thermal cycling and vibratory resonance testing, flightworthiness was purposely left out of the test plan to allow for complete focus on the performance aspects of the ADACS systems alone. Trust-but-verify is the status-quo when characterizing flightworthiness, that verification should be left to the Mission team assembling a Mission-specific spacecraft to their inherent qualification levels.

A foundational understanding of the bounds in which to test the ADACS unit specifically focusing on the performance aspects provided the guidance necessary to procure the test setup. Available to students studying space related topics within AFIT, is access to several laboratory spaces, hardware solutions, software development areas, and staff

supported by the CSRA. Of the items available for this testing was the opportunity to build a generic 6U CubeSat test unit specifically for testing ADACS operations for this research. The CSRA Mechanical Laboratory at AFIT possesses a Helmholtz Cage originally developed in 2012 [3], which has been maintained and updated over the years supporting occasional internal program testing and spacecraft development projects. Access to the cage allows for the variation of the magnetic field within the bounds of the cage providing a method to simulate the magnetic field estimated on-orbit. Additionally, within the cage rests and air bearing with a mounting platform purpose-built to receive a CubeSat chassis. The air bearing will allow for an extremely low friction rotational assembly representing the microgravity environment of space. Mounted around the cage are the six motion detection cameras of the PhaseSpace Motion Capture system, which provide the opportunity to measure and visualize the motion of the spacecraft during the test procedures. Beyond the large items that makeup the test suite are numerous lab workstations, software applications, tools, configuration items, cabling, power sources, and most importantly access to subject matter experts in every possible field related to this testing. The below subsections provide greater detail of the more critical test items.

### *Helmholtz Cage*

The AFIT Helmholtz Cage lies at the center of the ability to complete this research as described when referring to “flight-like” conditions. The cage provides the magnetic environment needed to test ADACS performance on Earth but as effected in Space. Specifically, the cage allows for the ability to vary the magnetic field within a small zone of influence, thus demonstrating the estimated magnetic field at a proposed orbital

altitude and inclination. The AFIT cage is built using three sets of square Helmholtz Coil pairs, aligned in the three primary axes of X, Y, and Z, of which more in-depth description can be found in Section 2.4.2 Helmholtz Coils and Cages. The large sizing of the coils, though requiring a larger amperage draw, delivers a larger area of uniform magnetic field in which the test chassis is mounted. The coils are controlled by the MATLAB script which has been updated by the CSRA staff since its initial commissioning in 2012 [3]. The truth magnetometer within the homogeneous zone performs as a feedback sensor thus allowing the cage to continually regulate current to each coil separately to ensure the least possible variation from the desired values. The desired values are estimated through a simulation run on Analytical Graphics Inc's (AGI) Systems Tool Kit (STK) Space Environment Effects Tool (SEET). The values are ingested into the script and driven by pre-specified time steps. Output from the MATLAB script return both desired values as well as measured values as registered by the truth magnetometer for analysis.

### *Air Bearing*

The available air bearing setup within the Helmholtz Cage at AFIT is of the cup and ball design. The chassis is mounted to the carrier plate which sits atop the ball. The ball rests within the socket where compressed air is pumped through miniature orifices allowing the ball/plate/chassis structure to hover in a very low friction environment. The cup and ball design allows for uninterrupted rotation about the Z axis (within the XY plane) but is limited to (+/-) 25 degrees above and below the XY plane. Critical to the setup of the test is the ability to balance the ball/plate/chassis structure on the air bearing. If the balance is

incorrect the air bearing will reach its equilibrium point below the available rotational limit, thus impacting or resting on the air bearing structure and rendering the test invalid. In addition to the potential of an unbalanced test, the potential for induced forces or rotations due to the flow of air around the cup and ball socket it always a potential, though proper cleaning and maintenance should provide for minimal impact.

### *PhaseSpace Motion Capture System*

Relying solely on the telemetry of the ADACS to verify its own performance is not the ideal solution when working towards a comparative analysis. As a secondary measure to have the performance of the ADACS verified by an external source, the implementation and usage of the PhaseSpace Motion Capture camera system was applied. The PhaseSpace system is a series of motion detecting cameras, six cameras for this experiment, physically mounted to the Helmholtz Cage approximately 1 meter above the mounting plate of the air bearing. The cameras are connected to the PhaseSpace server through an ethernet connection and controlled with the OWL Master Client software. Mounted to the chassis are a series of light emitting diodes (LED's) to which the cameras are tuned to sense. The Master Client software provides the ability to measure the initial positioning of the LED's and create a virtual rigid body from the positioning. The rigid body is then mapped to a reference coordinate system, in this case using the chassis frame of reference. The OWL Master Client then retrieves the measurements from each respective camera, analyzes the data, and outputs a solution for the motion of the rigid body in heading, physical positioning, and rotational quaternions. As an extra measure to package the timing, data capture, and output files a script in Python was developed by the



CSRA staff to streamline the PhaseSpace process. The data obtained from the PhaseSpace camera system will be used as a tool to satisfy the verification of the measured ADACS motion for all test objectives.

### *Generic Test Chassis*

The basis of which this set of tests falls is on the ability of an ADACS unit to perform determination and control functions on a 6U CubeSat chassis. To support this basis a generic chassis was sourced along with the minimally required components to operate within the laboratory confines. Within the chassis were various subsystems required for operation. A MAI-401 ADACS unit and supporting processor board and magnetometer add-on, with five Coarse Sun Sensors (the sixth would be obscured by the air bearing plate) supporting the ADACS. A Wi-Fi dongle acting as the Telemetry, Tracking & Command link. A Command & Data Handling System running AFIT's core Flight Software (cFS) for relaying commands to the ADACS as well as returning telemetry through the Wi-Fi link. An Electrical Power System with battery pack for powering the test unit, with a charge cable for keeping the battery pack supported when not testing. Of note were the lack of thermal control system deemed unnecessary for testing in the ambient indoor temperatures, the lack of solar panels which would interfere with the mounting of the chassis on the air bearing platform, and the addition of a mass model located opposite the solar panel face simulating the addition of a payload while also providing much needed counterweighting for the balancing process.

Commanding of the spacecraft was relayed from a lab workstation using the COSMOS software over a Wi-Fi connection to the C&DH, which then delivered the proper sequence of commands to the required subsystems. The COSMOS software also provided the ability to watch livestream telemetry data from the connected subsystems through 2-way communication.

#### *Computer Modeling for magnetic field*

The Helmholtz cage provides the opportunity to vary the magnetic environment within the cage to an almost unlimited number of combinations. Potential variations include setting the drivers to a zero current application to be affected only by Earth's magnetic field on location at AFIT, nulling Earth's field such that the cage truth measurements are at [0, 0, 0] milli-gauss in the respective [X, Y, Z] vectors, and simulating the space environment at any estimated orbital parameters. Discussions of current and planned Missions with members of the CSRA staff produced the request to study the operational performance of the ADACS at three specific simulated orbital altitudes, 450, 500, and 600 kilometers while at an orbital inclination of 50 degrees. These orbital parameters align with the bounds used by multiple other research projects run in conjunction with the CRSA. Analytical Graphics Inc's (AGI) Systems Tool Kit (STK) Space Environment Effects Tool (SEET) was used to produce the estimation of Earth's representative magnetic as felt on orbit at the above orbital parameters.

Setup of the SEET tool was completed using reference guides produced by STK for each separate orbit, with the main field set to use the International Geomagnetic Reference Field model (IGRF), and with no external model added as suggested by the SEET reference guide due to the low orbital altitudes required. The SEET tool requested the time steps in which to update the estimated magnetic field which was set to 1-minute intervals to save on both computing time for the simulation as well as allowing for enough time for the Helmholtz cage to equalize at each specified value. Each simulation was run for a period of 100 minutes under the assumption that 100 minutes would cover 1 full orbital period for the requested orbital altitudes in this test. The magnetic field data as then delivered in a .txt report with each time steps and respective magnetic intensity measured in nano-Tesla for the North, East, and Down reference frame. The report is imported into MATLAB, delimited, transformed into a more usable coordinate frame, and finally ingested into the Helmholtz Cage script driving the cage parameters.

### **3.3.1 Component Frames of Reference**

Complications can arise from a test setup running multiple stage tests on a complex system measuring the motion of a rotating test subject. The complications from component frames of reference and common nomenclature are potentially the most common and easiest to make. By simplifying each test component down to the base level frames, the entirety of the reference frame picture can be laid out allowing for smooth transformations when troubleshooting or analyzing data. Deciding on a common frame as the base frame as well as a naming and coloring convention eases the ability to assess each component and to visualize proper orientation. Understanding that the performance of the tested ADACS will be anchored to a relative but stationary pointing reference and

not tuned to Earth's NED configuration, the common frame can be chosen. For this test setup the common frame will follow that of the Helmholtz Cage with the three primary axes as shown in Figure 18. Additionally, the coordinate axes of X, Y, and Z will be color coded to Red, Green, Blue respectively for each component.

The chassis frame being developed as its own separate project has been described with its own individual coordinate frame. While operationally in space the attitude of the chassis and internal components with respect to the Earth is variable, but when installing parts and operating the unit within the effects of gravity on Earth the standard configuration of operation and carry is shown in Figure 18.

The orientation of the ADACS unit will likely vary by manufacturer and should be provided in the operations and reference material. Understanding the reference frame and coordinate system of the ADACS is required, but it is also critical to understand how the ADACS itself was mounted to within the chassis, thus making the first double coordinate transform of the process.

In the case of the MAI-401 test setup the magnetometers delivering measured magnetic field data to the determination function were provided on a separate board allowing for optional mounting positions throughout the chassis. As with the orientation of the ADACS with respect to the chassis, the orientation of the magnetometer board with respect to the ADACS is also a critically important task.

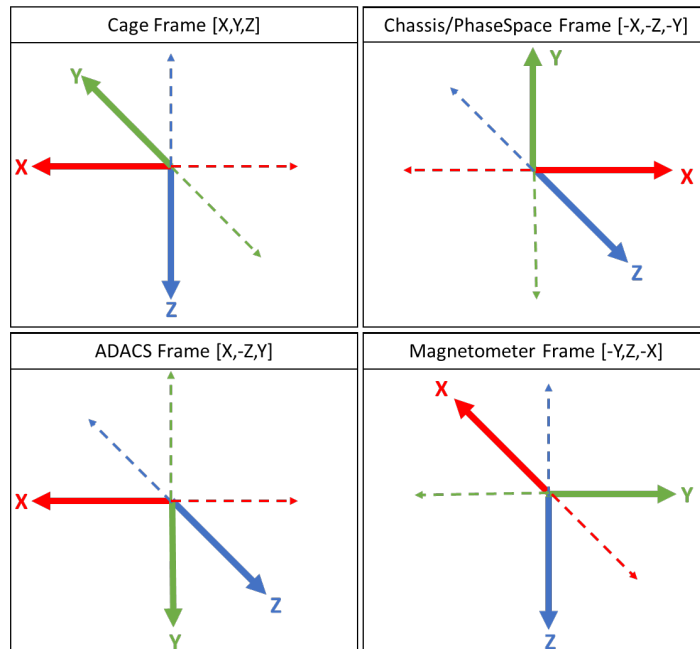


Figure 18 - Test Component Coordinate Frame

From the base level coordinate frames referenced in Figure 18 the remaining coordinate frames of the test setup can be managed. The MATLAB code running the Helmholtz Coils is inherently in the Cage frame but ingests the chassis frame to complete a coordinate transform such that the data delivered from the tests including that of the truth magnetometer can be obtained in the rotated frame for ease of analysis. The PhaseSpace camera system links its virtual rigid body to the chassis frame such that any rotation of the chassis is qualified and married to that of the rigid body.

In all cases it is beneficial to understand a common frame of reference to aid in the analysis of the data from each separate component. It is imperative to verify reference frames in all cases, but specifically for those that require coordinate transforms into other

reference frames. Additionally, it is beneficial to verify that for each reference frame and each transformation that the norm of the right-hand-rule is never violated.

### **3.4 Limitations**

Testing of space systems prior to launch and on-orbit operations is a significant requirement for the fact that the ability to re-contact a spacecraft for maintenance, repair, or modification is extremely difficult, costly, and rare. Subsequently, the effort and resources devoted to pre-launch testing is required to be high. With the increase in quantity of spacecraft on orbit coupled with an increase in capability-per-kilogram and interest in the exploitation of space resources, the knowledge base of the space environment is growing. An increase in knowledge of the environment in which a spacecraft will operate leads to more specific test scenarios. Ultimately the goal would be to test every operational characteristic of the spacecraft in a flight configuration and within a simulated space environment, though the cost and time required becomes prohibitive. From this realization it makes sense to test general operational characteristics in terrestrial environments which mimic space as close as possible and within the confines of what is reasonably available to the test team. For operations and test cases outside the norm or deemed unreasonable a simulated environment shall be an acceptable approach. The limitations that impacted this research were varied, as were the effects on the test procedures and results.

### *Star Tracker*

A primary component commonly used within an ADACS is that of a star tracker camera.

A star tracker can be utilized in two ways, with one significantly more complex. The first type operates with no a-priori information, such that the star tracker cyclically views captured images of the sky, tracking bright stars, and calculating rotational movement and rates from the imagery within the internal ADACS software. The second type is loaded with a star catalog such that the captured imagery can then be internally verified against the star catalog, providing not only rotational movement and rates, but estimated pointing vectors to assist the determination algorithm. Of the available ADACS units surveyed, the star trackers were heavily relied upon for internal data calls enhancing pointing accuracy and precision when in the more complex operational and command modes.

Testing of the star trackers requires either a real star field, or a simulated field. Testing in flight configuration on the real star field would require either an outdoors test, a roof opening, or positioning very near a large bank of windows, all of which become unreasonable when operating within the Helmholtz Cage. The other solution would be a simulated star field on a monitor placed directly in front of the star tracker camera. This becomes problematic when testing any motion of the spacecraft as the monitor would also be required to move with respect to the motion of the star tracker as to always keep it in frame. With the ability to test the star tracker limited within reasonable bounds, the ability to test the total performance of the ADACS system is also limited specifically with

respect to the pointing accuracy test which would rely heavily on the operational modes supported by the star tracker.

### *Sun Simulator*

Coarse Sun Sensors (CSS) are integral sensors providing data to the determination algorithms within the ADACS. Of the ADACS units surveyed, the CSS's were relied upon universally for detumble process, and occasionally in other commanded determination modes. Testing of the ADACS ability to detumble is then critically reliant upon the performance of the CSS's which are then reliant upon the test setup to provide a solar simulator as close as possible to the on-orbit environment. Energy from the Sun at the outer reaches of Earth's atmosphere is approximately 1350 (Watts/meter<sup>2</sup>), a value that is like what a spacecraft would encounter on orbit. In addition, the Sun's energy in space is spread across the entire electro-magnetic spectrum.

To simulate the Sun's energy on the CSS's a 200W incandescent lamp was placed approximately 20 cm from face of the rotating spacecraft to illuminate the CSS's to register the minimum photo-electric power required to simulate the spacecraft not in an eclipse period. Due to the proximity of the lamp to the face of the spacecraft, for each rotation as the lamp's influence left that of the closest CSS, the ADACS would err to an eclipsed condition before regaining enough energy to again become non-eclipsed at the next CSS. For this Sun simulator to work properly it is suggested to develop a collimated light source large enough to illuminate the entire chassis during a test period



and delivering enough light to satisfactorily trigger the ADACS into the illuminated state to not be limited by the constant flux between illuminated and eclipsed states.

#### **IV. Analysis**

With a suitable methodology laid out in Chapter III, coinciding with the development of a test plan sufficient to function as the framework for assessment between multiple ADACS units, the process of testing the on-hand MAI-401 ADACS unit was undertaken. From the beginning of the test period, it became apparent that the ability to command the spacecraft into the planned modes of operation through the flight-like Ground System – to C&DH – to ADACS pathway was not fully functional at the time of testing. Whether the issues arose from connectivity, the developed flight software, ground system software, commanding sequences, or a combination of the aforementioned, the ADACS unit did not respond as required. After much deliberation and consultation, it was agreed that though not all test objectives would be met, critical early testing was still beneficial and required for the program to succeed.

With the root cause of the commanding issue undetermined, the ultimate impediment for completion of the test sequence was identified as the inability to transition the ADACS from the initial boot mode known as Acquisition Mode, into any available mission mode where commands for attitude adjustments are accepted. Acquisition Mode, though unfortunate in the fact that pointing knowledge and slew rate would not be permitted to be explored, is the mode in which the detumble operation occurs, and as such will allow for one of the test objectives to be met. Performance analysis of the data obtained from the MAI-401 detumble along with the PhaseSpace camera system will not only permit a

deeper understanding of the detumble operation and performance but can also be extended to the operation of the ADACS in other modes. The sharing of sensors across modes allows the detumble analysis to benefit to the performance and effectiveness of the whole system.

The detumble tests followed directly from the test plan to comply with the baseline assumption that for any future comparative analysis to be performed, a strict adherence to a standardized test plan is required to be followed. The testing was performed, and aside from a small number of intermittent connectivity issues due to loss of wireless connection from the representative ground system to the C&DH leading to a loss of data and a necessary restart of the test, the tests progressed as expected. Each test scenario was completed, and data stored. The data files obtained from the tests were as expected, telemetry output from the ADACS by way of C&DH, Helmholtz Cage data from the MATLAB script, and motion data provided by the PhaseSpace camera system. Of the numerous data points to analyze, the most beneficial for analysis was derived from the telemetry taken with respect to the magnetic field. Additionally, the data from the PhaseSpace Motion Capture camera system provides a reliable supporting set.

#### **4.1 Magnetic Field Data Analysis**

The magnetic field data may be the most important point of analysis for this research for the reasoning that it is being measured both by the truth magnetometer within the cage and from the onboard magnetometers, as well as having the data point of what the intended magnetic field of the cage should be. The duplication of sensors provides the

ability for comparative analysis of one sensor against another in a common referenced frame. The first look at this data will be a comparison of three variables in the three major axes. The variables are:

- (1) Desired Helmholtz Cage magnetic field.
- (2) Helmholtz Cage magnetic field as measured by the truth magnetometers.
- (3) Helmholtz Cage magnetic field as measured by the ADACS magnetometers.

To view the values on a combined plot it is imperative to convert them all to a common frame of reference, and in this case it will be the “Cage” frame. The desired values and truth magnetometer measured values are provided in the chassis frame as is built into the MATLAB code, and thus need a rotation of 90 degrees about the X, followed by a 180-degree rotation about the Y. It is assumed that the coordinate transforms or rotations all share a similar baseline, in which each axis will only be varied by multiples of 90 degrees. In this case the rotation matrices are all simplified from trigonometric functions to combinations of 1, -1, and 0.

$$\begin{bmatrix} 1 & 0 & 0 \\ 0 & \cos(\theta) & -\sin(\theta) \\ 0 & \sin(\theta) & \cos(\theta) \end{bmatrix} = \begin{bmatrix} 1 & 0 & 0 \\ 0 & 0 & -1 \\ 0 & 1 & 0 \end{bmatrix} \begin{bmatrix} X \\ Y \\ Z \end{bmatrix} = \begin{bmatrix} X \\ -Z \\ Y \end{bmatrix} \quad (6)$$

Inserting the resultant coordinate frame vector into the next rotation to receive the total rotational transformation of the desired cage field and truth magnetometer.

$$\begin{bmatrix} \cos(\theta) & 0 & \sin(\theta) \\ 0 & 1 & 0 \\ -\sin(\theta) & 0 & \cos(\theta) \end{bmatrix} = \begin{bmatrix} -1 & 0 & 0 \\ 0 & 1 & 0 \\ 0 & 0 & -1 \end{bmatrix} \begin{bmatrix} X \\ -Z \\ Y \end{bmatrix} = \begin{bmatrix} X \\ -Z \\ -Y \end{bmatrix} \quad (7)$$

In a similar fashion, the onboard magnetometer is required to go through a series of rotations to reach the common “cage” frame, in this case specifically due to multiple

components being mounted to and working with each other in different relations. The magnetometer is mounted onto the ADACS with a specified NED orientation, while this should clarify the relationship, the NED label was only specified with a single arrow, leading to an ambiguous understanding of the true relationship. To understand the true relationship, the cage was set to X, Y, Z values of [0, 0, 0] respectively, and then each axis was increased to 1000 milligauss. This process allowed for the known cage axes to be traced to the unknown spacecraft magnetometer axes as described in the ADACS axes empirically.

The magnetometer data is passed to the ADACS which has a known orientation per manufacturers specifications, which then outputs the telemetry in the ADACS frame to the C&DH where it can be read out. Since the ADACS works as an intermediary in this process, the addition of the ADACS frame rotation is also a necessary piece. The ADACS frame is transformed into the cage frame with a single -90-degree rotation about the X axis, this is the expected value of the onboard magnetometer if aligned with the ADACS.

$$\begin{bmatrix} 1 & 0 & 0 \\ 0 & \cos(\theta) & -\sin(\theta) \\ 0 & \sin(\theta) & \cos(\theta) \end{bmatrix} = \begin{bmatrix} 1 & 0 & 0 \\ 0 & 0 & 1 \\ 0 & -1 & 0 \end{bmatrix} \begin{bmatrix} X \\ Y \\ Z \end{bmatrix} = \begin{bmatrix} X \\ -Z \\ Y \end{bmatrix} \quad (8)$$

The measured values of the onboard magnetometers resulted in the following matrix with respect to the cage frame, though given in the ADACS frame.

$$\begin{bmatrix} -Y \\ Z \\ -X \end{bmatrix} \quad (9)$$

With the known experimental values as well as the expected resultant, the rotation matrix from the magnetometer frame to the ADACS frame can be solved for.

$$\begin{bmatrix} X \\ -Z \\ Y \end{bmatrix} = [?]_{3 \times 3} \begin{bmatrix} -Y \\ Z \\ -X \end{bmatrix} = \begin{bmatrix} 0 & 0 & -1 \\ 0 & -1 & 0 \\ -1 & 0 & 0 \end{bmatrix} \quad (10)$$

From which the ADACS frame to Cage frame rotation of -90 degrees about X can then take place, proving the combination of rotations does is in-fact net the originally driven [X, Y, Z].

$$\begin{bmatrix} 1 & 0 & 0 \\ 0 & \cos(\theta) & -\sin(\theta) \\ 0 & \sin(\theta) & \cos(\theta) \end{bmatrix} = \begin{bmatrix} 1 & 0 & 0 \\ 0 & 0 & 1 \\ 0 & -1 & 0 \end{bmatrix} \begin{bmatrix} X \\ -Z \\ Y \end{bmatrix} = \begin{bmatrix} X \\ Y \\ Z \end{bmatrix} \quad (11)$$

With the specified rotations performed upon the requisite data sets, the data is then plotted for analysis. It is important to note that of the three orbital scenarios completed only one will be followed in this analysis, the detumble scenario at an orbital altitude of 500 kilometers and an inclination of 50 degrees. The results of the remaining simulations will not be deeply explored as the results are all in agreement and follow similar trending.

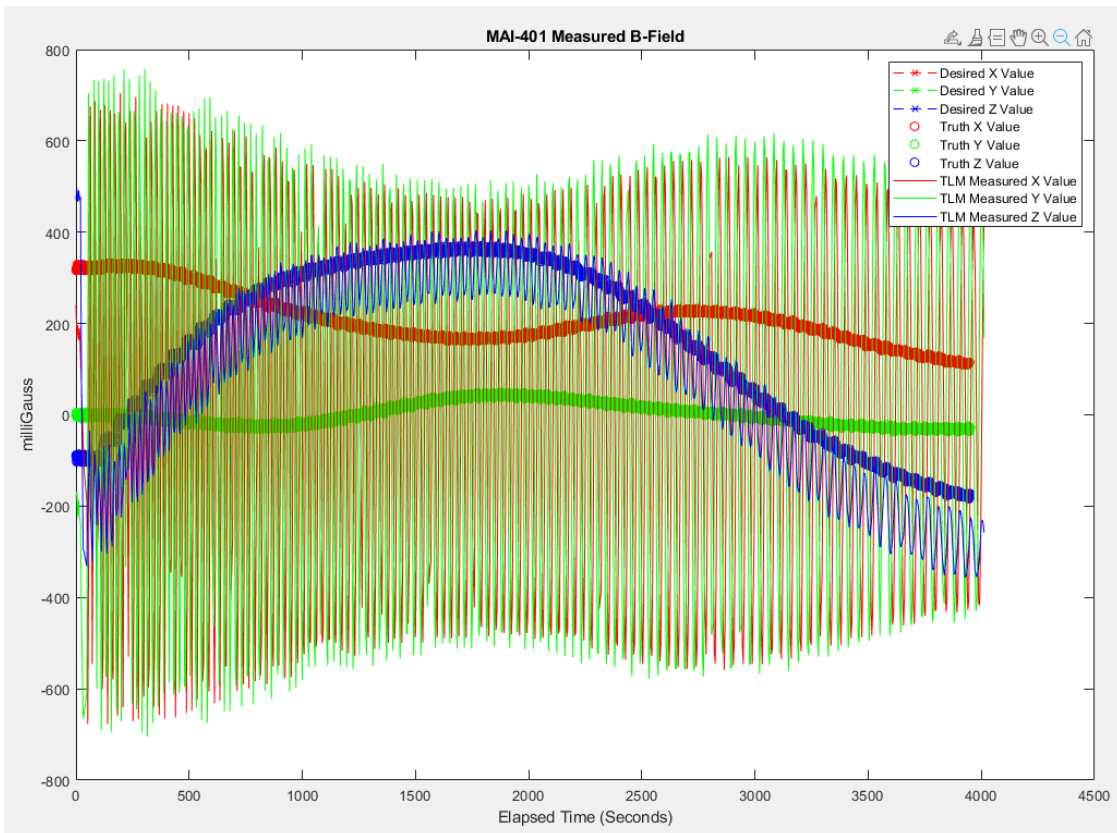


Figure 19 – Magnetic Field Measured Data for simulated 450 KM Orbital Altitude at 50 degrees inclination.

Various conclusions can be drawn from the data plotted in Figure 19 representing magnetic field values in milligauss over an elapsed time in seconds on both a large scale as well as in more compact views. From Figure 19 the desired and truth values appear as solid lines progressing across the chart, though when enlarged as in Figure 20 the data points become more apparent, while the MAI-401 telemetry data is plotted as a solid line of a sinusoidal nature.

When taking an enlarged view of the magnetic field data within the Helmholtz cage as shown in Figure 20, as expected, the desired values of the magnetic field represented by the "--\*--" line progressed in a series of time steps at 60 second intervals for the entirety

of the test period. Additionally, from the same enlarged view the measured data shown with the “o” points taken from the truth magnetometer within the cage provides a closer look at the how well the cage algorithm performs in driving the Helmholtz coils to produce the intended magnetic field. The variation in the truth values from the desired values as explained by Brewer (2010) are due to the interaction, or more specifically the bleed of magnetic energy between each specified axis due to the overlap of the magnetic field lines. To mitigate the effects of the transfer of energy, the code driving the Helmholtz cage employs a feedback loop for each axis comparing the current field values against the desired values, and adjusting the electrical current applied to each coil to vary the field [3].

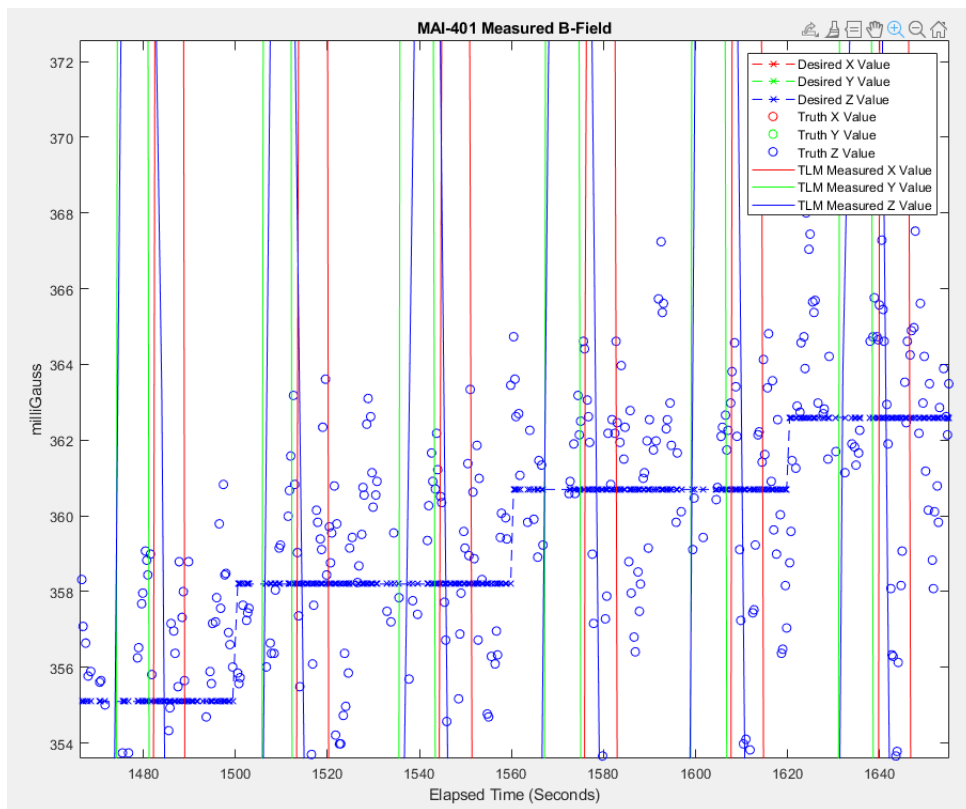


Figure 20 – Enlarged View: Magnetic Field Data for simulated 450 KM Orbital Altitude at 50 degrees inclination

With the plots of the desired and truth cage data proving to be sufficient and as expected, it is then key to begin looking at the measured ADACS telemetry data for performance. The telemetry data appears to follow similar trends as the desired and truth values, but with a readily apparent increase in magnitude of values as well as added offsets for X and Z axes. This increase in magnitude and addition of offset will be further explored in Section 4.3. Furthermore, and what is not specifically apparent to the naked eye is the increase in time spread from peak-to-peak value as time progresses in all three axes. The increase in spread describes an increase in time between each successive peak magnetic field as the spacecraft rotates, or more specifically that it is taking more time for the spacecraft to rotate the same distance. This trend is promising in that the slowing of the rotational rate of the spacecraft is the desired outcome of the detumble capability.

To enhance and clarify the understanding of the plot of the measured B-Field data against time, the simple derivative of the data can be taken.

$$\frac{dB}{dt} = \frac{\text{Change in B Field}}{\text{Change in time}} \quad (12)$$

The derivative is applied independently to each of the three primary axes, X, Y, and Z producing the rate of change of the magnetic field in each axis. The rate of change data can then be plotted against time for each respective axis, resulting in the plot shown in Figure 21.



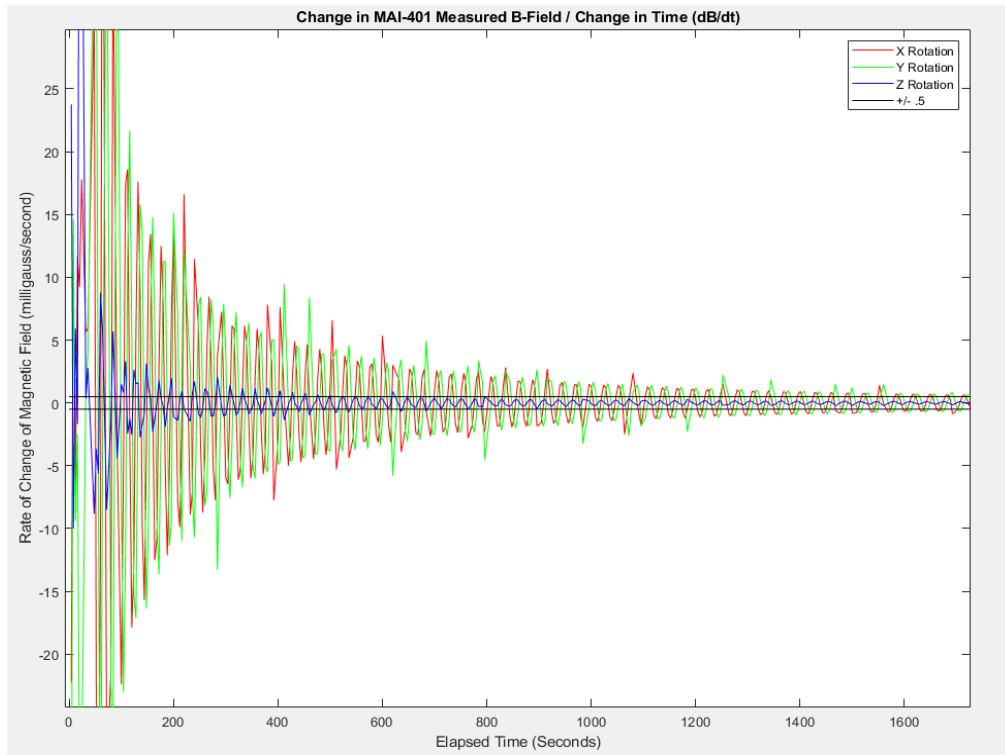


Figure 21 - Rate of Change on the Measured Magnetic Field

Figure 21 represents the rate of change data as solid line with the X axis as red, Y axis as green, and Z axis as blue following the predetermined coloring scheme and plotted in the cage frame of reference. As expected, the X and Y values are similar as they are on the same plane of rotation and should follow each other out of phase by 90 degrees. The Z values are expected to be much smaller in magnitude which is supported by the plot. The mechanism of the air bearing limits of freedom of movement in the Z axis which in turn limits how the test operator can exert force simulating ejection from the cannister onto the chassis. This requires the perturbation to be focused in the XY plane, and thus the Z values will be much smaller in scale. All three data sets follow the same trending of large initial rate of change values trending down towards a stagnation.

Of the important takeaways from Figure 20 is the general shape of the plot's maximum values as time progresses. In a rotational system at a constant rate of spin with no damping effects one would expect to see a linear fit line at a single value as the rate of change would be constant. In a system with a constant damping effect such as one with an induced drag or applied force opposite of the direction of travel, one would expect to see a decreasing rate of change as a linear set of values trending towards zero, and likely ending at an equilibrium value. The data in this plot follows a decreasing rate of change in a polynomial trend which is indicative of the damping force becoming less effective as time progresses due to less time spent at the maximum magnetic dipole.

An additional takeaway is specific to the Z axis. Though starting at a lower initial value of rate of change, the maximum values of the Z axis decrease and come to a stagnation point much more rapidly than that of the X and Y axes. The overlying difference comes from the interaction with the gravitational force on the system. Where the air bearing provides a simulated micro-gravitational environment when describing the frictional forces in space, it does not reduce the force of gravity on the spacecraft itself. Gravity thus acts as an additional damping force on the motion of the chassis in the Z axis ultimately leading to the chassis coming to a static position of equilibrium in the Z direction. The minimal but present cyclical perturbations in the Z axis continuing throughout the duration of the test data can likely be attributed to slight imbalances of the spacecraft remnant from test setup and persisting due to the constant rotation in the XY plane.

## 4.2 PhaseSpace Motion Capture Data Analysis

The PhaseSpace Camera system is a secondary point of data that allows for the analysis of spacecraft motion with regards to the static frame of reference. The PhaseSpace cameras are hard mounted on the cage, with LED emitters and controllers mounted to the chassis. Through the PhaseSpace server any motion of the LED emitters is detected by the sensors, transmitted to the PhaseSpace client server, where it is available to view on the lab workstation. This process is tunable with various data outputs that can be used for analysis. Initial setup of the Cameras, emitters, and a virtual rigid body within the PhaseSpace software linking the chassis and emitters to the Cage frame provides the PhaseSpace software the information required to output values of both heading angle as well as deviation from centroid. In the case of these specific tests, the data output with regards to heading was questionable in all cases, leading to the belief that a deficiency in setup procedure was likely to blame. With the heading angle data left out, the remaining data from PhaseSpace, specified in millimeters of deviation from the assumed centroid in cartesian coordinates (X, Y, Z) became the focal point for analysis.

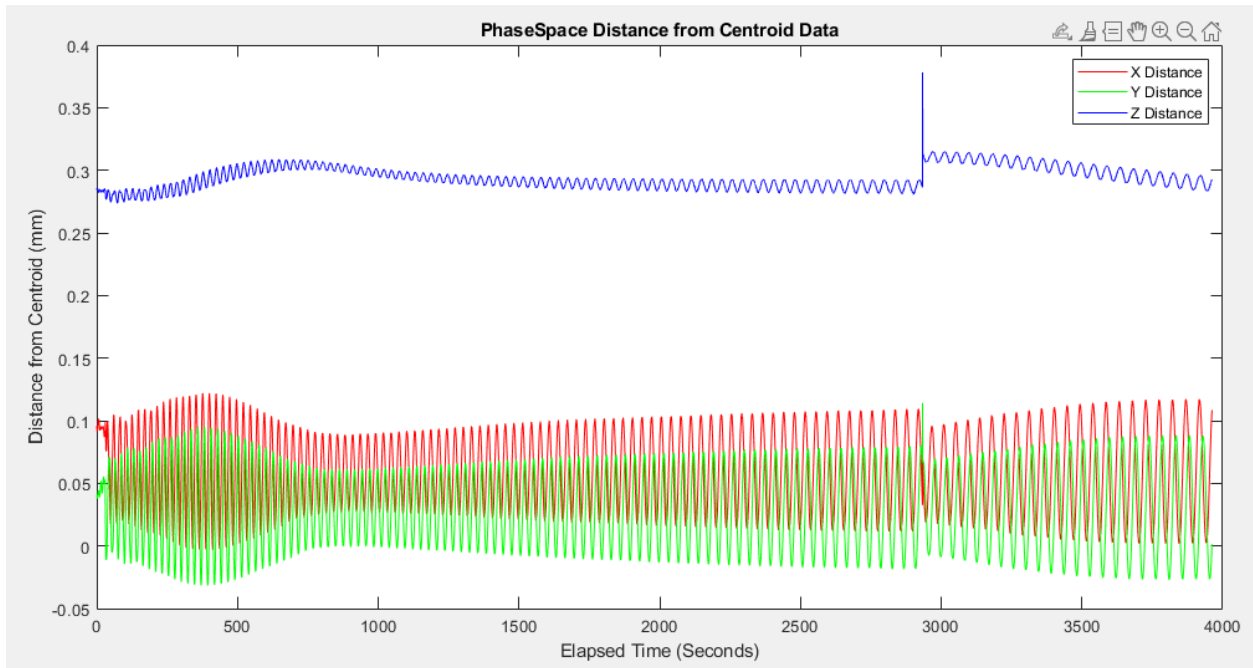


Figure 22 – PhaseSpace Raw Distance from Centroid Measurements

Figure 22 plots the raw measurements obtained from the PhaseSpace server of millimeters of offset of the centroid of the virtual rigid body to the centroid of rotation. The data is measured separately across all three axes of rotation, and is aligned through the MATLAB code to the cage axis, as such shares the same cage coordinate system so that  $X, Y, Z = X, Y, Z$ . The magnitude of the measured values separated by axis informs on the degree of deviation from the centroid. As expected, the X and Y values are similar though out of phase as would suggest a rotation within the XY plane, and the slight discrepancy in median value would suggest that the centroid of the rigid body is shifted slightly from the centroid of rotation. In addition, the discrepancy nearing the 3000 elapsed second period would suggest a bump or external perturbation which was not expected. Like the magnetic field measurement data, the deviation from centroid data is not specifically focused on the magnitude of the values, but on the cyclical nature of the values. Complimenting the data obtained from the MAI-401 ADACS B-Field telemetry,

values of all three axis are sinusoidal in nature, with peak-to-peak elapsed time periods growing longer as time progresses suggesting a decreasing speed of rotation.

When taking the derivative of the offset data with respect to time in each axis, a plot of linear velocity can be produced as in Figure 23;

$$\frac{dl}{dt} = \frac{\text{Change in offset distance}}{\text{Change in time}} \quad (13)$$

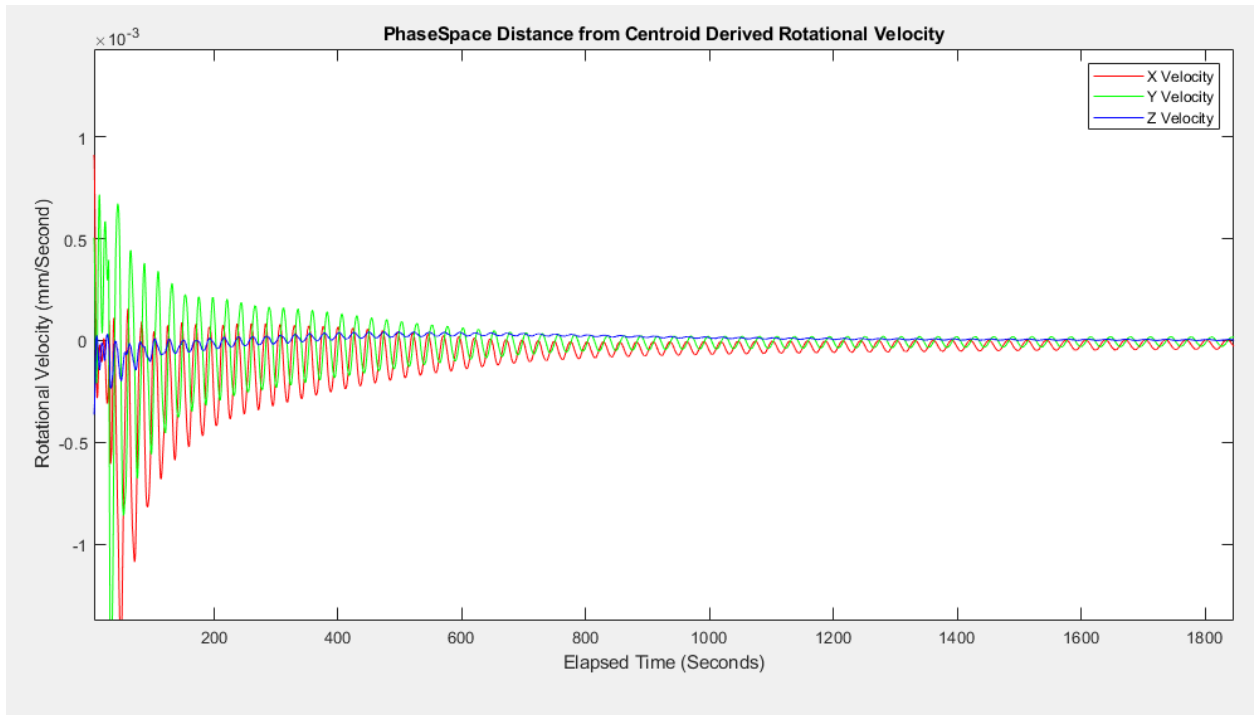


Figure 23 – PhaseSpace Derived Linear Velocity from Centroid Measurements

Supporting the assertions from the magnetic field data, the time derivative of the centroid offset data reveals that the velocity values of the spacecraft within the test scenario also decrease as time progresses. While making assumptions on rotational systems from inferences on data and plots describing linear measurements is a potentially poor choice, it can be beneficial. In a linear system one would assume that constant motion of an

object would be visible as a straight line in a distance vs. time plot, which when viewing solely the maximum values of the data in Figure 22 would largely agree. Similarly, when applying a reduction or friction force to an object, the plot of velocity vs. time would decrease as time moves right as which is supported when viewing the maximum values of each axis in Figure 23. Due to the rotational nature of the system, the velocity with respect to each axis is at the maximum values where the plot trends support the assumptions specifically because the velocity component vectors are at 0 and 90 degrees to the axis of rotation. As the rotation continues and deviates away from 90 degrees the assumptions become less accurate. It is then suggested that the cartesian coordinates and measurements be transformed into spherical coordinates for ease of understanding and analysis.

The process of transforming cartesian coordinates (X, Y, Z) as measured by the PhaseSpace camera system to Spherical Coordinates (r, theta, phi) is a trigonometric problem resulting in the formation of three entwined components. The resultant components become; r, the radius from the centroid,  $\theta$ , angle of rotation in the XY plane, and  $\phi$ , the angle off the +Z axis. The three spherical components are calculated from the X, Y, Z values as:

$$r = \sqrt{X^2 + Y^2 + Z^2} \quad (14)$$

$$\theta = \tan^{-1}\left(\frac{Y}{X}\right) \quad (15)$$

$$\phi = \left(\frac{\sqrt{X^2 + Y^2}}{Z}\right) \quad (16)$$

Plotting the measured values of the PhaseSpace camera system as transformed into spherical coordinates shown in Figure 24 can provide a few clarifying data points.

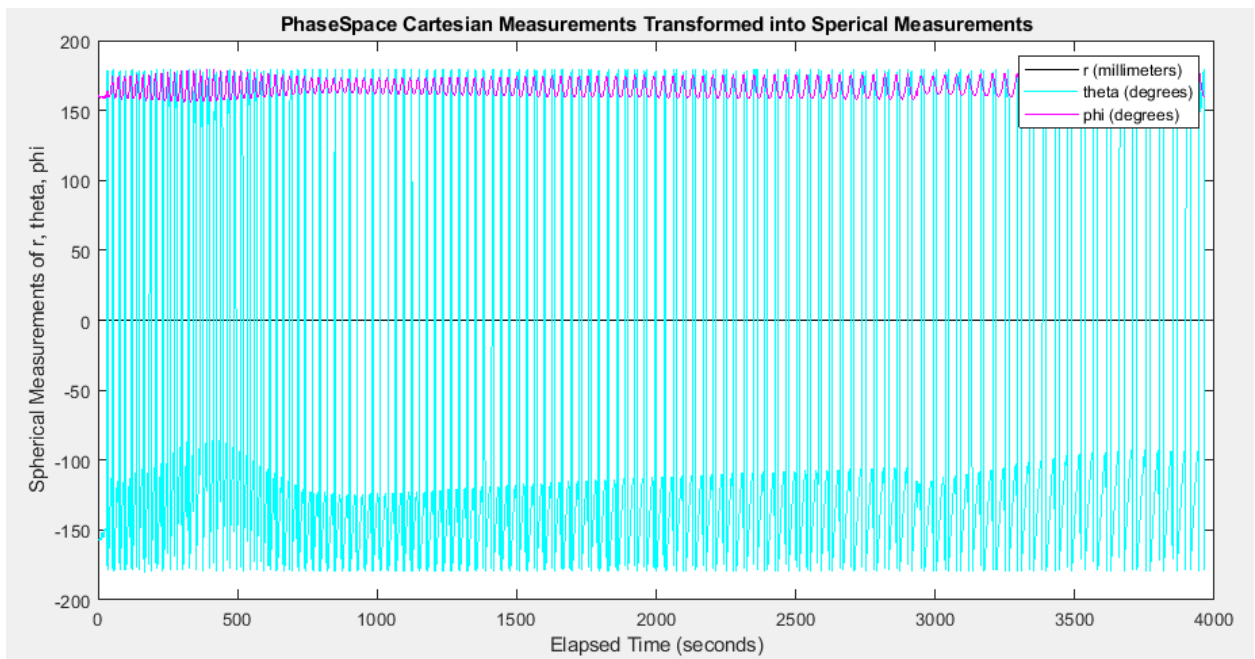


Figure 24 - PhaseSpace Measured Motion in Spherical Representation

The values of r across the plot shown by the solid black line and hold steady across the entirety of the plot as expected. The relatively static values suggest that the radial distance from the centroid of the virtual rigid body to the centroid of rotation is stable, confirming that the chassis is not translating on the air bearing, and that the measured data is correct.

The values of  $\theta$  shown in cyan are cyclical as expected with magnitudes between -180 and 180 degrees verifying that the chassis is in fact rotating through a full 360-degree rotation. The values across the plot between -90 and -180 degrees show what looks like an additional mode or inconsistency syncing with changes in the phi values. Due to the origination of the data coming from linear measurements, this inconsistency may be attributed to the addition or subtraction of distance of travel across the XY plane as induced by the perturbation component in the Z direction.

The  $\phi$  data as shown in magenta invites a degree of interpretation which may be dependent upon assumptions. As viewed the values are of sinusoidal nature and consistent with prior data analysis, with the magnitude ranging from roughly 150 to 180 degrees and symmetrical about the median. The magnitude of values varies along the curve as could be attributed by a rotating system that was out of balance. The range of values suggests a total deviation from the XY plane of approximately 30 degrees, or 15 degrees in both the positive and negative directions, which is consistent with the maximum usable range inherent to the air bearing mechanism. The offset of the median value of the curve from 0 degrees expected to the approximately 165 degrees derived suggests a potential error in calculation or understanding of coordinate frame but may also be attributed to the view angle of the chassis from the XY plane of the camera system. A combination of the former and latter is likely the culprit as the camera system is mounted approximately 1 meter above the chassis resulting in a large look angle,



though it would presumably be a negative value as the camera system is looking down on the chassis.

Regarding both the  $\theta$  and  $\phi$  curves, the plot values and trends coincide with the prior analysis of the B-Field measurements as well as the data obtained from the cartesian centroid offset measurements. The trend of the spherical measurements follows the cyclical nature with time splits between peaks increasing as time progresses, again reasserting the assumption that this is indeed a slowing nature applied to the rotation of the spacecraft. As with the previous data sets it is beneficial to take the time derivative of the motion data and in this case with respect to the spherical coordinate data.

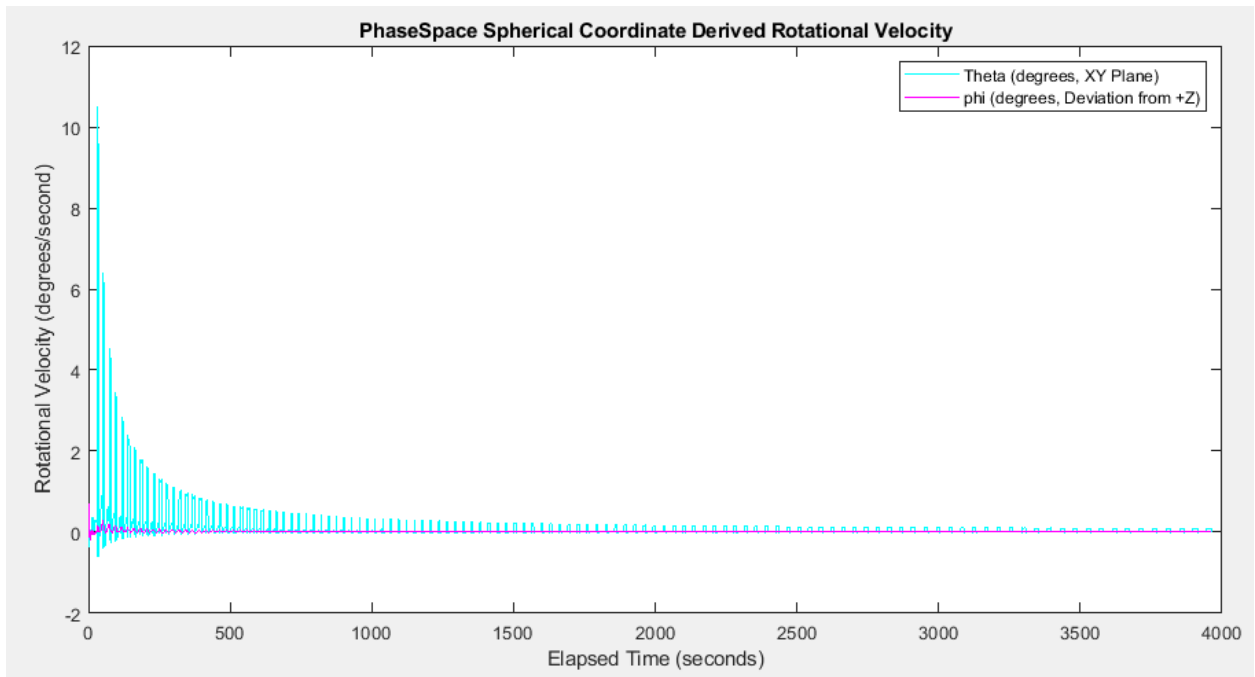


Figure 25 – PhaseSpace Derived Rotational Velocity in Spherical Representation

Figure 25 plots the time derivative of the motion capture data as represented in spherical coordinates with the rotational velocity on the Y axis of the plot in degrees per seconds, and elapsed time on the X-axis recorded in seconds. What is shown as three differing measurement values in the plot of the original data is simplified down to only two data sets for this plot, as the time derivative of the change in distance between the rotational centroid and the centroid of the virtual rigid body is zero when looking at a static measurement. The resultant is a plot of the change in  $\theta$ , the degree of rotation within the XY plane, and the change in  $\phi$ , the degree of rotation from the Z-axis, per change in time.

$$\frac{d\theta}{dt} = \frac{\text{angular change in XY plane (degrees)}}{\text{change in time (seconds)}} \quad (17)$$

$$\frac{d\phi}{dt} = \frac{\text{angular change of Z axis (degrees)}}{\text{change in time (seconds)}} \quad (18)$$

Both variables  $\theta$  and  $\phi$  form a sinusoidal pattern representing the rotational nature as expected, and both initialize at a large magnitude and decrease to a relatively stable equilibrium value as time progresses. Due to the perturbation force being applied primarily in the XY plane the magnitude of the values measured of  $\theta$  are much larger than those of  $\phi$ . The values of both sets trend downward, signifying a slowing in the rotational rate of the spacecraft across all axes. In addition, a trend like that seen in the preceding plots is continued whereas the rate of change becomes less significant as time progresses.

### 4.3 Bias and Gains

As with any data analysis task, an understanding of the general narrative of the data can be performed with relative ease and speed, but an understanding of the nuances which are essential to the truth of the data set require a much more exhaustive and robust approach. While the test data does in-fact support the ADACS unit performance, there exist a host of nuances understood from the data which not only deserve investigation, but that may change the initial understanding of the data. One such nuance can be viewed when looking more closely at the plots of the magnetic field data obtained from the MAI-401 ADACS telemetry. When backing out and viewing the entirety of the data run from Figure 19, there is a significant visible trend in all three axis that leads to the belief that the measured telemetry data is requires additional investigation.

The trend, though apparent in all three axes can be showcased by looking at a single axis, such as the Z-axis is this case. The data for the measured B-Field sourced directly from the ADACS telemetry follow the same visual trending of both the desired and truth values, but a variability in magnitude of the measured data is significantly larger than that of the truth data. In addition to the increase in magnitude, the data is also offset from the midline of the desired values in the negative direction for the x-axis data. The variation in magnitude and the offset of the data being apparent in all axes, constant through the entire data collect, and visible in all test scenarios, leads to the belief that the variation is not an anomaly. Additionally, the variation is likely due to two separate causes. It is speculated that the cause of the increased magnitude of the measured data likely stems from the addition of noise in the system which could be attributed to an electro-magnetic

source onboard the test unit. The offset of the data can likely be attributed to poor calibration of the test setup.

Locating the source of the noise began with a test to understand better the impact of the magnetorquers. If the noise is due to the application of magnetic dipole moment resulting from the current applied to the magnetorquers to adjust attitude, then the noise cannot be removed unless the usage of the magnetorquers is discontinued. To test this hypothesis, it was decided to disable the magnetorquers built-in to the ADACS, and a command was sent transitioning the ADACS into Test Mode. As was expected from Test Mode, telemetry verified that there was no current being sent to the magnetorquers, and a test scenario was run. In addition to running this test in Test Mode, the Helmholtz Cage was set to a stationary B-Field such that the variation of the measured data could not be attributed to the performance of the cage itself. The goal of this test was to investigate if the magnetorquers were in fact the source of the noise. The data shown in Figure 26 verifies that even with no current to the magnetorquers, the noise was still present though now at a reduced level.

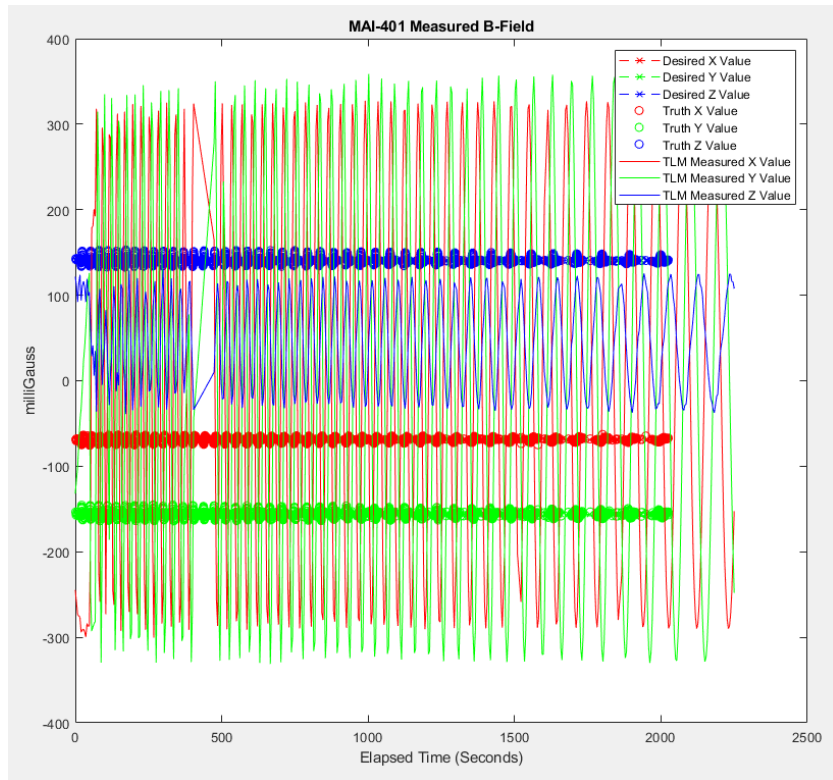


Figure 26 – Magnetic Field Data in Test Mode with no current to magnetorquers

With the magnetorquers contributing only a partial source of the noise as the magnitude of the values was decreased by approximately half, a continuance in the investigation of noise was warranted. The investigation shifted then to assess the calibration of the test setup and the ADACS itself. Calibration of the test setup would be focused on the values measured by the truth magnetometers, while calibration of the ADACS would look at the synchronicity of the values between the measured telemetry from the onboard sensors and that of the truth magnetometers. Variable bias and gain settings built-in to the MAI-401 ADACS software allows for the tuning of the internal bias and gain values to overcome internal variations and achieve measurements consistent with truth values.

At this time, the ADACS unit was extracted from the chassis to perform additional testing not related to the performance metrics in this study. The calibration of the ADACS unit itself would have a far greater effect if still contained within the chassis so to perform the inherent operations within a flight-like condition and encountering all electro-magnetic effects of the full build. Though not permitted due to the additional outside demand for study, the data obtained through the calibration of the ADACS as the sole system is still pertinent and will be applied to the test data in a post-processing manor, albeit with the efficacy likely reduced. Additionally, the ADACS will be forced to be commanded from and retrieve telemetry from a separate source, Aspire Studios, since the connection to the C&DH system within the chassis was terminated when the ADACS unit was extracted. Aspire Studios while providing a similar service does deviate in areas such as data types and scaling factors from the AFIT flight software, such that additional attention to the data types referenced within the MAI-401 User Manual must be carefully maintained.

To calibrate the truth magnetometers the estimated values of Earth's magnetic field at the latitude, longitude, and elevation of AFIT on the date of the test was required. The estimated values were sourced from the National Geophysical Data Center (NGDC) Magnetic Field Calculator [29] for the following inputs;

AFIT Latitude: 39.783878° N  
AFIT Longitude: 84.08379° W  
AFIT Elevation: 800.0 ft Mean Sea Level

Once the estimated values for AFIT specific location were obtained and converted from the native nano-tesla values of the calculator to milli-gauss, the truth magnetometer milli-gauss meter could be then be calibrated to the estimated values. The estimated values were very similar in magnitude to the current readings of the milli-gauss meter such that very little tuning was required. The similarity suggests that the calibration of the milli-gauss meter was very likely within realistic error for the prior tests.

With the truth magnetometer calibrated to the estimated magnetic field at AFIT as the base values, the next calibration would be tuning the ADACS magnetometers to the truth magnetometers. To set the initial point, the Helmholtz Cage was driven to [X, Y, Z] values of [0, 0, 0] as measured by the truth magnetometer. Once equilibrium was maintained, the measured B-field telemetry values of each axis were recorded with the median values of.

$$[X, Y, Z] = [1190, 800, 509]$$

These values correspond to an offset from the ADACS measured B-field to the truth magnetometer measured values, and as such can be viewed as a bias in measurement. From the MAI User Manual, bias values are added to the measured values by using the command SetMagBias, which reads in user values and converts them to bias with the following.

$$\text{Magnetic Field (uT)} = [\text{Mag Output (lsb)} + \text{Mag Bias (lsb)}] * \text{Mag Gain} * 0.032 \text{ uT/lsb}$$

[27]

From the knowledge of how MAI intends to use the bias values, the values obtained from the telemetry in lsb can then be converted into a form usable for analysis such as milli-gauss and applied to the test data as post-processing. It is known in this case that lsb refers to “least significant bit” and the resultant values are in micro-tesla, so the conversion is straight-forward.

With the initial bias known, the gain settings could then be found. Each primary axis of the Helmholtz cage was individually increased to a value of 1000 milli-gauss with respect to the calibrated truth magnetometer. The measured values of the magnetic field obtained from the ADACS telemetry with respect to the corresponding axis were subsequently found. In all three axes, the measured values of the magnetic field exceeded the truth values by approximately 30 to 40 percent. With the bias having been previously found with its application directed by the ADACS User Manual, the same process shall be followed while deriving the gain scaling factors.

$$\text{Magnetic Field (uT)} = [\text{Mag Output (lsb)} + \text{Mag Bias (lsb)}] * \text{Mag Gain} * 0.032 \text{ uT/lsb} \\ [27]$$

As with the bias, the telemetry values obtained through the Aspire Studios GUI used to calculate the gain are also measured in lsb and micro-tesla and as such also need to be converted. The calculated gain scaling factors found for each respective axis were thus found to be;

$$[X, Y, Z] = [.75, -.708, .682]$$



For each case, both bias and gain, the values found were relayed in the ADACS frame of reference requiring a coordinate transformation into the cage frame for consistency when plotting the data. Also of note is the negative value of the gain in the Y position, a product of the variation in coordinate frames.

To test the efficacy of the empirically determined bias and gain values, the values were first applied to the Test Mode scenario data using the above referenced equation shared by both the SetMagBias and SetMagGain commands in Equation 18. Applying the bias and gains first to the Test Mode scenario where the current being applied to the magnetorquers was verified to be zero would likely produce the lowest noise values of all test scenarios due to the removal of the induced magnetorquer B-field. The plot of the data with the applied bias and gain as shown in Figure 27 can then be compared to Figure 26 to assess any benefit from the bias and gain. From the study of the comparative data, the bias values did in fact shift the median values of each axis, with the Y and Z data sets shifting as expected towards the measured truth values. The shift towards the truth values suggests that the assumptions and operations performed to mitigate the bias were sound. When looking solely at the X axis data the median of the telemetry shifts farther away from the truth values in an unexpected occurrence, to which an explanation is not readily available. Furthermore, when looking at the range of the magnitude of telemetry values it is apparent that the range is decreasing with the application of the gain factors as expected from the calibration process.

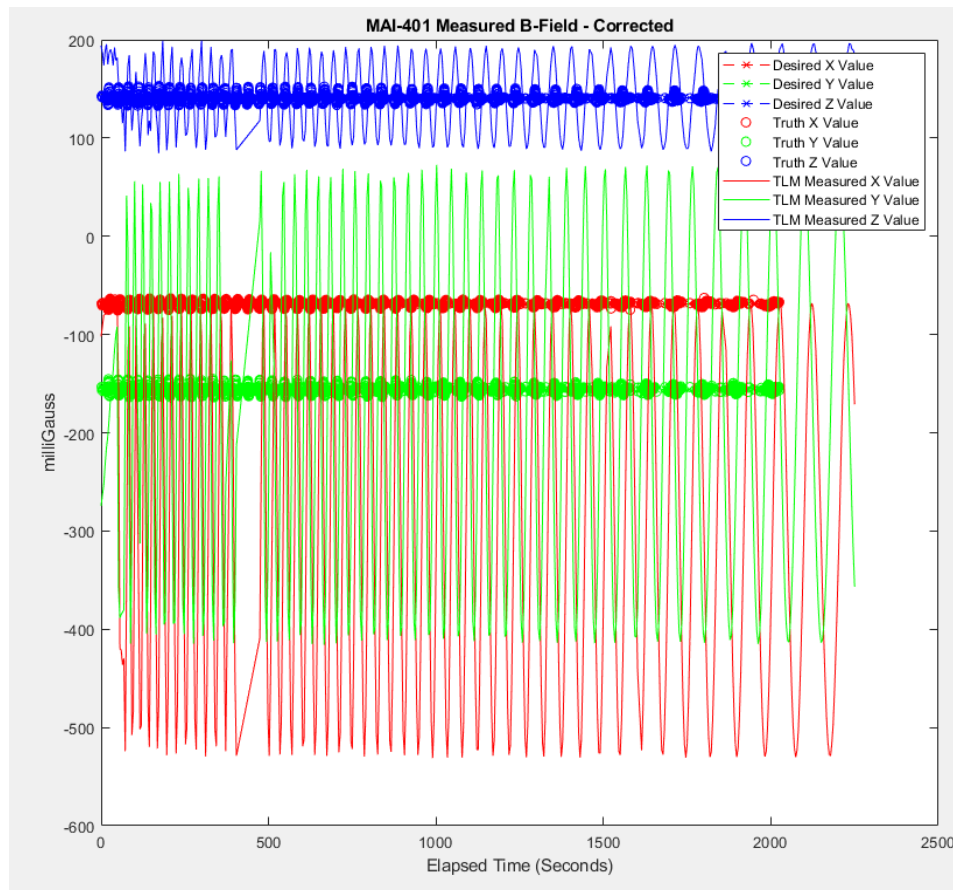


Figure 27 – MAI-401 Magnetic Field Telemetry Corrected for Bias and Gain

The determination of the bias and gain values leveraging the Test Mode scenario data follows the process MAI describes in the User Manual. The application of the bias succeeded in aligning the offset values of the measured values in two of three axes. A reduction in noise across all three axes is also attributed to the application of the gain scaling. Noting the success of the bias and gain on the Test Mode data, it is suggested to apply the same bias and gain values as a post-process to the original test data. Figure 28 plots the corrected or altered values of the original magnetic field obtained from the ADACS telemetry after applying the bias and gain values determined above. When

compared against the original data shown in Figure 19 the benefits do not meet with expectations. While the level of noise across each axis does decrease to by a significant degree signifying a benefit from the application of the gain, the offset of the median of ADACS telemetry data departs even more-so in the X-axis than the test case, and completely unexpectedly in the Y-axis. This trend of deviation away from the Test Mode scenario occurs in every tested orbital scenario. The commonality of the deviation suggests that not only would the bias and gain determination work have been better suited with the ADACS mounted within the chassis in a full-build configuration, but also that determining the bias and gains with the magnetorquers unpowered likely led to an errant understanding of the bias values specifically.

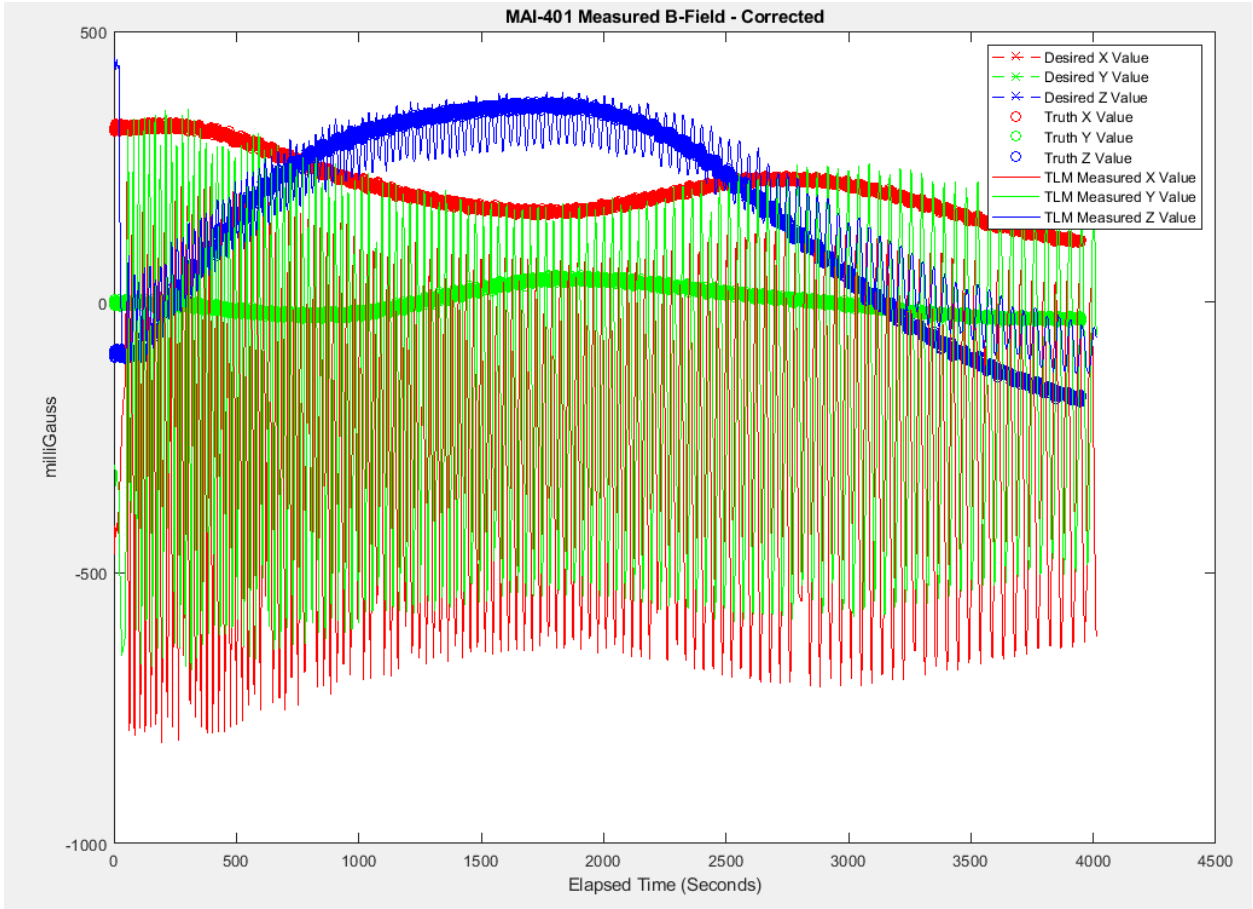


Figure 28 – Bias and Gain altered B-Field Data for simulated 450 KM Orbital Altitude at 50 degrees inclination

#### 4.4 Conclusion of Test Results

The data collected from each separate orbital scenario all point to the same overall conclusion when analyzing the raw and time derivative data from both the ADACS telemetry and the PhaseSpace Motion Camera system; that the MAI-401 ADACS does in-fact support a detumble operation. For all cases, the spacecraft yielded an equilibrium rotational rate of less than 0.5 degrees per second per axis occurring in a time frame of less than 30 minutes, both of which fall within reasonable performance requirements.

While the detumble operation did not in any case result in a completely stationary hold

position, this was not necessarily a requirement or seen as a detriment and can be further managed by altering default settings such as rotisserie rate within the ADACS configuration.

This information while helpful must be qualified as it has been collected on a generically built 6U CubeSat bus. Due to the generic build, specific configuration items such as payloads which are in most cases limited to singular missions have not been accounted for. By testing performance metrics of components on a generic build with intent to apply the gained knowledge to Mission specific builds, one must pay special attention to what has and has not been accounted for to not overvalue the essence of the data.

Purpose-built Mission-specific spacecraft may deviate from the generic build in multiple areas such as total mass, center of mass, moment of inertia, internal magnetic characteristics, and others all of which would greatly influence the performance characteristics of the ADACS unit. It is due to this that the generic chassis must follow strict adherence to the test plan to create a truly comparative analysis of each available ADACS unit. Simultaneously the test team must understand and deliver to the Mission team that the data collected and analyzed is only representative of the ability of the ADACS as tested and will vary based on their specific Mission configurations.

The intent of this research remains to understand the performance measures of the commercially available CubeSat specific ADACS units available on the market. More specifically the root questions become;

- 1) Will the ADACS perform to the marketed specifications when operated as a functional spacecraft and subjected to flight-like environments?
- 2) Does the performance and operation of the ADACS unit as tested lend itself to specific Mission sets based on the acquired data?

Subjecting the test article to the prescribed test procedure outlined both in the Methodology of Chapter III and more specifically in Test Plan included in Appendix A. provides the framework to answer question one above. The Test Plan lays out test setup including hardware, software, data points for active simulations, operations, usage, and how to draw out the required data for analysis. The analysis then leads the test team to the facts of performance which can be used as the basis for comparative analysis. As a generality this question is simple in the understanding that measurements and facts are exactly what they are.

What becomes difficult is understanding and answering question two, what Mission set is the tested ADACS unit best prepared to handle? This question is the bane of the Engineer and analogous to the question of “Which is better?”. Understanding the physical properties of the system may in fact qualify or disqualify a unit from specific Missions, but the physical properties alone do not tell the entire story. Commanding and operating a spacecraft from hundreds of kilometers away is a difficult task. This task is made even more difficult by any number of Mission influences such as orbital parameters, eclipse cycle, ground station locations, time of day, or power system charge level. Beyond the external complications comes the internal connections, interfacing, and interrelated activity by combinations of the Electrical Power System, Command & Data

Handling System, Telemetry, Tracking & Control System, ADACS, Thermal Control System, and the addition of payloads.

From this understanding comes two fundamentally differing approaches by which the ADACS manufacturer can allow a user to interact with the ADACS system. One approach provides a “Black Box” system in which the user cannot easily see the inner workings of the ADACS, separated from how the determination and control functions perform, and given only enough information and options for commands to provide a specified level of Attitude Determination and Control. Black Box offerings may provide robust operations within a specified number of available operations, and if the Mission requirements fall within those bounds, then a Black Box solution may be preferred. Conversely, if Mission requirements fall outside of the normal operations available to the specific Black Box solution, then the team must either find a work-around or alter the Mission plan.

The second approach, referred to as the “Open-Source” approach is quite opposite, providing the user direct access to the inner workings of the ADACS with the assumption that more options may be more beneficial, but with the inevitable warning of any changes the user makes after taking ownership becomes the owner’s problem. Open-Source offerings provide the user with a plethora of options and possibilities when it comes to tailoring the solution to specific Mission needs, which can be extremely beneficial in a research oriented program working to develop new and novel operations and test cases in Space. Alternatively, for a University team with high turnover rate and a relatively low-

level understanding of the intricate settings and operations, an open source solution may prove too complex or time intensive for the simpler Missions.

As for the definitive answer of how to determine which Mission each ADACS is better suited to perform, this becomes the inherent problem with recommendations....the answer will likely depend heavily on a variety of factors. The test team's understanding of the test unit, comfort level with intricacies of ADACS operations and internal configurations, code changes, commanding capabilities, and knowledge of both the Mission profile as well as the capability level of the Mission and Operations Team. In any case, it is imperative to understand the Mission requirements on multiple levels before making a down-selection of an ADACS unit for any specified Mission set.

## **V. Conclusion**

### **5.1 Summary**

As AFIT continues to expand its CubeSat program into more units with varying Missions, the focus of this research becomes increasingly important. Testing and characterizing CubeSat ADACS units for performance and application to specific Mission sets such as RPO is crucial to the Development Team's ability to make informed choices. From increased levels of detail on performance and operational capability the Mission profile can be selectively matched to a specified ADACS cutting down on the required resource demand and gaining components best suited for the proper application. The total performance characterization of the MAI-401 ADACS unit as intended in Chapter I was unsuccessful, though a portion of the test requirements were achieved



through the Detumble test, garnering sufficient data to provide a narrative on the test campaign.

Formulation of the test plan was facilitated by the knowledge gained as referenced in Chapter II, and the test methodology outlined in Chapter III. Chapter II investigated multiple facets of spacecraft operational life including the space environment, attitude determination and control algorithms, sensors, actuators, CubeSat configurations, reference frames, as well as a looking to prior Missions for guidance. Chapter III provided the justification for the testing, the basis of the performance evaluation, and explained the test setup with regards to providing a simulated space environment as achieved on Earth. Chapter III also includes a section on limitations which aids in qualifying the ability to extend the results of the test to future Mission performance.

The results and analysis from the test campaign are discussed in Chapter IV. While the full analysis and characterization of the ADACS was not able to be performed due to recurring errors when transitioning ADACS modes of operation, the detumble analysis was available for evaluation. The detumble analysis is broken down into two specific areas, the first which investigates the rotational data with respect to the measured magnetic fields, and the second which investigates the physical motion of the chassis. From the data and the subsequent time-derivatives, the performance of the ADACS is understood as it relates to the test chassis, proving from both analytical data sets that a suitable detumble operation in the simulated space environment was successful. In addition, the data provides a deeper understanding of the test setup as well as the

performance of the test plan. Recommended modifications to both the test setup and plan are discussed to provide not only enhanced and less noisy data, but a more standardized test procedure aiding in comparatives with subsequent tests.

## **5.2 Conclusion**

Limited by the inability to change ADACS modes of operation, the Detumble test became the central point of the test campaign from which conclusions about both the capabilities of the tested ADACS unit in the current configuration as well as the suitability of the test plan could be made. Direct observations of each test case for the varying orbital altitudes provided the understanding that the chassis was in-fact stabilizing over time within the magnetic field as supplied by the Helmholtz Cage in all three axes, performing the detumble operation as expected.

Measured data from the truth magnetometer when overlaid with the desired magnetic field of the cage supports that the performance of the Helmholtz Cage is sufficient to the complete the test scenarios. Further investigation into noisy data did result in the re-calibration of the truth magnetometer, though the adjustments made to the base level readings of the milli-Gauss meter were of insignificant values such that the truth magnetometer readings are recognized as reliable.

An additional test case was added to ensure that the forces imparted on the spacecraft due to Earth's gravitational field were not the primary cause of the detumble. With the current applied to the ADACS internal magnetorquers set to 0 amperes as verified by the

ADACS telemetry, the rate of deceleration of the chassis could be attributed solely to the effects of gravity and related friction. Data then analyzed from both the magnetic field and motion capture cameras system supported the presumption that the frictional forces are of a negligible value in all three axes, thus supporting the detumble conclusion.

Conclusions on the rate of detumble with respect to the variation in magnetic field as the orbital altitude increases are not conclusive. Due to the decrease in strength of Earth's magnetic field as distance from the Earth increases, the predicted rate of detumble if reliant upon magnetic dipole moment of magnetorquers as with the MAI-401, would decrease. Stated in a more concise manor, as orbital altitude increases so too does the time it takes to detumble from specified rotational rate. Due to inconsistencies in the initial application of the perturbation force simulating ejection from the deployment cannister, the time and rate of detumble could not be satisfactorily compared. This inconclusivity is further discussed in recommendations for future development.

Detumble is synonymous with and in many cases is referred to as rate nulling, such that the goal of the process overall is to reduce or null the rotational rate of the chassis in each axis. While the assumption may be that the rate nulling is completed when the chassis has reached a static hold in all three axes, the configuration, settings, and logic of the ADACS software is what ultimately controls the final motion of the chassis. In the case the two ADACS investigated for this research the rate nulling is essentially over-ridden once a threshold values is reached at which time the software begins performing a Sun Search operation to locate the Sun and then drive the solar panel face to a Sun pointing

attitude. Each ADACS performs the Sun search differently, and the rate and pattern to how the Sun is located can be configured in the settings. In the specific operation of the MAI-401 during this test campaign the chassis never came to a full static position. After investigating further into the operation of the Detumble and Sun Safe modes it was found that the ADACS will drive a default rotisserie rate until the Sun is located at which time the configured solar panel face is aligned with the Sun vector. A secondary look at the ADACS telemetry showed that the eclipse flag was in a state of constant flux with the assumption that the Sun simulator lamp was too close to the face of the chassis. Due to the rotation the chassis corner would block the next sensors causing a few second eclipse followed by a few second illuminated phase. To alleviate this problem a secondary sensor such as a gyroscope or magnetometer could be used to continue the rate nulling to a zero, or a change the Sun simulator could be made.

Finally, this test campaign and research points to the need for modifications to the test plan and test setup to enhance the standardization and basis for comparison, as well as a new requirement that a full software package including operational checkout has been completed before testing shall commence in the future. The recommendation is that the testing and analysis of performance completed on the MAI-401 as referenced in this research be used solely as a test-plan dry-run and operational checkout, and that the MAI-401 be tested again once the recommend modifications have been added. Once the recommendations have been integrated, the test plan shall provide for the standardized test and characterization of any commercially available CubeSat-specific ADACS unit

available with the ability to provide recommendations for use in specific Missions based on performance criteria as was the initial intent of this research.

### **5.3 Recommendations for Future development**

As this is the first available ADACS to be tested in this chassis configuration, in this test setup, and following this specific test plan, the comparative analysis is not necessarily a valid mindset when describing the performance. This notion, along with various other observations and assumptions throughout the testing process encourage the evolution of the current test plan to perform more as a stand-alone hard-measurement test where the results of the test provide numerical values more applicable to day-to-day engineering decision discussions. It is from these ideas that this section, Recommendations for Test Changes, has developed.

#### *Test Setup Calibration*

With any test setup, the test data is only as good as the calibration of the test system. In the case of this set of tests the initial calibration of the system was not performed as the data was not necessarily taken with respect to any specific known baseline but used as a comparison against itself in a relative sense. While this methodology works when limited to a single test campaign, the overall goal is to provide a comparative analysis for multiple ADACS units over what could amount to years between tests. As such, the entire test setup shall be completely calibrated before beginning testing for all future tests providing a common baseline for a true comparison. In addition, the test calibration shall

be performed with the test unit built into a standard test configuration outlined in the Test Plan. By following the specified plan, the results will not be skewed by factors emanating from changes in the configuration.

#### *ADACS Setup and Developing Bias and Gain Values*

For each ADACS unit, the tools provided by the manufacturer to operate in both the hardware and software domain must be fully understood to maximize performance and understand the true capability of the offering. Testing a unit without first performing one's due diligence in learning the tools available will likely skew the results of any test procedure. Not only is it imperative to calibrate the Test Setup within which the ADACS is operating, but also imperative to use the tools available to calibrate the ADACS and its integral components to the test setup as well. In many cases, and as found with the MAI-401, values observed within the calibration process can then be applied to the configuration of the ADACS, promoting a continued increase in performance. This concept is demonstrated with when understanding at the Bias and Gain settings of the MAI-401. The Bias and Gain values are developed within the calibration process, incorporated into the system configuration, and are then applied to the measured values such that the telemetry output is augmented to produce enhanced values. Acquiring the maximum potential performance from the ADACS requires more than proper setup and calibration, but also in-depth knowledge of the test unit calibration process, and how to maximize performance using the provided settings intrinsic to the ADACS and shall be incorporated into the initial setup process of the test plan moving forward.

### *Understanding Gravitational and Frictional Forces*

The measured data obtained from running the test procedure with the MAI-401 ADACS in Test Mode provided additional understanding which led to the requirement of additional data required for improved analysis. In Test Mode, the ADACS provides no current to the magnetorquers verified by the telemetry, and which are the only active component attempting to null the rate of rotation. With no active control of the spacecraft, the resulting data still showed a slowing of the rotational rate in all three axes. The uncontrolled slowing is likely the result of both gravitational damping specifically in the Z axis, and frictional slowing in the rotation within the XY plane. Testing the rotational characteristics in Test Mode after calibration and before performing operational test scenarios shall provide the ability to understand the gravitational and frictional forces acting upon the chassis. The baseline external forces can then be removed from the measured data during the data analysis process resulting in the performance metrics being attributed solely to the ADACS.

### *Initial Perturbance Force*

Comparative analysis between multiple units requires a strict adherence to the test process to ensure that each test unit is subjected to the same variables. What was initially assumed in the original test plan was that the initial perturbation force applied to the chassis to simulate ejection from the canister would be easily measured, providing for the ability to compare performance of the detumble operation with regards to the initial rotational velocity. The data analysis proved this assumption to be incorrect as the immediate decrease in rotational velocity prevents the ability to get a repeated

measurement as a method to verify the initial conditions. Without a verified initial measurement of the rotational velocity, it is difficult to assess if the ADACS does in fact perform to the required performance metrics. In addition, due to the polynomial nature of the detumble velocity reduction, the determination of how well the detumble works as a comparative measure is reliant upon the initial conditions. To combat this unknown and further standardize the test process it is suggested that each test case be subjected to the same initial rotational rate to simplify analysis. The process by which this solution can be implemented is likely an issue and may be offered as a follow-on tasking.

#### *Test Chassis Modifications*

The data accumulated from each test scenario is based on how well the ADACS performs within the test chassis, from which conclusions can be made moving forward as to how the ADACS will perform on a Mission chassis with physical properties likely much different. From this understanding it would be beneficial to develop a test chassis at the upper limits of the acceptable range of physical properties, in essence providing a worst-case scenario. By testing on what would be assumed as a worst-case scenario, the data that is then applied to the Mission configurations would in almost all cases provide an increase in performance over the test case. The current configuration provides a test case that is likely smaller in mass than the Mission spacecraft it is providing data to, and thus the performance metrics derived from the test case are less conservative than that of the Mission. With the current arrangement the Mission Team must be aware in all cases that the performance of the test unit is likely an overestimation of the performance as applied



to the Mission platform and must make careful assumptions about expected Mission performance.

#### *Increased Understanding of Telemetry Values and Modes of Operation*

Of the items that plagued the ease of testing and analysis of this research, the most problematic of all was the inability to retrieve certain telemetry streams from the ADACS dependent upon chosen mode of operation. As referenced in the introduction to Chapter IV, the inability to transition to Mission modes left the ADACS in Acquisition mode for the detumble tests. For an unknown reason, the MAI-401 limits the telemetry outputs gathered while in Acquisition mode, limiting the knowledge of the user. The specific telemetry point that would have been extremely beneficial to the analysis of the rotational data of the test is that of the body rate measurements. In Acquisition Mode the spacecraft is rate nulling using magnetorquers as the control function and rate of change of the magnetometers as the determination function [27]. Due to this setup, the 3-axis MEMS accelerometer / gyroscope is left unpowered, and this cannot measure or provide data to the telemetry flow. Limitations of system characteristics such as this prevent the test team from truly understanding total system performance in all states and modes but does provide the opportunity to learn and pass on information to the Mission and Operation teams down the line.

## **Appendix A. Test Plan**

### **CubeSat Attitude Determination and Control System (ADACS) Characterization and Testing for Rendezvous and Proximity Operations (RPO)**

**Captain Steven Bednarski**

**Test Plan**

## Table of Contents

1. Introduction .....	110
1.1 Purpose .....	110
1.2 Scope .....	110
1.3 Limitations .....	112
1.4 Objectives .....	<b>Error! Bookmark not defined.</b>
2. Resource Requirements .....	113
2.1 Facilities .....	<b>Error! Bookmark not defined.</b>
2.2 Personnel .....	114
2.3 Documentation.....	114
2.4 Material/Equipment/Software Requirements .....	115
3. Test Configuration .....	116
4. Test Procedure.....	122

## **I. Introduction**

### **1.1 Purpose**

The continued growth of the CubeSat mission areas as well as component availability leads to an increased flexibility afforded to spacecraft developers. Flexibility consumes resources as each option must be carefully assessed against all other options within the available pool. The goal is the development of a test plan broad inclusive enough to accommodate any market available ADACS offering, providing a standard data set by which each offering can be compared against for further analysis. The standard data set will aid in the component selection process and likely lead to reduced time and budgetary expenditures.

### **1.2 Scope**

There exist multitudes of specific data points and discrete nuances to each mission, though when opening the focus, the overall characterization of ADACS can be broken down into two specific areas: physical attributes, and operational performance.

Physical attributes while important to the overall development of the spacecraft will not be included. For this test, only CubeSat specific ADACS will be tested, and as a result both the size and mass limitations have already been set by the CubeSat form factor standardization. Power draw, another physical attribute will not be covered, as the development of the spacecraft Electrical and Power System (EPS) will take power as a design consideration.

Operational performance of an ADACS is further broken down into two categories, determination of the spacecraft attitude, and the control of the spacecraft attitude. Determination of the spacecraft attitude is largely a function of the sensors capturing data with respect to the surrounding environment and the determination algorithm employed. The determination is then fed into the control algorithm which will then process command requirements and deliver commands to the control components. It is the overall control performance which is critical to characterize and will be the focus of this test plan.

Of the missions investigated, the operational performance requirements common are listed in Table 1. In developing a standardized test plan as the concept of this test, the required objective and threshold values for each requirement based on mission is not indicated as the measured performance of each offering for comparison is the objective.

Table 4 - Operational Performance Requirements

Reference #	Name	Description
ADACS.1	Detumble Capability	ADACS shall automatically recover and stabilize from an externally induced torque .
ADACS.2	Pointing Knowledge	<del>ADACS shall provide current attitude estimates as telemetry.</del>
ADACS.3	Pointing Accuracy	ADACS shall provide spacecraft attitude control to a specified vector
ADACS.4	Slew Rate	ADACS shall provide spacecraft-controlled slewing.

#### ADACS.1

Detumble Capability is a requirement seen on the vast majority of spacecraft. When launched, or in the case of CubeSats ejected from the deploying mechanism, the addition of an external torque is often generated. This external torque when applied to the spacecraft creates added rotation to the spacecraft that may be measured across all three primary axes. The requirement is that the ADACS shall reduce the rotation of the spacecraft and stabilize into a pre-specified pointing or controlled rotational attitude. As detumble is the first required task of the spacecraft after deployment, this requirement earns a high priority. Deploying mechanisms provide not-to-exceed rates of rotation that spacecraft may be subject to, and for this test the maximum value will be set to 10 degrees/second/axis. An additional point of data to be measured for comparison is the rate at which the spacecraft performs the detumble operation.

#### ADACS.2

Pointing Knowledge is the requirement assessing the ADACS' ability to determine precise attitude within a known frame of reference, in most cases the celestial frame. This requirement falls squarely under the purview of spacecraft attitude determination. Pointing knowledge is an extremely important input to spacecraft control, but one which is very difficult to test within the confines of a laboratory environment. To fully assess the pointing knowledge of the spacecraft, the laboratory would need to setup a 100% true representation of the space environment including the placement of all celestial bodies and their mechanics such as the sun and star field, or provide simulated signals to the ADACS. Though signal simulation would indeed test the operation of the spacecraft determination, the control aspect would be limited as would the operation of the physical determination sensors. Due to this limitation, ADACS.2 Pointing Knowledge will not be tested specifically, and the performance of the ADACS determination will be assessed with respect to a local origination point, and as part of ADACS.3 Pointing Accuracy.

#### ADACS.3

Pointing Accuracy is the requirement that a ADACS control the attitude of spacecraft such that a specified spacecraft body frame, vector, or plane orient in the direction of a specified target vector within an external known frame. Typically pointing accuracy is referenced to the celestial frame, but as with Pointing Knowledge, the ability to create a perfect representation of the celestial field without signal simulation in the laboratory is not achievable within the physical and budgetary constraints. Testing Pointing Accuracy

will form the basis on the assumption that the spacecraft will be oriented to an origination point within a local frame. The accuracy will be assessed based on commanding within the local frame. When commanded to specific pointing or attitude parameters, all deviations whether sinusoidal variance, overshooting, bounce, or any other phenomena will be investigated during data analysis.

#### ADACS.4

Slew rate requires that the ADACS control the slewing action of the spacecraft, or in other words a deliberate rotational rate about a specified point. Slew rate can refer to a spacecraft being nadir pointing, sun pointing, or with respect to RPO missions following another spacecraft's signal. In each case the spacecraft will be required to continuously perform attitude adjustments at a set rate. Each ADACS offering likely has preset maximum slew rates, and performance at these rates will be tested.

### 1.3 Limitations

As described in the previous sections, the available test setup for characterizing ADACS operational performance precludes testing of certain test activities and asserts the reliance upon assumptions for others. With the selected limitations in mind, the goal of the test setup is still to create the most flight-like space-environment possible within the laboratory bounds. The remaining test requirements, setup and control will be scrutinized to deliver the highest quality data products and analysis possible.

### 1.4 Objectives

Test objectives in generality are characterized as pass/fail or successful/unsuccessful when based off strict mission specific requirements. In the case of this research it is not a specified value that is the goal, but an understanding of the capability of the ADACS offering itself and how it reacts in a simulated space environment and when applied to the 6U spacecraft on-hand. The ADACS offerings are specified to performance standards from the provider, though characterization in flight-like testing may show deviation from the performance standards. Hypothetically an ADACS may have the strongest Attitude Determination functionality on paper, but when combined with sub-par control system or undersized control components for the mass or inertial center of the spacecraft, the performance would surely suffer. It is precisely these types of situations which make flight-like testing a requirement.

Based on the current set of Operational Performance Requirements, the following test objectives shall be investigated with successes appropriate to satisfy requirement verification. Further explanation of each test will follow in the test configuration and setup sections.

Table 5 - Overview of ADACS Tests and Success Criteria

<b>Test</b>	<b>Test Name</b>	<b>Success Criteria</b>
<b>ADACS.1.Test</b>	Detumble Analysis	<b>Success:</b> When perturbed by an external torque the ADACS will minimize the disturbance forces on the spacecraft in a controlled manor leading culminating with stabilization <b>Failure:</b> ADACS fails to control external torques, or fails to control external torques within a sufficient period
<b>ADACS.3.Test</b>	Pointing Accuracy	<b>Success:</b> ADACS controls spacecraft attitude to reach a commanded point or vector <b>Failure:</b> ADACS fails to adjust attitude or reaches a predetermined time limit
<b>ADACS.4.Test</b>	Slew Rate	<b>Success:</b> ADACS controls the rate of rotation of the spacecraft to a specified limit <b>Failure:</b> ADACS allows for uncontrolled rotation of the spacecraft either above or below predetermined limits.

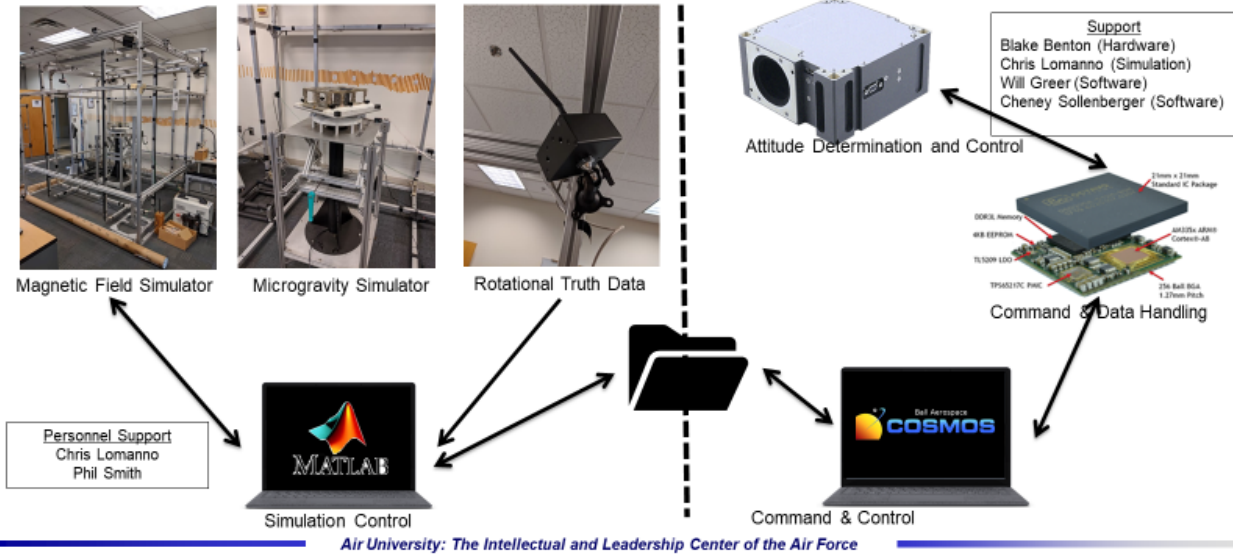
## II. Resource Requirements

### 2.1 Facilities

The Air Force Institute of Technology's (AFIT) Center for Space Research and Assurance (CSRA) occupies a variety of laboratory spaces on the AFIT campus with a multitude of test and experimentation setups. The testing referenced within this Test Plan will occur within the CSRA Mechanical Lab in room 103 of Building # 646 and will leverage the pre-existing experimental structures. To create the most flight-like environment for the ADACS, several modeling solutions will also be used in concert. A Helmholtz Cage will provide the magnetic environment estimated at an orbital altitude, an air bearing will provide a semi-unobstructed rotational capability in a simulated micro-gravity environment, solar illumination simulation will be achieved, as well as control of the ADACS. In addition to the test setup itself, access to a 6U CubeSat and required componentry will provide the basis the test case including access to the telemetry.



The AFIT of Today is the Air Force of Tomorrow.



Air University: The Intellectual and Leadership Center of the Air Force

Figure 29 – CSRA Mechanical Lab ADACS Test Setup Overview

## 2.2 Personnel

In addition to the laboratory apparatus and materials available from the CSRA, there are also personnel employed by the Center filling multiple roles across the engineering and software spectrum. The personnel have backgrounds in Mechanical, Electrical, and Systems Engineering, as well as Software Engineering, Design, and Development. As individuals and as a collective the personnel have provided an immense amount of support to the students in experimental design, setup, and performance.

## 2.3 Documentation

Documentation required to support the testing process will be categorized in two distinct categories, reference documents for the testing environment, and ADACS model specific reference documents for referred to as ADACS Specifications.



Table 6 – Reference Documentation

<b>Reference Category</b>	<b>Reference Document</b>
<b>Testing Environment</b>	Helmholtz Cage Users Guide v2.3 WIP (Work in Progress)
<b>Testing Environment</b>	Air Bearing Operation v1
<b>Testing Environment</b>	PhaseSpace Camera Users Guide
<b>Testing Environment</b>	ASYS 632 Lesson 10 – Commanding through COSMOS
<b>ADACS Specifications</b>	MAI-401 Mini ADACS (17 June 2020), Adcole Maryland Aerospace, Inc.
<b>ADACS Specifications</b>	** BCT GN&C Users Guide Rev A**
<b>ADACS Specifications</b>	** XACT Gen3 Interface Control Document Rev B **

**\*\* Note \*\***

For this test, the MAI-401 will be the test subject, but for reference in developing a broad and inclusive test plan for any available COTS ADACS the BCT XACT will be studied as a concurrent case for planning activities.

#### **2.4 Material/Equipment/Software Requirements**

Though students, CSRA Technologists, and external Mission Partners have exercised testing within the CSRA Mechanical Lab using the experiment configuration and setup in the past, the testing completed was not aimed at specific ADACS characterization. As such, the current setup may need to be further massaged to work for the exact testing scenarios required for this research. The materials, equipment and software required to complete the testing are initial estimates until the testing begins, at which time the configuration will be subject to change to support the test objectives. Any deviance from the initial base-line test configuration will be monitored and updated such that repeatable testing can be performed on successive test platforms.

Table 7 – Required Test Equipment

Equipment	Location	Category	Supporting	Acquired/Changed
Lab Computer	Mechanical Lab	Hardware		
MATLAB	Lab Computer	Software		
COSMOS	Lab Computer (VM)	Software		
Data Acquisition System (DAQ)	Lab Computer	Software		
Master Client	Lab Computer	Software		
Helmholtz Cage (HC)	Mechanical Lab	Hardware		
Air Bearing (AB)	Mechanical Lab	Hardware		
Air Compressor	Mechanical Lab	Hardware		
PhaseSpace Camera System (PS)	Mechanical Lab	Hardware		
Grissom 6U Integrated CubeSat	Mechanical Lab	Hardware		
MAI-401	Mechanical Lab	Hardware		
Grissom C&DH	Mechanical Lab	Hardware		
Flight Software Chip	Mechanical Lab	Hardware		
Wi-Fi Dongle	Mechanical Lab	Hardware		
cFS Flight Software	Software Lab	Software		

### III. Test Configuration

#### Helmholtz Cage

Many ADACS rely heavily on magnetic sensors such as magnetometers for informing the attitude determination algorithm, while magnetic control components such as magnetic torque rods rely on the creation of magnetic dipole moments in relation to the ambient magnetic field for attitude control. Simulating a realistic magnetic environment in which the ADACS will be required to perform once on orbit will be a requisite part of the test setup and will require the use of the AFIT Helmholtz Cage. The AFIT Helmholtz Cage is a square coil 3-axis cage within the Mechanical Lab. The Helmholtz cage is controlled through MATLAB scripting and holds the prescribed ambient magnetic field using truth magnetometers on a feedback loop. Systems Tool Kit (STK) from AGI is leveraged to estimate the magnetic field at an orbital altitude and can simulate point-in-time and positional fields, as well as full orbital pass simulations. The testing for this research will only require a single 3-axis point-in-time magnetic field estimate. Additional information about the AFIT Helmholtz Cage can be found in the thesis by Brewer [3].

### Air bearing

A hemispherical air bearing is located in the center of the Helmholtz Cage within the area of assumed homogenous magnetism. The CubeSat chassis is mounted to the air bearing which allows for freedom of movement in the three primary axes. Due to the construction of the air bearing, the freedom of rotation about the z-axis (vertical/nadir axis) is unlimited, while the rotation about the remaining two axes is limited by the support structure to +/- XX degrees in the vertical plane. In addition to providing the ability for rotational motion, the air bearing also simulates an environment of microgravity by drastically reducing felt friction. The air bearing achieves this with a cup and ball design, where the ball floats on air pressure thus negating the gravity induced friction. Gravity will still influence the behavior of the spacecraft as a whole on the air bearing, and as such a careful balancing of the integrated chassis is required to minimize any external torques.

### PhaseSpace Motion Capture System

To verify the true motion of the spacecraft a set of positional truth sensors will be needed and optical sensors are the most sensible and available options. The PhaseSpace Motion capture System has been mounted to the Helmholtz Cage structure with cameras in 6 locations. These cameras are optically tuned to capture light emitted by a set of controlled LED markers. The markers are mounted to the spacecraft chassis, and the marker positions are stored within the PhaseSpace master Client software. The Master Client software enables the creation of a known frame which can then be aligned to a local origination point. The motion of the spacecraft can then be precisely tracked with the PhaseSpace system.

### “GRISSOM” 6U Spacecraft

The goal of the research is to characterize the performance of ADACS offerings in flight-like conditions, and as such the access to a spacecraft chassis and operational components is central to the testing. The test article in use is a 6U chassis owned by the CSRA. For a completely accurate test flight for a specific mission all required mission components would be presumed necessary for integration before testing. In the case of this research the 100% flight model is both unnecessary and unable to be used. Unnecessary because this research is validating performance in a generality and not mission specific, so the understanding of which components are necessary would be in question. To solve this, a minimum viable product stance is taken, and only the base level components required for operation will be integrated. Additionally, due to the limitations of the air bearing and test platform, the ability to perform spacecraft rotation with the solar panels deployed would cause the interference disrupting the test. For standardization moving forward, the minimum viable products will be the Chassis, Electrical Power System (EPS), Command & Data Handling System (C&DH), Attitude Determination and Control System (ADACS) including any external sensors such as Coarse Sun Sensors, and mass models for additional weighting and balance. Slight modifications to a component or performance aspects of a component such will be allowed so long as a standard is kept and referenced.

### Wi-Fi Connectivity

Sending commands and receiving telemetry in the laboratory environment is generally accomplished with a direct ethernet connection into a flatsat configuration from the command software. The push towards flight-like testing requires an integrated satellite build and coupled with the requirement that the spacecraft rotate unencumbered drives the need for a wireless connection to the C&DH which then communicates with the down stream components. On orbit this wireless connection would be waveform transmissions from a ground-based antenna to the satellite antenna incurring the need to obtain certifications and spectrum allocation through the FAA. Access to the Wi-Fi network in the laboratory allows for the circumvention of the certification steps by allowing for the usage of a pre-defined transmission system requiring only the addition of a Wi-Fi dongle to an existing C&DH input. The Wi-Fi connection thus provides the means for commanding the spacecraft wirelessly as well as capturing telemetry from the spacecraft with the ability to store the data directly on the network.

### COSMOS

With the physical process by which commands and telemetry are delivered between the spacecraft and laboratory computer system solved by utilization of the Wi-Fi network, the obstacle of the software requirement then appears. The Grissom Program currently uses Ball Aerospace's COSMOS Operation and Test Environment for command and control. Access from the laboratory workstation to a virtual machine running the COSMOS software enables a consistent user interface and data handling software to be applied to the test case. The challenge with this software moving forward will be the ability for the laboratory technologists and software development team at AFIT to produce the required command and telemetry library for each new ADACS offering required to fully benefit from the available data stream.

### Timing

Complications on timing between differing data collection systems is one issue that needs to be continually monitored within these test cases. As an overview there are essentially three data types being collected; Spacecraft Telemetry (from COSMOS), and Simulation truth data and PhaseSpace truth data (both collected from MATLAB). The issue is that all three of these data sets are measured and saved with differing timing conventions. Spacecraft telemetry is kept in GPS seconds, Helmholtz cage directionality is based on elapsed seconds past a Julian Data start time (start time may not be accurate), and PhaseSpace positional data is based on Unix microseconds. Conversions between these timing conventions is not problematic aside from the loss of fidelity based on significant figures. The PhaseSpace positional data is the most stringent with microseconds, while the Helmholtz Cage data is only tracked to hundredths, and by far the worst case is the spacecraft telemetry which is only linked to the transmitted time stamp which is every 4 seconds with the exact timing of the data. In addition to the format of the timing, the synchronization of the data will need to be carefully studied during the analysis if data matching will be performed.

Table 8 – Data Time Conventions

<b>Data Type</b>	<b>Time Convention</b>	<b>Data Example</b>
Spacecraft Telemetry	GPS Seconds	1209168176 seconds
PhaseSpace Capture	Unix Micro-Seconds	1600201057.0728998 seconds
Helmholtz Cage	Elapsed Seconds from Start	2458384.57916667 + 15.79 seconds

**ORIENTATION**

Integration of the individual components of the spacecraft requires careful tracking of the orientation of each component that will influence or be influenced by the pointing of the spacecraft. Within this research there exist external components which also necessitate the alignment of a specified axis to work as a cohesive unit and deliver understandable metrics. For tracking purposes Table 6 has been created to allow for quick references between the components.

The Helmholtz cage rests within the laboratory and is positioned in a general sense where the X vector is mostly North pointing, the Y vector is normal to the x vector and mostly East pointing, and the Z vector is normal to both the X and Y vectors. The Z vector in compliance with the right-hand rule, is positive in the downward direction, or Nadir pointing. The positioning with respect to the Earth's true magnetic field is not specifically pertinent other than to make the reference point from which the test can track directionality of the cage magnetic field. This is due to the operation of the Helmholtz cage itself, where the strength of the cage magnetic field can be commanded to simulate any directionality, overcoming and negating the forces from Earth's magnetic field.

The Helmholtz Cage field is controlled through the MATLAB code and requires the usage of truth magnetometers placed within the homogeneous portion of the cage field. When the field is commanded the truth magnetometers provide measured data in a feedback loop in order to allow the cage to continually adjust the field to maintain a stability. The truth magnetometer data is also captured by the MAATLAB script and can be used as an additional data source.

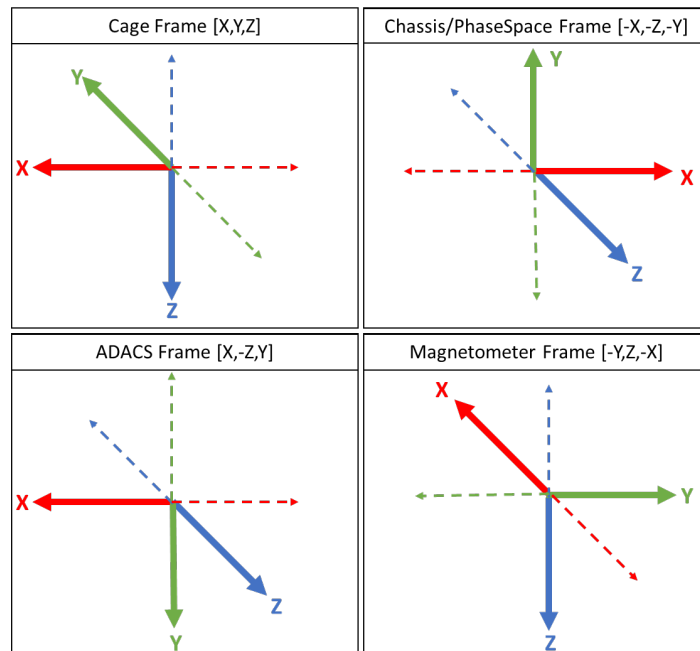


Figure 30 - Component Frame Diagrams

The Air Bearing is located directly within the center of the Helmholtz Cage and is used to provide the spacecraft with a simulated micro-gravity experience. The microgravity environment is described as a friction free or minimal friction induced environment with free rotation in three axes. The Air Bearing is level to the Earth and provides a single orienting vector in the Z direction.

The Spacecraft chassis is mounted in the center of the cage within the homogeneously controlled magnetic field. More specifically the chassis will be mounted to the Air Bearing which will allow for the unhindered rotation of the chassis about the center of the Air Bearing, in this case the Z axis. The test chassis has been configured such that it will be attached to the Air Bearing on the 6U face. The orientation of the chassis body-frame has been agreed upon by the entire development team and has been the standard for development of the flight software. Pictured is a representation of the CubeSat chassis with the directional vectors in both positive and negative directions from the origin corner.

Mounted within the chassis reside determination and control components which also require alignment to a known frame. The ADACS itself is mounted within the chassis and has a known directionality built-in to the integral software for use with the internal determination sensors and control components. The three-axis magnetometer delivers it's own three-axis frame which needs alignment to a known frame. The six sun sensors are themselves non-directional but will need to be wired to specific ports on the ADACS to signal illumination on the proper face of the chassis. From these documented component frames, a standard set of transforms can be developed and input into the software at required points creating a known frame directory.

The Chassis-frame is aligned to the Helmholtz Cage frame within the MATLAB script to sync the directionality of chassis pointing vectors with the “truth” of the cage. This is to say that since the cage provides a relative frame, that the chassis will acknowledge the cage frame, such that chassis X, Y, and Z will be rotated and transformed into cage X, Y, and Z for the purposes of anchoring the data for consistency. The Chassis frame will then be considered the basis frame for all spacecraft components to be aligned to. With the cage setup as well as the prior-to agreed upon body frame of the chassis, this transform was the most complicated to reach the required transform in the least number of rotations.

The ADACS needs to undergo a coordinate transform to align the ADACS frame with the Chassis frame.

In this case the transform was relatively easy as the directionality of the chassis frame was solely rotated 180 degrees around the Z axis.

The last significant transform is required to align the magnetic frame of the cage with that of the spacecraft 3-axis magnetometer. The difficulty became apparent when looking at the inscription of the frame reference inscribed upon the magnetometer, NED with a single arrow. To understand a 3-vector frame, two distinct vector arrows would be required with the assumption that the 3<sup>rd</sup> axis would be normal to the initial two. Due to this incongruency, the directionality was found by physically manipulating the magnetic field and reading the spacecraft magnetometer data. By commanding the cage to 0 on two of three axes, the third axis would reveal itself. From this data, the frame of the spacecraft magnetometer was determined along with the required transform.

Table 9 – Component Transforms

<b>Component Transforms</b>	<b>From</b>	<b>To</b>
From Chassis to Helmholtz Cage	Chassis X Chassis Y Chassis Z	Cage -X Cage -Z Cage -Y
From ADACS to Chassis	ADACS X ADACS Y ADACS Z	Chassis -X Chassis -Y Chassis Z
From Cage to Spacecraft Magnetometer	Cage X Cage Y Cage Z	Magnetometer -Y (-Y) Magnetometer Z (X) Magnetometer -X (Z)

### Test Setup

The final portion of the test configuration is determined by the operation of the selected ADACS offering that is being subjected to the test procedure. Each ADACS will likely have differing methodologies on operation as well as command and telemetry structures,

and potentially component builds, but trends can be found throughout the industry. Potential trends can be searched for in any number of scenarios, and for this research the methodology is to understand the trends that allow for the simplification of test scenarios that best allows for a comparative testing of multiple ADACS. With this methodology is it beneficial to break down the operation of each ADACS into the requirements necessary for operation of the specific test. For this plan a referenced in Section 1.4, there will be three primary tests; Detumble, Pointing Accuracy, and Slew Rate, of which slew rate will be combined with the Pointing Accuracy tests.

Detumble operations have shown the apparent trend that each ADACS uses the Coarse Sun Sensors and magnetometers for attitude determination while using the internal magnetorquers to reduce the tumbling effect caused by the forces imparted on the spacecraft from tip-off and ejection. This solidifies the basic needs of the experimental setup for the testing; a Helmholtz cage for the magnetic field, air bearing for the friction reduction, and a light source providing a sufficient wattage to the sun sensors.

Pointing Accuracy operations provide a much more difficult case to trend. Though each offering encompasses very similar component structure, the utilization of the sensor data along with the performance characteristics of both the determination and control algorithms can provide results with very different outcomes. The laboratory setup at AFIT does not have the apparatus required to accommodate star trackers or provide simulated star tracker data into the determination algorithms which makes the trend more convenient. The test cases will be reliant upon their magnetometers, IMU's, and sun sensors as the sole input to their determination algorithms. This standardization while not a true representation of a flight-like test will allow for a comparative analysis of the ADACS.

#### **IV. Test Procedure**

In developing this test plan there were various reference documents called upon to aid in the understanding of the equipment and setup, as well as to aid in the effort to combine a number of differing and prior tests as well as configuration plans into one seamless document. These references have been used, updated, changed, works-in-progress, and the latest editions have been prioritized. The documents referenced are as follows;

1. Helmholtz\_Cage\_Users\_Guide\_v2.3\_WIP.docx
2. phase\_space\_satellite\_user\_guide\_r3.docx
3. AIR BEARING OPERATION rev1.docx

The Test procedure will include the setup of the experiment as well as an initial checkout period to ensure the proper working for the CubeSat

#### **\*\*NOTE\*\***

It is important to note that the setup of the experiment is the critical component of the testing procedure and not the specific tests themselves. The experimental setup will be



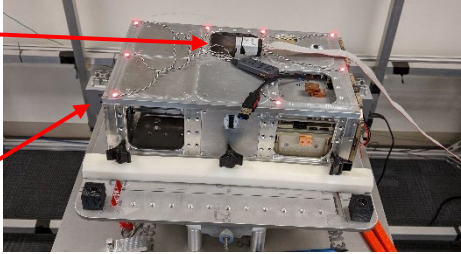
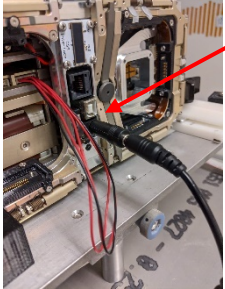
the key to whether the data collected can be used as a comparative against all other ADACS tests performed. The operation of the actual test and subsequent data collection is relatively straight forward but all rely upon a consistent and repeatable setup.


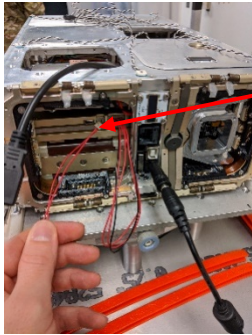
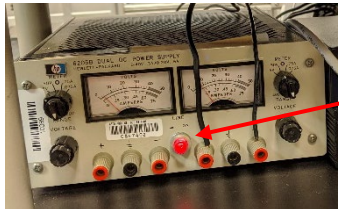
In addition, the specific test cases mentioned within this test plan there are a number of tests that can be included that will likely benefit the analysis and ability to compare and contrast performance metrics in the future. Testing the physical characteristics of the test chassis in full flight-configuration as mention in the preceding sections can be indicative of how well the ADACS and overall system performs with respect to the physical attributes. For example, if an ADACS performs control measures at a slower pace than an alternative ADACS can this be due to an increase in system mass or MOI? Such measurements though not specifically required for this test will allow for ultimately a better understanding in the global perspective, as well as providing a secondary measure to aid in the transference of knowledge learned to a mission chassis.

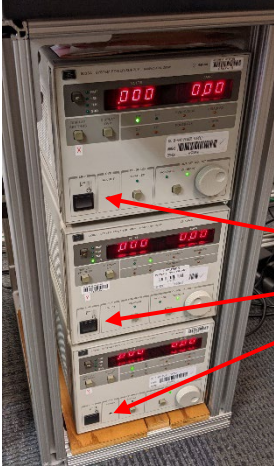
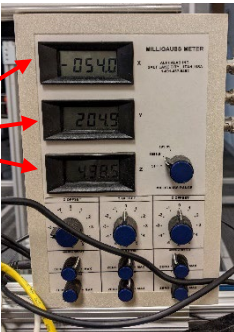
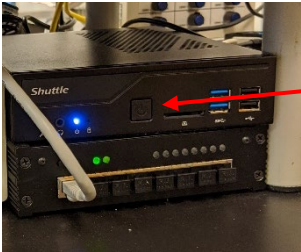
Furthermore, the deep investigation into the operations and configuration settings of the ADACS is what will likely provide a greater understanding of the modes of operation and configuration settings that will provide the highest level of performance of the ADACS. Each ADACS likely uses a different methodology for developing the determination and control algorithms, different starting algorithms, processes, sensors, and sensor types, and with the goal to characterize performance it is reliant upon the tester's due diligence to ensure that the true capabilities of the ADACS are being tested.

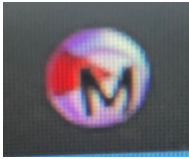

#### **4.1 Experiment Setup and CubeSat Checkout**

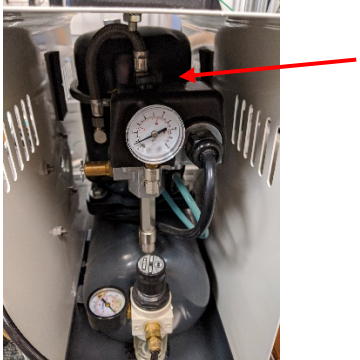

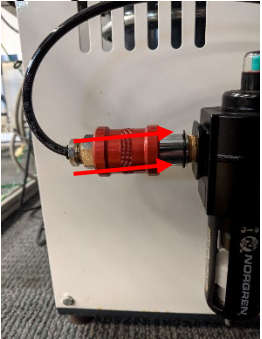
Setup of the experiment is a complex series of steps spanning a significant number of operations and devices all working in unison to create a relative Space environment simulation on Earth. The environment must allow for unrestricted motion and operation of the spacecraft in a way which does not interfere with the expected operation in Space. The AFIT CSRA Staff has developed user guides for the more complex systems which can be referred to at any time to gain a more in depth understanding of the specific system and its proper operation. The following procedure for setup will outline the procedure and an in depth reading and understanding of each user guide will provide the test team with additional information on mounting and balancing the satellite, cage setup and operation, air bearing setup, calibration, safety, and connectivity. The test environment is controlled through MATLAB script on the Lab Workstation and is currently being transitioned from a code-based interface to a GUI. The satellite is being controlled by a virtual machine on the same workstation running an instance of COSMOS. COSMOS represents the ground station which sends commands to the C&DH, which then controls the sub-components such as the ADACS.

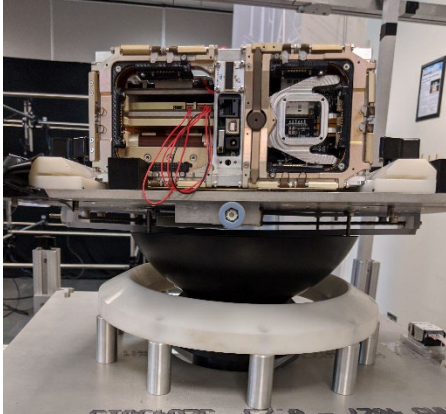

Step	Activity	Complete	Notes
<b>SECURING THE TEST ARTICLE TO THE AIR BEARING</b>			
1.	With the AIR BEARING MOUNTING PLATE raised and secured above the air bearing cup surface protected from debris and scratches, mount the TEST ARTICLE to the AIR BEARING MOUNTING PLATE with the provided mounting brackets and hardware.		This is a very unscientific way of mounting the CubeSat, but the mount will need to be adjusted at a later step for balancing the chassis.
2.	<p>Attach PHASESPACE LED's to the top plate of the chassis in the 4 corners and then evenly distributed along the long side of the chassis with sticky-tack [careful not to get stick-tack on anything but the aluminum chassis] plug in USB power pack to the LED HARNESS and</p>  <p>secure to chassis with sticky-tack. The LED's will automatically turn on when powered.</p>		The PhaseSpace LED's needed to be attached in a non-uniform pattern so that we can tell the difference in which sensor is picking up which LED from the MATLAB viewer.
3.	<p>Connect the CubeSat power supply A/C line to the power supply input jack on the chassis.</p> 		This will charge the EPS and allow for continuous testing and performance during the test when disconnected and running off battery power. Running the battery to a zero power level will harm the battery, a full charge is preferred at all times.

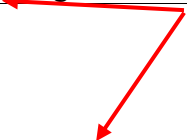
4.	<p>Remove the remove before flight cover by holding in the cover and pulling the pin,</p>  <p>releasing the ejection sensor enable switch.</p>		
5.	<p>Insert the jumper-wired enable plug on the</p>  <p>front of the chassis.</p>		<p>The secondary enable switch is normally released with the solar panel deployment, this jumper simulates the deployed state.</p>
<b>INITIALIZING THE HELMHOLTZ CAGE</b>			
6.	<p>Power on the coil relays using the RELAY POWER device. Click the button in the middle labeled “Line”, when power is on the</p>  <p>red circular button will illuminate.</p>		
7.	<p>Power on the X, Y, Z coils using the COIL POWER SUPPLIES. Flip the switches on the bottom left corner labeled “Line” to the up position.</p>		

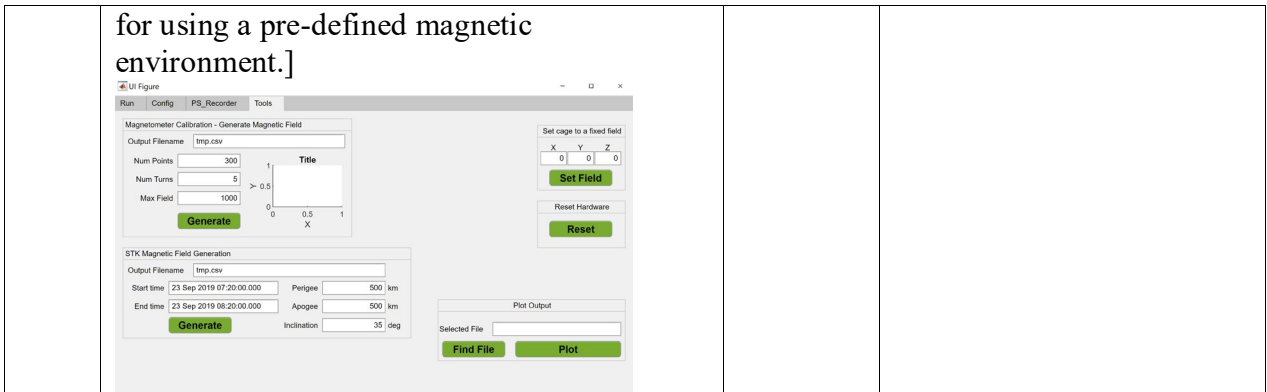
			
<p>8.</p>	<p>Verify the MILLIGAUSS METER is receiving signal from the TRUTH</p>  <p>MAGNETOMETER</p>		<p>X = Y = Z =</p>
<p>9.</p>	<p>INITIALIZING THE PHASESPACE CAMERAS</p>		
<p>10.</p>	<p>Power on the PhaseSpace server and cameras using the PHASESPACE SERVER device. Click the small circular button near the</p>  <p>middle labeled "ON/OFF". The LED labeled "POWER" will turn on when powered on.</p>		

11.	Open PhaseSpace Master Client on the lab workstation 		
12.	Wait ~1 minute for the server to boot and the cameras to connect.		
13.	Verify that the cameras are connected in PhaseSpace Master Client on by navigating to the cameras tab..		
14.	Verify that the PHASESPACE CAMERAS are seeing the PHASESPACE LED's		
<b>SUN SIMULATOR SETUP</b>			
15.	Place the solar simulator LIGHT SOURCE (incandescent XXX W lamp) on a cart at the same level as the center of the SPACECRAFT as close to the cage as possible (extend the neck of the lamp towards the CubeSat, turn off room lights and darken the shades.		This lamp will simulate the sun, the power sensed will decrease the farther from the CSS's by $1/r^2$
<b>INITIALIZING THE AIR BEARING</b>			
16.	Check and verify the oil level of the AIR COMPRESSOR through the oil level sight 		
17.	On the AIR COMPRESSOR rotate the power knob clockwise from Off to ON		

			
<p>18. Verify that the AIR COMPRESSOR pressure gauge has reached beyond 75 psi before continuing to the next step.</p>			
<p>19. Once the AIR COMPRESSOR has reached above 75 PSI send air pressure to the air bearing pedestal by sliding the red slide valve on the side of the AIR COMPRESSOR to the open position.</p>			
<p>20. Verify by touch that the AIR BEARING cup is releasing air</p>			

			
	<p>DO NOT lower the AIR BEARING PLATE onto the AIR BEARING CUP unless the compressor is above 75 PSI or damage will occur.</p>		
	<p>INITIALIZING THE HELMHOLTZ CAGE SOFTWARE</p>		
<p>21.</p>	<p>On the lab desktop computer, in MATLAB, open the file Helmholtz_Cage_Main within MATLAB, it is the main driver for the cage, as well as data acquisition and collection for</p>  <p>the cameras. The script opens in App Designer, hut RUN to run the APP.</p>		
<p>22.</p>	<p>Both static and dynamic magnetic fields can be implemented by the MATLAB software. For this research a static field will be solely used. For a dynamic field STK can be used to output an estimated field at given orbital parameters.</p>		<p>Want a static field for this test.</p>
<p>23.</p>	<p>Within Helmholtz_Cage_GUI in MATLAB on the LAB COMPUTER setup the variables to configure the cage controller for the preferred test, the GUI will initialize with a default configuration.</p>		
	<p>SETTING A MAGNETIC FIELD</p>		
<p>24.</p>	<p>Within the Cage GUI click the Tools tab, focus on the lower left hand box labeled “STK Magnetic Field Generation.” This is where the magnetic field for a specific target orbit can be simulated from STK and used as the input to the Cage simulation. [See step 39</p>		<p>This configuration will be stored as a configuration file and will need to be uploaded by following the next steps.</p>





25. To use a pre-established magnetic environment Navigate to Helmholtz\_Cage\_main > Config and click on Load Config. Load config will give multiple options. Choose the best-fit for your test.

For this test use the pre-established file HALONet\_Dawn\_Dusk\_E CI\_Inertial to set the field.

26. Under the run tab, select Run Cage to run the currently configured simulation. The cage will run through the magnetic environments at the specified time basis within the simulation. At any point you can hit Pause Cage which will hold the magnetic field at the current position.

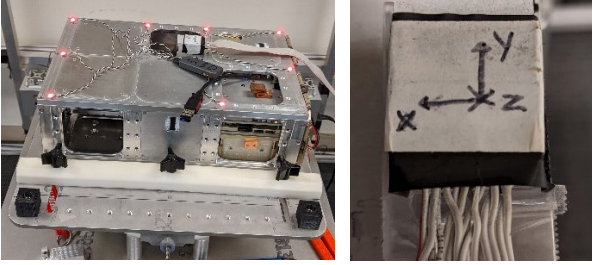
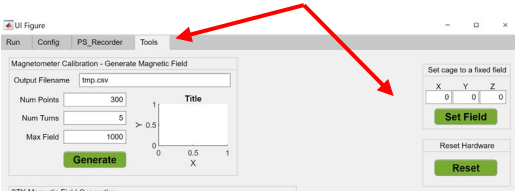
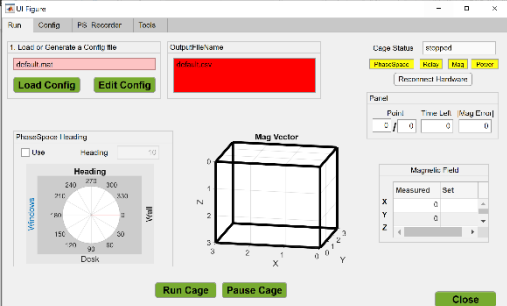
The Pause function is critical specifically for the Pointing Accuracy test, knowing that the magnetic field is stationary allows for the measurement of the variation of the ADACS pointing to determine in a general frame how well the control function of the ADACS performs.

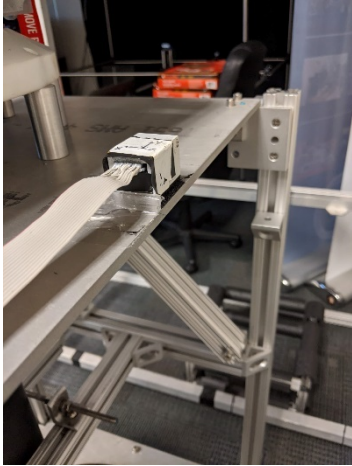
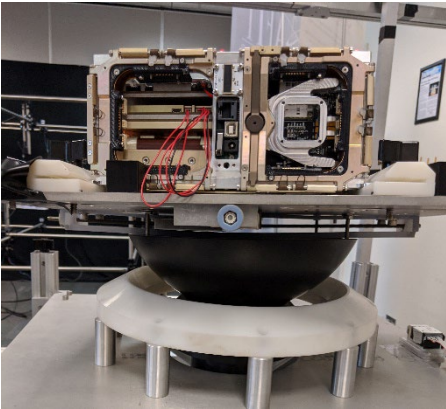
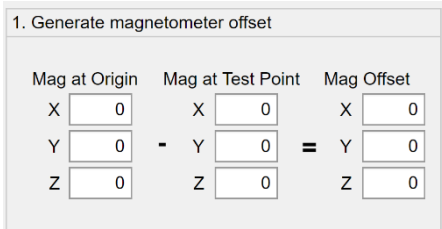
**TRUTH MAGNETOMETER**

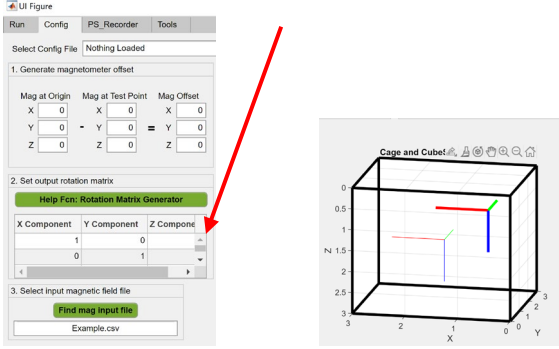
27. Set the truth magnetometer as close as possible to the center of the cage with the labeled x, y, z axes pointing in the same directions as the cage

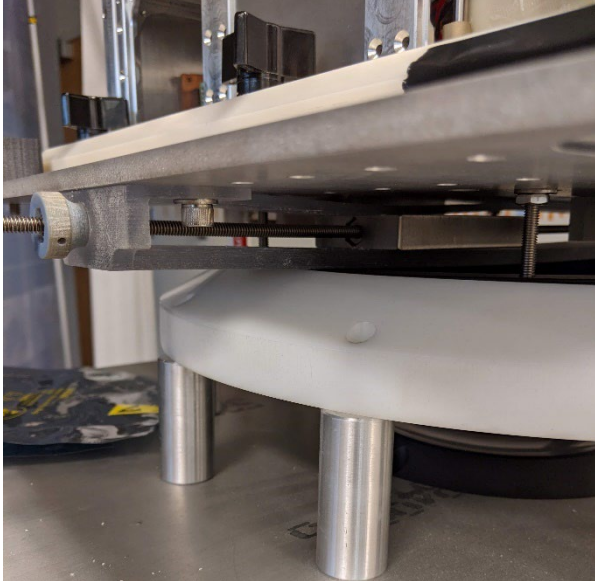
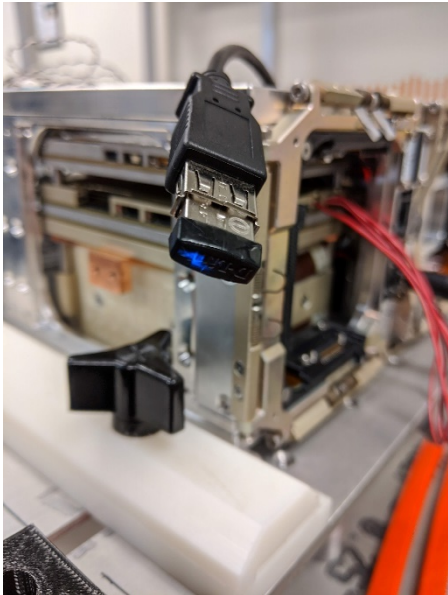

Note: Loading a pre-existing configuration will input all offsets and translations, it is advised to save the new configuration at this point and make it

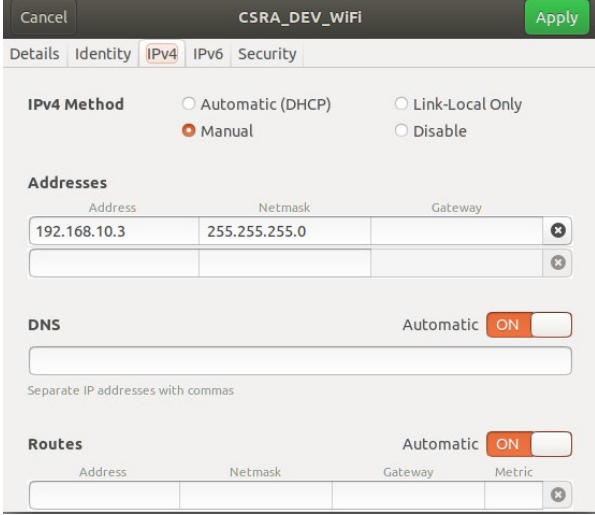
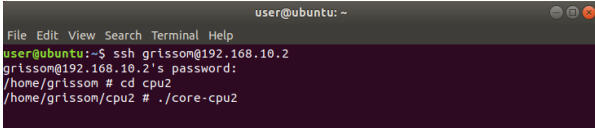
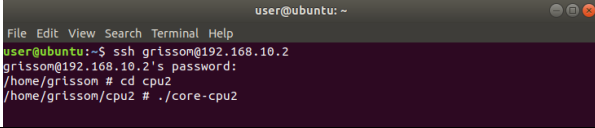


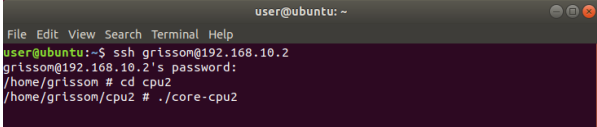
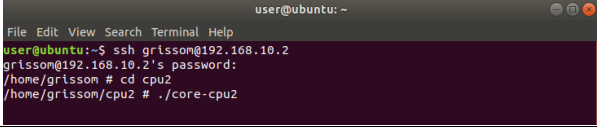
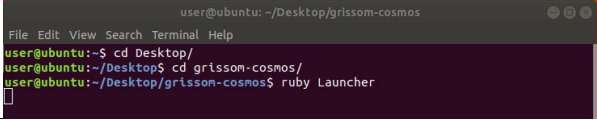
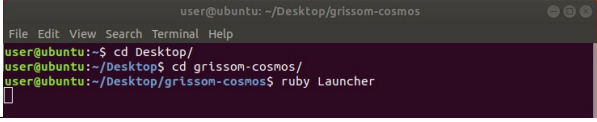
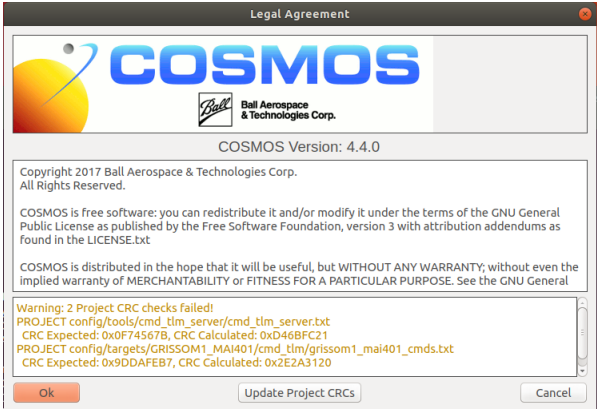
		<p>your own.</p> <p>Note the approximate location away from the center of the chassis for reference .</p> <p>X =</p> <p>Y =</p> <p>Z =</p>
<p>28.</p>	<p>Within Helmholtz_Cage_Main open the Tools tab and set the cage field to [0, 0, 0] and click Set Field</p> 	<p>Drive Field to 0, let the field settle, and then take measurements of what the truth mags are reading.</p>
<p>29.</p>	<p>Navigate to Helmholtz_Cage_main &gt; Config and store the values off the Milligauss Meter in the config tab under mag at origin, this will be used to create an offset due to the</p>  <p>dislocation of the truth magnetometer.</p>	<p>X1=</p> <p>Y1 =</p> <p>Z1 =</p> <p>These numbers will jump around as the cage is continually working towards hitting the commanded values with a feedback loop. FYI, when the satellite is off, the cage is much more stable.</p>

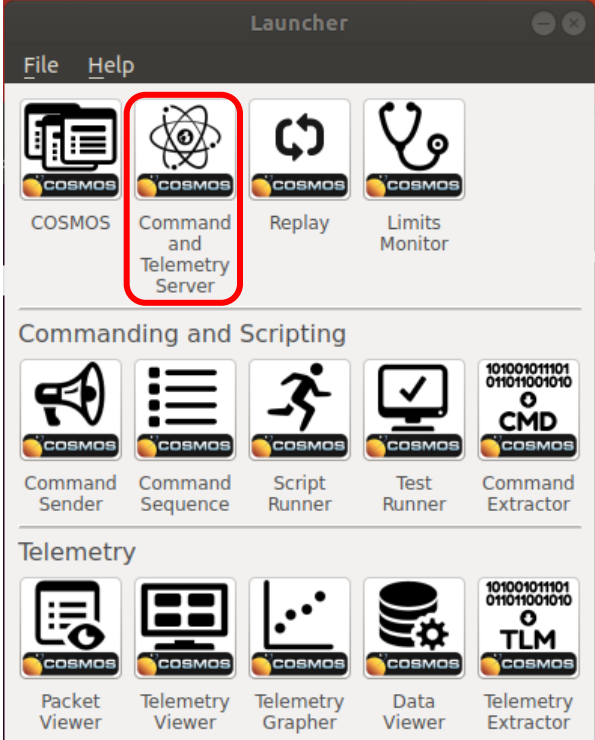
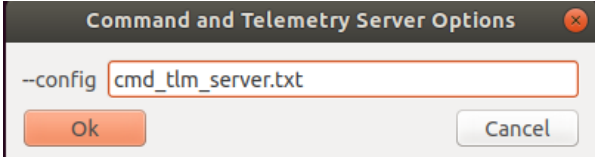
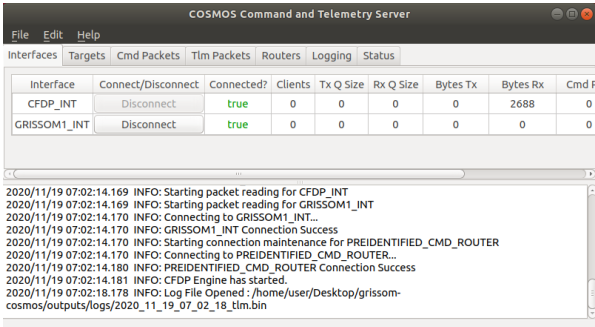
<p>30.</p>	<p>Move the truth magnetometer to the Velcro spot on the -X side where the magnetometer will stay for the duration of the test.</p> 		
<p>31.</p>	<p>Raise the pedestal to where the air bearing takes the full weight of the system, platform and CubeSat combined.</p> 		<p>Verify the compressor is above 75 lbs. of pressure before raising the platform off the support ring.</p>
<p>32.</p>	<p>Take another reading of the Milligauss Meters and enter it into the config tab under Mag at Test Point</p>		<p>X2= Y2 = Z2 =</p>
<p>33.</p>	<p>Subtract current Milligauss readings from initial Milligauss readings to find the magnetic offset, store as offset in the config</p> 		<p>X(1-2) = Y(1-2)= Z(1-2) = This is your magnetic offset location.</p>

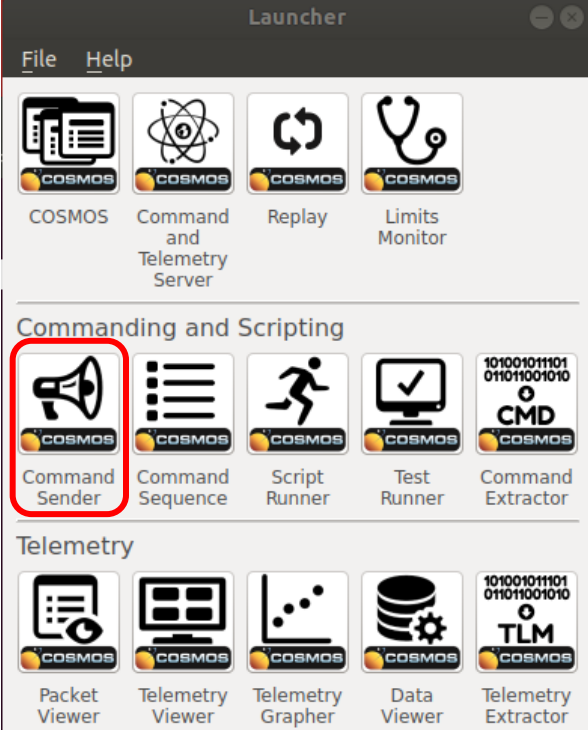
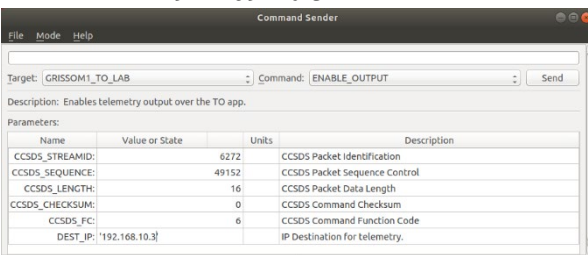
	tab under offset. The GUI will calculate the offset for you.		
34.	<p>Within Helmholtz_Cage_main &gt; Config be sure to implement the correct coordinate rotation matrix which will relay the coordinate frame of the satellite chassis to the cage. The diagram shows the translation in 3-dimetsnional graphics.</p> 		This is especially important as the chassis frame is the central frame to which the components are fundamentally derived from.
35.	Click Save Config to save your mag offset baseline.		It is important that the CubeSat is on and running during the Cage Setup process, as the magnetic field will change due to the current within the CubeSat.
<b>INITIALIZING THE SATELLITE</b>			
36.	With the air bearing “floating” the likelihood that the CubeSat is bottomed out on a side is high. Use mass adjusters on the underside of the AIR BEARING pedestal bracket to balance the system. The goal is for the entire system to float and be flat.		This step is a continual process of adjust and reassess and will likely take a long time to perfect. The ability to balance is necessary to reduce any possible eternal torques compounded by the gravitational force.

			
<p>37.</p>	<p>Check that the Wi-Fi Dongle is blinking blue, this means that it is connected to the Wi-Fi network.</p> 		
<p>INITIALIZING THE GROUND SOFTWARE</p>			
<p>38.</p>	<p>Open VMWare Workstation 15 app on the Lab Workstation, this is the virtual machine</p>  <p>that will link to COSMOS software providing the ground commanding to the C&amp;DH (VM</p>		<p>THE VM runs on an instance of Linux, and as such a good understanding of Linux will be beneficial.</p>

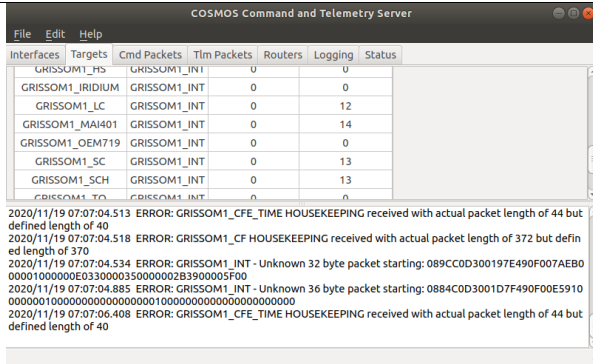
	will be called cFS v2) and click 'Play virtual machine.'		
39.	Ensure the Wi-Fi dongle in the front of the lab workstation is blinking blue and ready for connection. Connect the virtual machine to the Wi-Fi signal CSRA_DEV_WiFi on the Lab workstation.		
40.	Go to Wi-Fi setting and set the IP address to 192.168.10.3 and the Net mask to 255.255.255.0.		Computer IP needs to be 192.168.10.3 Satellite IP needs to be 192.168.12.2
			
41.	Open a terminal window, send the to connect to the C&DH over Wi-Fi to remotely connect into the C&DH <code>ssh grisson@192.168.10.2</code>		
			
42.	Likely there will be a warning message that pops up, if so re-enter the ssh command from step 48 above and continue on. It is a good idea to copy the error message for later in case the connection continues to fail.		
43.	Enter in the password for the C&DH when prompted by the terminal window		
			
44.	Once connected to the C&DH change directories into the core flight software using the following command: <code>cd /home/grisson/cpu2</code>		cFS and cpu2 should be the same software but something is broken in cFS, USE CPU2

	 <pre> user@ubuntu: ~ File Edit View Search Terminal Help user@ubuntu:~\$ ssh grisson@192.168.10.2 grisson@192.168.10.2's password: /home/grisson # cd cpu2 /home/grisson/cpu2 # ./core-cpu2 </pre>		
45.	<p>Initialize the core flight software using the following command:</p> <pre>./core-cpu2</pre> 		Data streams will be visible as the C&DH will be locating and initializing all integrated components.
46.	<p>Open a secondary terminal window in the VM</p>		
47.	<p>Change directories to where the cosmos software is located with the following command:</p> <pre>cd Desktop/grissom-cosmos</pre> 		
48.	<p>Open the COSMOS launcher with the following command from the terminal window:</p> <pre>ruby Launcher</pre> 		Ignore all warnings and continue
49.	<p>Accept the default user configuration, click OK</p> 		
50.	<p>Choose the command and telemetry server icon within the launcher</p>		

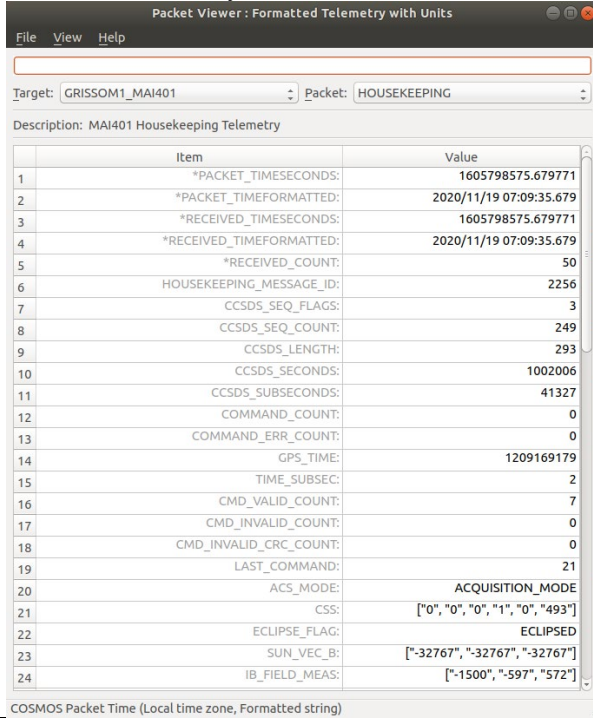
																														
51.	<p>Select OK to use the default telemetry configuration file.</p> 																													
52.	<p>Verify through the command and telemetry window interface tab the connection to the CubeSat is valid and data packets are being sent and delivered</p>  <table border="1" data-bbox="347 1373 938 1457"> <thead> <tr> <th>Interface</th> <th>Connect/Disconnect</th> <th>Connected?</th> <th>Clients</th> <th>Tx Q Size</th> <th>Rx Q Size</th> <th>Bytes Tx</th> <th>Bytes Rx</th> <th>Cmd F</th> </tr> </thead> <tbody> <tr> <td>CFDP_INT</td> <td>Disconnect</td> <td>true</td> <td>0</td> <td>0</td> <td>0</td> <td>0</td> <td>2688</td> <td>0</td> </tr> <tr> <td>GRISSOM1_INT</td> <td>Disconnect</td> <td>true</td> <td>0</td> <td>0</td> <td>0</td> <td>0</td> <td>0</td> <td>0</td> </tr> </tbody> </table>	Interface	Connect/Disconnect	Connected?	Clients	Tx Q Size	Rx Q Size	Bytes Tx	Bytes Rx	Cmd F	CFDP_INT	Disconnect	true	0	0	0	0	2688	0	GRISSOM1_INT	Disconnect	true	0	0	0	0	0	0		Connection should be TRUE
Interface	Connect/Disconnect	Connected?	Clients	Tx Q Size	Rx Q Size	Bytes Tx	Bytes Rx	Cmd F																						
CFDP_INT	Disconnect	true	0	0	0	0	2688	0																						
GRISSOM1_INT	Disconnect	true	0	0	0	0	0	0																						
53.																														
<b>ENABLING TELEMETRY</b>																														
54.	Choose the Command Sender icon within the launcher window.																													

																															
<p>55.</p>	<p>To enable telemetry output from the C&amp;DH to COSMOS, from COMMAND SENDER send the following command from the drop down menu:  <b>TO_ENABLE_OUTPUT_CC</b>  Make sure to change Dest_IP to the computer IP address: 192.169.10.3.</p>  <table border="1" data-bbox="349 1312 933 1438"> <thead> <tr> <th>Name</th> <th>Value or State</th> <th>Units</th> <th>Description</th> </tr> </thead> <tbody> <tr> <td>CCSDS_STREAMID:</td> <td>6272</td> <td></td> <td>CCSDS Packet Identification</td> </tr> <tr> <td>CCSDS_SEQUENCE:</td> <td>49152</td> <td></td> <td>CCSDS Packet Sequence Control</td> </tr> <tr> <td>CCSDS_LENGTH:</td> <td>16</td> <td></td> <td>CCSDS Packet Data Length</td> </tr> <tr> <td>CCSDS_CHECKSUM:</td> <td>0</td> <td></td> <td>CCSDS Command Checksum</td> </tr> <tr> <td>CCSDS_FC:</td> <td>6</td> <td></td> <td>CCSDS Command Function Code</td> </tr> <tr> <td>DEST_IP:</td> <td>192.168.10.3</td> <td></td> <td>IP Destination for telemetry.</td> </tr> </tbody> </table>	Name	Value or State	Units	Description	CCSDS_STREAMID:	6272		CCSDS Packet Identification	CCSDS_SEQUENCE:	49152		CCSDS Packet Sequence Control	CCSDS_LENGTH:	16		CCSDS Packet Data Length	CCSDS_CHECKSUM:	0		CCSDS Command Checksum	CCSDS_FC:	6		CCSDS Command Function Code	DEST_IP:	192.168.10.3		IP Destination for telemetry.		<p>This will allow the C&amp;DH to send updated telemetry packets to the COSMOS telemetry tracker and will include telemetry from all active components at a 4 second interval.</p>
Name	Value or State	Units	Description																												
CCSDS_STREAMID:	6272		CCSDS Packet Identification																												
CCSDS_SEQUENCE:	49152		CCSDS Packet Sequence Control																												
CCSDS_LENGTH:	16		CCSDS Packet Data Length																												
CCSDS_CHECKSUM:	0		CCSDS Command Checksum																												
CCSDS_FC:	6		CCSDS Command Function Code																												
DEST_IP:	192.168.10.3		IP Destination for telemetry.																												
<p>56.</p>	<p>Verify telemetry is being sent by selecting the Tlm Packets tab within the COSMOS Command and Telemetry Server and watching packet numbers increment up</p>																														





57. Click Packet Viewer for the target, Grissom\_MAI401 to view the entire spread of ADACS telemetry.



All telemetry can be further explained in the MAI-401 System Manual (updated 10 January 2020).

This concludes the Test Procedure 4.1 – Initial Setup

At this point the following setup should be true and you can proceed to the test activities:

- Cage on and configured
- Truth Magnetometer Calibrated
- Chassis mounted and balanced
- Air Bearing on and floating
- PhaseSpace LED's on
- PhaseSpace Cameras collecting
- Fight Software initialized

## 4.2 Detumble Test

In the operation of the spacecraft on orbit, Detumble is generally the second priority operation following spacecraft initialization, and the first test of the ADACS. When the spacecraft, CubeSat in this case, is deployed from the canister will have introduced upon it rotation from launch canister friction as well as a tip-off from the host satellite. It is a common assumption that the combined torques needed to be overcome by the spacecraft and more specifically the ADACS should not exceed 10 meters/second per axis. Detumble is a critical operation as it brings the spacecraft under control and sets the spacecraft up for both solar charging and communication with the ground site.

Step	Activity	Complete	Notes
1.			
2.	From COSMOS set ACS mode to TEST_MODE MAI401_SET_ACS_MODE_CC [0 = TEST_MODE]		
3.	From COSMOS send REQUEST TELEMETRY from ADACS MAI401_SEND_ORBIT_TLM_CC [empty]		
4.	Verify ADACS ACK of command by looking for changes in the telemetry data		
5.	From SOH data confirm the following sensors and quantities are recognized, powered on: (3) MAGNETOMETERS, (3) MeMS accelerometers, (1) Sun Sensor, (1) Star Tracker, (3) Magnetorquers, (3) Reaction Wheels in the telemetry data flow		
6.	Verify magnetometer data streamed from ADACS to C&DH through COSMOS matches the data output file from the truth magnetometer readings in order to baseline the magnetic field measurements.		
7.	IF any previous steps FAIL, proceed to TROUBLESHOOTING		
8.	Scan the completed test plan or section with all Pass/Fail boxes, initials, and dates filled, and post it in the shared drive under ADACS Test Reporting Folder [Create this folder when in Lab]		
	This concludes the Test Procedure 4.2.1 – ADACS Power-Up and Initialization Test		

Step	Activity	Complete	Notes
1.	From GUI reset HC B-field parameters to the saved orientation from the initial setup (Step #33)		
2.	Verify alignment of the TRUTH MAGNETOMETERS to the saved orientation from the initial setup (Step #34)		
3.	Verify alignment of the ADACS MAGNETOMETERS to the saved orientation from the initial setup (Step #36)		
4.	Verify alignment of the PHASESPACE CAMERAS to the saved orientation from the initial setup (Step #37)		
5.	From COSMOS send REQUEST TELEMETRY from ADACS at current position MAI401_SEND_ORBIT_TLM_CC [empty]		
6.	From COSMOS command ADACS to point to a specified location (between +/- 18 degrees from XY plane due to air bearing limitations) MAI401_SET_RV_CC [ECI position X, Y, X] [insert pointing location in table format]		
7.	MANUALLY PERTURB the Chassis <b>GENTLY</b> , the goal is to rotate the spacecraft on the air bearing at a rate estimated to be 10 degrees/second around the z axis (some wobble is OK, this is to simulate ejection of the spacecraft and detumble. Analysis of ADACS telemetry as well as PhaseSpace Camera data after the test will reflect if the ADACS can keep up with this rotation rate		
8.	OPEN PhaseSpace data and ADACS telemetry to assess the maximum rotation rate experienced. IF rate is less than (<) 10 degrees/second repeat at a greater rate IF rate is greater than (>) 10 degrees/second AND less than (<) 15 degrees/second STOP and CONTINUE TO #62 IF rate is greater than (>) 15 degrees/second REPEAT at a lower rate		
9.	Scan the completed test plan or section with all Pass/Fail boxes, initials, and dates filled, and post it in the shared drive under ADACS Test Reporting Folder [Create this folder when in Lab]		
	This concludes the Test Procedure 4.2.5 – ADACS Detumble Test		

### 4.3 Pointing Accuracy and Slew Rate

Pointing accuracy is an integral part of characterizing the performance of an ADACS. The determination function of the ADACS will provide an estimated pointing based on

the sensor input received. The desired pointing can be provided to the ADACS in multiple manners such as pre-loaded vectors, pointing tables, or direct commands uplinked through the TT&C system. The method in which the desired pointing can be provided ranges from vector specific, to LVLH, to ECEF. Desired pointing can follow a direct vector, include rotation rates, or follow a nadir position, all of which are options within the code as provided by the manufacturer. For this test the cage will be set to a static position so as not to invalidate the test, a desired attitude will be commanded, and the data from the controlled motion to reach the desired attitude will be captured and analyzed. The specific data points requested are desired heading, measured heading, and timestamps from each measurement. The data collected shall allow for derivations of rates and deviations for analysis.

#### Pointing Accuracy

Step	Activity	Complete	Notes
1.	From MATLAB reset HC B-field parameters to the saved orientation from the initial setup (Step #33)		
2.	Verify alignment of the TRUTH MAGNETOMETERS to the saved orientation from the initial setup (Step #34)		
3.	Verify alignment of the ADACS MAGNETOMETERS to the saved orientation from the initial setup (Step #36)		
4.	Verify alignment of the PHASESPACE CAMERAS to the saved orientation from the initial setup (Step #37)		
5.	From COSMOS send REQUEST TELEMETRY from ADACS at current position MAI401_SEND_ORBIT_TLM_CC [empty]		
6.	From COSMOS command ADACS to point to a specified location (between +/- 18 degrees from XY plane due to air bearing limitations) MAI401_SET_RV_CC [ECI position X, Y, X] [insert pointing location in table format]		
7.	Note pointing location commanded (this will be used analyze and compare the pointing attitude telemetry from the ADACS and the PhotoSense Cameras to the commanded value after testing has been completed to satisfy part 1)		
8.	Perform tasks 40 & 41 a total of 9 times for 9 differing pointing locations, and then an 10 <sup>th</sup> time returning the to the attitude commanded in the first iteration.		
9.	Allow the ADACS to hold the last commanded position for 30 minutes (continually sending data on positioning to be analyzed later to satisfy Part 2)		
10.	Scan the completed test plan or section with all Pass/Fail boxes, initials, and dates filled, and post it in the shared drive under ADACS Test Reporting Folder [Create this		

	folder when in Lab]		
	This concludes the Test Procedure 4.2.3 – ADACS Pointing Accuracy Test		

Slew

Step	Activity	Complete	Notes
1.	From GUI reset HC B-field parameters to the saved orientation from the initial setup (Step #33)		
2.	Verify alignment of the TRUTH MAGNETOMETERS to the saved orientation from the initial setup (Step #34)		
3.	Verify alignment of the ADACS MAGNETOMETERS to the saved orientation from the initial setup (Step #36)		
4.	Verify alignment of the PHASESPACE CAMERAS to the saved orientation from the initial setup (Step #37)		
5.	From COSMOS send REQUEST TELEMETRY from ADACS at current position MAI401_SEND_ORBIT_TLM_CC [empty]		
6.	From COSMOS command ADACS to point to a specified (between +/- 18 degrees from XY plane due to air bearing limitations) MAI401_SET_RV_CC [ECI position X, Y, X] [insert pointing location in table format]		
7.	From COSMOS command ADACS to point to a specified position 90 degrees from initial point every 180 seconds for a total of 10 maneuvers (if the ADACS telemetry show that it can indeed hit these orientations in the time allotted, then the rotational rate can be confirmed as greater than (>) .5 degrees/second MAI401_SET_RV_CC [ECI position X, Y, X] [insert pointing location in table format]		
8.	Perform Steps 59 and 60 for a 180degree/180 second rate (simulating a 1 deg/second rate)		
9.	Perform Steps 59 and 60 for a 180degree/90 second rate (simulating a 2 deg/second rate)		
10.	Scan the completed test plan or section with all Pass/Fail boxes, initials, and dates filled, and post it in the shared drive under ADACS Test Reporting Folder [Create this folder when in Lab]		
	This concludes the Test Procedure 4.2.3 – ADACS Maximum Rotational Rate test		

## **Appendix B. MATLAB Analysis Code**

**CubeSat Attitude Determination and Control System (ADACS) Characterization  
and Testing for Rendezvous and Proximity Operations (RPO)**

**Captain Steven Bednarski**

**MATLAB Analysis Code**

## Code Setup

```
% Steven Bednarski
% Test: Detumble, Acquisition Mode, Static Cage
% Grad Mar 2021

clear all; close all; clc;
format long
set(0,'DefaultFigureWindowStyle','docked')
f = 1; % figure stepper

% 3 Primary data types
% ADACS Telemetry
% PhaseSpace Cameras
% Helmholtz Truth Magnetometer

% ADD YOUR FILE INPUTS HERE, AND CHANGE WHERE THEY SAVE BELOW
% (CTRL-F SAVEAS)
addpath('60050\'); % add path where your data is
stored
cagedata = 'BednarskiTest_201211_1639.csv'; % add filepath of your
cage data
phasespacedata = 'BedTest600x50.txt'; % add filepath of your
phasespace data
telemetrydata = '20201211600x50Partial.txt'; % add filepath of your
ADACS telemetry data
```

## IMPORT DATA Files as Tables

```
%TELEMETRY IMPORT
t1m = readtable(telemetrydata,'Delimiter'... % importing txt file,
delimited
,{' ','[',']',',','\t'}, 'MultipleDelimsAsOne', true); % headers: TARGET,
PACKET, GPS_TIME, ACS_MODE, CSS, ECLIPSE_FLAG
disp('Telemetry Imported') % SUN_VEC_B,
IB_FIELD_MEAS, B_DOT, TORQUE_COIL_CMD, GC_TORQUE_COIL_CMD
% QBI_HAT, QBI_HAT_ST,
OMEGA_B, BODY_RATE

% PHASESPACE IMPORT
psDetAcq = readtable(phasespacedata, "Delimiter",{' ','[',']',... % importing txt file,
delimiting for multiple delimiters
,{' ','[',']'}); % headers: time(us), frame,
heading(deg), pos_X, pos_Y, pos_Z, rot_w, quat_x, quat_y, quat_z
```

```

disp('PhaseSpace Imported')

% CAGE IMPORT (MATLAB)
cageDetAcq = readtable(cagedata);           % importing .csv file
disp('Cage Data Imported')                % headers = elapsed_seconds,
mag_des_x, mag_des_y, mag_des_z, mag_act_x_rot, mag_act_y_rot, mag_act_z_rot,
mag_act_x, mag_act_y, mag_act_z, norm_mag_error

```

### Cage Data

```

% Cage time in elapsed seconds passed the Julian start time
cagetimeinit = 2458384.57916667;           % Julian Date start time -
2458384.57916667, time in elapsed seconds
cagetime = cageDetAcq.elapsed_seconds;

% Desired cage magnetic field
descagex_chas = cageDetAcq.mag_des_x;     % x component,
desired value, in chassis frame
descagey_chas = cageDetAcq.mag_des_y;     % y component,
desired value, in chassis frame
descagez_chas = cageDetAcq.mag_des_z;     % z component,
desired value, in chassis frame

% Truth magnetometer measured cage magnetic field
truthBFieldx_chas = cageDetAcq.mag_act_x_rot; % x component
measured value in chassis frame, mag is in milliGauss (mG)
truthBFieldy_chas = cageDetAcq.mag_act_y_rot; % y component
measured value in chassis frame, mag is in milliGauss (mG)
truthBFieldz_chas = cageDetAcq.mag_act_z_rot; % z component
measured value in chassis frame, mag is in milliGauss (mG)

cageBField = [cagetime, truthBFieldx_chas, truthBFieldy_chas, truthBFieldz_chas]; %
measured composite [x, y, z] magnetic field

```

### ADACS Data

```

tlmtime = tlm.Var3;                       % time in GPS Seconds, packets
at 4 second intervals
tlmtimeelapsed = tlmtime - tlmtime(1, 1); % ADACS telemetry
GPSTime is wrong, and resets to May 1 2018, unless
% rerunning all the data with a specified
times stamp, the ability to

```



```

% exactly match data up is poor, so a
general time step will be used.

% Telemetry Rotational Data (Omega_B telemetry point) smoothed(2 sec
time constant) body rate in body frame using mag and sun sensors
tlm_omega_B = rad2deg([tlm.Var35, tlm.Var36, tlm.Var37]); % rads/sec to
deg/sec, [x, y, z] components

% Telemetry measured B Field
tlmBFieldx = (tlm.Var15); % x component in ADACS
frame, in lsb counts
tlmBFieldy = (tlm.Var16); % y component in ADACS
frame, in lsb counts
tlmBFieldz = (tlm.Var17); % z component in ADACS
frame, in lsb counts

```

### PhaseSpace Data

```

% Time Data Time in Unix Microseconds
(actual time found on top line of .txt doc
pstimeinit = 1606839527.236135; % (not needed unless
syncing) Tuesday, December 1, 2020 4:18:47.236 PM
timegap = 315964800; % (not needed unless syncing)
standard gap from unix to gps time with no leap seconds
pstime = psDetAcq.time_us_((13:10:end), 1); % raw data @ ~100
Hz, sample every 10 or change if wanted
pstimeelapsed = pstime - pstime(1,1); % total time elapsed
pstotaltime = psDetAcq.time_us_((13:10:end), 1);
pstotaltimeelapsed = pstotaltime - pstotaltime(1,1);

% Positional Data ***Measured mm from
phasespace centroid in Body Frame [0, 0, 0]***
ps_pos_x = psDetAcq.pos_X(13:10:end)/1000; % x component,
changed mm to meters (/1000)
ps_pos_y = psDetAcq.pos_Y(13:10:end)/1000; % y component,
changed mm to meters (/1000)
ps_pos_z = psDetAcq.pos_Z(13:10:end)/1000; % z component,
changed mm to meters (/1000)
ps_pos = [ps_pos_x, ps_pos_y, ps_pos_z]; % [x, y, z]

% Heading Data
ps_heading = rad2deg(unwrap(deg2rad(psDetAcq.heading_deg_(13:10:end)))); %
unwrap allows top values to begin again at the bottom (359 deg + 1 deg = 0 deg)

```

## Plotting Magnetic Field Data

```
% Magnetic Field Plot
figure(f)
pbaspect([2 1 1])
plot(cagetime, (-1 * descagex_chas), '--xr')           % chassis frame rotated to
cage frame, cage x = chassis -x
hold on
plot(cagetime, (-1 * descagez_chas), '--xg')         % chassis frame rotated to
cage frame, cage y = chassis -z
plot(cagetime, (-1 * descagey_chas), '--xb')         % chassis frame rotated to
cage frame, cage z = chassis -y

plot(cagetime, (-1 * truthBFieldx_chas), 'Or')       % driven as chassis put in
cage x frame, chassis x = cage -x (to aid in data management)
plot(cagetime, (-1 * truthBFieldz_chas), 'Og')       % driven as chassis put
in cage y frame, chassis y = cage -z (to aid in data management)
plot(cagetime, (-1 * truthBFieldy_chas), 'Ob')       % driven as chassis put
in cage z frame, chassis z = cage -y (to aid in data management)

plot(tlmtimeelapsed, (-1 * tlmBFieldy) * 32 / 100, 'r') % put in cage frame,
cage x = ADACSmag -y
plot(tlmtimeelapsed, tlmBFieldz * 32 / 100, 'g')     % put in cage frame,
cage y = ADACSmag z
plot(tlmtimeelapsed, (-1 * tlmBFieldx) * 32 / 100, 'b') % put in cage frame,
cage z = ADACSmag -x
title("MAI-401 Measured B-Field")
xlabel("Elapsed Time (Seconds)")
ylabel("milliGauss")
legend("Desired X Value", "Desired Y Value", "Desired Z Value", "Truth X Value",
"Truth Y Value", "Truth Z Value", "TLM Measured X Value", "TLM Measured Y
Value", "TLM Measured Z Value")
saveas(figure(f), [pwd '/60050/gainMAI-401 Measured B-Field.pdf'])
f = f + 1; % step to next figure
disp('MAI-401 B-Field measurement plot complete')
```

## BIAS(offset) and GAINS(scaling) at B-Field Measurement

```
% Magnetic Field Plot
figure(f)
pbaspect([2 1 1])
plot(cagetime, (-1 * descagex_chas), '--xr')           % chassis frame rotated to
cage frame, cage x = chassis -x
hold on
```

```

plot(cagetime, (-1 * descagez_chas), '--xg') % chassis frame rotated to
cage frame, cage Y = chassis -Z
plot(cagetime, (-1 * descagey_chas), '--xb') % chassis frame rotated to
cage frame, cage Z = chassis -Y

plot(cagetime, (-1 * truthBFieldx_chas), 'Or') % driven as chassis put in
cage x frame, chassis x = cage -x (to aid in data management)
plot(cagetime, (-1 * truthBFieldz_chas), 'Og') % driven as chassis put
in cage y frame, chassis y = cage -z (to aid in data management)
plot(cagetime, (-1 * truthBFieldy_chas), 'Ob') % driven as chassis put
in cage z frame, chassis z = cage -y (to aid in data management)

plot(tlmtimeelapsed, (.75 * ((-1190 + (tlmBFieldy)) *32/100)), 'r') % put in cage
frame, cage x = ADACSmag -y
plot(tlmtimeelapsed, (.708 * ((-800 + (tlmBFieldz)) *32/100)), 'g') % put in cage
frame, cage y = ADACSmag z
plot(tlmtimeelapsed, (.682 * ((509 + (-1 * tlmBFieldx))*32/100)), 'b') % put in cage
frame, cage z = ADACSmag -x
title("MAI-401 Measured B-Field - Corrected")
xlabel("Elapsed Time (Seconds)")
ylabel("milliGauss")
legend("Desired X Value", "Desired Y Value", "Desired Z Value", "Truth X Value",
"Truth Y Value", "Truth Z Value", "TLM Measured X Value", "TLM Measured Y
Value", "TLM Measured Z Value")
saveas(figure(f), [pwd '/60050/gainMAI-401 Measured Corrected B-Field.pdf'])
f = f + 1; % step to next figure
disp('MAI-401 B-Field measurement plot complete')

```

### Magnetic Rotational Data (change in mag field over time)

```

step = 0;
for step = 1:(length(tlmtimeelapsed) - 1) %764
    d_mag_x(step) = tlmBFieldx(step + 1) - tlmBFieldx(step); % x component,
change in magnitude B field (mG) at each tlm point
    d_mag_y(step) = tlmBFieldy(step + 1) - tlmBFieldy(step); % y component,
change in magnitude B field (mG) at each tlm point
    d_mag_z(step) = tlmBFieldz(step + 1) - tlmBFieldz(step); % z component,
change in magnitude B field (mG) at each tlm point
    tlm_B_omega_x(step) = d_mag_x(step)/tlmtimeelapsed(step); % x
component, body rate in dB / dt
    tlm_B_omega_y(step) = d_mag_y(step)/tlmtimeelapsed(step); % y
component, body rate in dB / dt
    tlm_B_omega_z(step) = d_mag_z(step)/tlmtimeelapsed(step); % z
component, body rate in dB / dt

```

```

end

figure(f) % plotting derived body rate velocity
vs time
plot(tlmtimeelapsed(1:end - 1), ((tlm_B_omega_y.)*32/100), 'r') % plotted
ADACS values in cage frame, lsb to mG, cage x = ADACS y
hold on
plot(tlmtimeelapsed(1:end - 1), ((tlm_B_omega_z.)*32/100), 'g') % plotted
ADACS values in cage frame, lsb to mG, cage y = ADACS z
plot(tlmtimeelapsed(1:end - 1), ((tlm_B_omega_x.)*32/100), 'b') % plotted
ADACS values in cage frame, lsb to mG, cage z = ADACS x
baselinetop = zeros(length(tlmtimeelapsed(1:end - 1)),1) + .5;
plot(tlmtimeelapsed(1:end - 1), baselinetop, 'k')
baselinebottom = zeros(length(tlmtimeelapsed(1:end - 1)),1) - .5;
plot(tlmtimeelapsed(1:end - 1), baselinebottom, 'k')

% ylim([-10 10])
title("Change in MAI-401 Measured B-Field / Change in Time (dB/dt)")
xlabel("Elapsed Time (Seconds)")
ylabel("Rate of Change of Magnetic Field (milligauss/second)")
legend("X Rotation", "Y Rotation", "Z Rotation", "+/- .5 ")
saveas(figure(f), [pwd '/60050/gainMAI-401 B-Field Derived Rotational Velocity.pdf'])
f = f + 1; % step to next figure
disp('MAI-401 B-Field derived Velocity plot complete')

%%%%%%%%%%%%%%%%%%%%%%%%%%%%%%%%%%%%%%%%%%%%%%%%%%%%%%%%%%%%%%%%%%%%%%%%
%%%%%%%%%%%%%%%%%%%%%%%%%%%%%%%%%%%%%%%%%%%%%%%%%%%%%%%%%%%%%%%%%%%%%%%%

% Magnetic acceleration (change in mag field over time, over time)
step = 0;
for step = 1:(length(tlmtimeelapsed) - 2) %764
    d2_mag_x(step) = tlm_B_omega_x(step + 1) - tlm_B_omega_x(step); % x
component, change in mag derived velocity
    d2_mag_y(step) = tlm_B_omega_y(step + 1) - tlm_B_omega_y(step); % y
component, change in mag derived velocity
    d2_mag_z(step) = tlm_B_omega_z(step + 1) - tlm_B_omega_z(step); % z
component, change in mag derived velocity
    tlm_B_omega2_x(step) = d2_mag_x(step)/tlmtimeelapsed(step); % x
component, change in mag field over time, over time again
    tlm_B_omega2_y(step) = d2_mag_y(step)/tlmtimeelapsed(step); % y
component, change in mag field over time, over time again
    tlm_B_omega2_z(step) = d2_mag_z(step)/tlmtimeelapsed(step); % z
component, change in mag field over time, over time again
end

```

```

figure(f) % plotting derived body rate
acceleration vs time
plot(tlmtimeelapsed(1:end - 2), (tlm_B_omega2_x.'), 'r')
hold on
plot(tlmtimeelapsed(1:end - 2), (tlm_B_omega2_y.'), 'g')
plot(tlmtimeelapsed(1:end - 2), (tlm_B_omega2_z.'), 'b')
pbaspect([2 1 1])
ylim([-.5 .5])
title("Telemetry B-Field Derived Rotational Acceleration")
xlabel("Elapsed Time (Seconds)")
ylabel("Rotational Acceleration (Units?)")
legend("X Rotation", "Y Rotation", "Z Rotation")
saveas(figure(f), [pwd '/60050/gainMAI-401 B-Field Derived Rotational
Acceleration.pdf'])
f = f + 1; % step to next figure
disp('B field derived acceleration plot complete')

```

### Plotting ADACS measured Omega B

```

% figure(f) % plotting telemetry mag field
measurements vs time
% plot(tlmtimeelapsed, tlm_omega_B(:, 1), 'r')
% hold on
% plot(tlmtimeelapsed, tlm_omega_B(:, 2), 'g')
% plot(tlmtimeelapsed, tlm_omega_B(:, 3), 'b')
% pbaspect([2 1 1])
% title("MAI-401 Measured Rotational Velocity (Body Frame)")
% xlabel("Elapsed Time (Seconds)")
% ylabel("Rotational Velocity (Degrees/Second)")
% legend("X Rotation", "Y Rotation", "Z Rotation")
% saveas(figure(f), [pwd '/60050/gainMAI-401 Measured Rotational Velocity (Body
Frame).pdf']);
% %saveas(figure(1),[pwd '/subFolderName/myFig.fig']);
% f = f + 1; % step to next figure
% disp('Telemetry rotational measurement plot complete')

```

### PhaseSpace

```

% in m from centroid
figure(f)
plot(pstimeelapsed, (ps_pos_x), 'r') % plotting phasespace
measured offset from centroid x direction, cage frame
hold on

```

```

plot(pstimeelapsed, (ps_pos_y), 'g') % plotting phasespace
measured offset from centroid y direction, cage frame
plot(pstimeelapsed, (ps_pos_z), 'b') % plotting phasespace
measured offset from centroid z direction, cage frame
pbaspect([2 1 1])
title("PhaseSpace Distance from Centroid Data")
xlabel("Elapsed Time (Seconds)")
ylabel("Distance from Centroid (m)")
legend("X Distance", "Y Distance", "Z Distance")
saveas(figure(f), [pwd '/60050/gainPhaseSpace pointing data.pdf'])
f = f + 1; % step to next figure
disp('phasespace distance from centroid plot complete')

%%%%%%%%%%%%%%%%%%%%%%%%%%%%%%%%%%%%%%%%%%%%%%%%%%%%%%%%%%%%%%%%%%%%%%%%
%%%%%%%%%%%%%%%%%%%%%%%%%%%%%%%%%%%%%%%%%%%%%%%%%%%%%%%%%%%%%%%%%%%%%%%%

% Velocity Data from off-centroid measurement
step = 0;
for step = 1:(length(pstime) - 1) %2672
    d_time(step) = pstimeelapsed(step + 1) - pstimeelapsed(step); % phasespace
    linear change in time for each iteration
    d_ps_pos_x(step) = (ps_pos_x(step + 1) - ps_pos_x(step)); % phasespace
    linear change in x offset, cage frame
    d_ps_pos_y(step) = ps_pos_y(step + 1) - ps_pos_y(step); % phasespace
    linear change in y offset, cage frame
    d_ps_pos_z(step) = ps_pos_z(step + 1) - ps_pos_z(step); % phasespace
    linear change in z offset, cage frame
    ps_omega_x(step) = d_ps_pos_x(step)/d_time(step); % phasespace linear
    change in x offset over change in time, cage frame
    ps_omega_y(step) = d_ps_pos_y(step)/d_time(step); % phasespace linear
    change in y offset over change in time, cage frame
    ps_omega_z(step) = d_ps_pos_z(step)/d_time(step); % phasespace linear
    change in z offset over change in time, cage frame
end

figure(f) % plotting change in phasespace
change in offset/change in time
plot(pstimeelapsed(1:end - 1), abs(ps_omega_x.'), 'r')
hold on
plot(pstimeelapsed(1:end - 1), abs(ps_omega_y.'), 'g')
plot(pstimeelapsed(1:end - 1), abs(ps_omega_z.'), 'b')
pbaspect([2 1 1])
ylim([0 .025])
title("PhaseSpace Distance from Centroid Derived Rotational Velocity")
xlabel("Elapsed Time (Seconds)")
ylabel("Rotational Velocity (m/Second)")

```

```

legend("X Velocity", "Y Velocity", "Z Velocity")
saveas(figure(f), [pwd '/60050/gainPhaseSpace derived velocity.pdf'])
f = f + 1; % step to next figure
disp('PhaseSpace derived velocity plot complete')

ps_omega_x_max = max(ps_omega_x);

%%%%%%%%%%%%%%%%%%%%%%%%%%%%%%%%%%%%%%%%%%%%%%%%%%%%%%%%%%%%%%%%%%%%%%%%
%%%%%%%%%%%%%%%%%%%%%%%%%%%%%%%%%%%%%%%%%%%%%%%%%%%%%%%%%%%%%%%%%%%%%%%%
% Acceleration Data from off-centroid measurement
step = 0;
for step = 1:(length(pstime) - 2) %2672
    d_time(step) = pstimeelapsed(step + 1) - pstimeelapsed(step); % phasespace
    linear change in time for each iteration
    d2_omega_x(step) = (ps_omega_x(step + 1) - ps_omega_x(step)); % phasespace
    linear change in dx/dt, cage frame
    d2_omega_y(step) = (ps_omega_y(step + 1) - ps_omega_y(step)); % phasespace
    linear change in dy/dt, cage frame
    d2_omega_z(step) = (ps_omega_z(step + 1) - ps_omega_z(step)); % phasespace
    linear change in dz/dt, cage frame
    ps_accel_x(step) = d2_omega_x(step)/d_time(step); % phasespace linear
    d2x/dt2, cage frame
    ps_accel_y(step) = d2_omega_y(step)/d_time(step); % phasespace linear
    d2y/dt2, cage frame
    ps_accel_z(step) = d2_omega_z(step)/d_time(step); % phasespace linear
    d2z/dt2, cage frame
end

figure(f) % plotting phasespace d2x/dt2 (x, y,
and z)
plot(pstimeelapsed(1:end - 2), abs(ps_accel_x.), 'r')
hold on
plot(pstimeelapsed(1:end - 2), abs(ps_accel_y.), 'g')
plot(pstimeelapsed(1:end - 2), abs(ps_accel_z.), 'b')
pbaspect([2 1 1])
ylim([-0.005 .005])
title("PhaseSpace Distance from Centroid Derived Rotational Acceleration")
xlabel("Elapsed Time (Seconds)")
ylabel("Rotational Acceleration (m/second/second)")
legend("X Acceleration", "Y Acceleration", "Z Acceleration")
saveas(figure(f), [pwd '/60050/gainPhaseSpace derived acceleration.pdf'])
f = f + 1; % step to next figure
disp('PhaseSpace derived acceleration plot complete')

```

## Heading Data from PhaseSpace Data

```
% figure(f)
% plot(pstotaltimeelapsed, (ps_heading), 'k')
% pbaspect([2 1 1])
% title("Detumble Heading Visualization from PhaseSpace Cameras")
% xlabel("Elapsed Time (seconds)")
% ylabel("Heading (degrees)")
% %% legend("")
% f = f + 1;
%
% %% Rotational Velocity (change in heading (deg) / Change in time(s))
% step = 0;
% for step = 1:(length(pstotaltimeelapsed) - 1) %764
%   dH(step) = ps_heading(step + 1) - ps_heading(step);% change in angular value
%   (degrees)
%   dt(step) = pstotaltime(step + 1) - pstotaltime(step);%change in time (seconds)
%   dHdt(step) = dH(step)/dt(step);%change in angele/change in time (deg/s)
% end
% figure(f)
% plot(pstotaltimeelapsed(1:end-1), (dHdt), 'k')
% pbaspect([2 1 1])
% title("Angular VelocityDerived from PhaseSpace Heading")
% xlabel("Elapsed Time (seconds)")
% ylabel("Angular Velocity (degrees/second)")
% %% legend("")
% f = f + 1;
```

## PhaseSpace Cartesian to Spherical Coordinate

```
r = sqrt((ps_pos_x).^2+(ps_pos_y).^2+(ps_pos_z).^2);
theta = rad2deg(unwrap(atan2(ps_pos_y, ps_pos_x))); %atan2d is the 4
quadrant atan, competed in degrees, unwrap wraps 359 deg + 1 = 0 deg
phi = atan2d(sqrt(ps_pos_x.^2+ps_pos_y.^2), ps_pos_z);
```

```
figure(f) % Plotting phasespace data after
change to spherical coordniates
plot(pstotaltimeelapsed, (r), 'k')
hold on
plot(pstotaltimeelapsed, (theta), 'c')
plot(pstotaltimeelapsed, (phi), 'm')
pbaspect([2 1 1])
ylim([-200 200])
title("PhaseSpace Cartesian Measurements Transformed into Spherical Measurements")
```



```

xlabel("Elapsed Time (seconds)")
ylabel("Spherical Measurements of r, theta, phi")
legend("r (millimeters)", "theta (degrees)", "phi (degrees)")
f = f + 1;

```

### PhaseSpace Spherical Coordinate Rotational Velocity

```

step4 = 0;
for step4 = 1:(length(pstotaltime) - 1)
    dtime(step4) = pstotaltime(step4 + 1) - pstotaltime(step4);           % time stepping
    d_theta(step4) = (theta(step4 + 1) - theta(step4));                   % change in theta
    if d_theta(step4) > 20                                               % if step is too big then data is
likely wrong (like 2 deg - 358 deg...) so discard it
        d_theta(step4) = NaN;
    end
    d_phi(step4) = (phi(step4 + 1) - phi(step4));                         % change in phi
    d_theta_d_time(step4) = abs(d_theta(step4)/dtime(step4));            % change in theta /
change in time
    d_phi_d_time(step4) = abs(d_phi(step4)/dtime(step4));                % change in phi /
change in time
end

total_dtheta_dt = 0;                                                    % creating an average theta
changing for the addition of each iteration
for step6 = 2:(length(pstotaltime) - 1)
    if isnan(d_theta_d_time(step6))
        d_theta_d_time(step6) = mean(d_theta_d_time);
    end
    total_dtheta_dt(step6) = (total_dtheta_dt(step6-1) + d_theta_d_time(step6));
    runavg_dtheta_dt(step6) = total_dtheta_dt(step6) / step6;
end

total_dphi_dt = 0;                                                      % creating an average phi changing
for the addition of each iteration
for step6 = 2:(length(pstotaltime) - 1)
    if isnan(d_phi_d_time(step6))
        d_phi_d_time(step6) = mean(d_phi_d_time);
    end
    total_dphi_dt(step6) = (total_dphi_dt(step6-1) + d_phi_d_time(step6));
    runavg_dphi_dt(step6) = total_dphi_dt(step6) / step6;
end

figure(f)                                                                % plotting d/dt of theta, phi, and
iterative averages

```

```

plot(pstotaltimeelapsed(1:end-1), ((runavg_dtheta_dt).'), 'k')
hold on
plot(pstotaltimeelapsed(1:end-1), ((runavg_dphi_dt).'), 'r')
plot(pstotaltimeelapsed(1:end-1), (d_theta_d_time), 'c');
plot(pstotaltimeelapsed(1:end-1), (d_phi_d_time), 'm')
pbaspect([2 1 1])
ylim([0 20])
title("PhaseSpace Spherical Coordinate Derived Rotational Velocity")
xlabel("Elapsed Time (seconds)")
ylabel("Rotational Velocity (degrees/second)")
legend("Theta (degrees, XY Plane)", "phi (degrees, Deviation from +Z)", "Running Average d_theta/dt", "Running Average d_phi/dt")
f = f + 1;
saveas(figure(f), [pwd '/60050/gain PhaseSpace Spherical Rotational Velocity.pdf'])

```

### PhaseSpace Spherical Coordinate Rotational Acceleration

```

step5 = 0;
for step5 = 1:(length(pstotaltime) - 2)
    d2_theta(step5) = abs(d_theta(step5 + 1) - d_theta(step5));           % Change in
    theta velocity
    d2_phi(step5) = abs(d_phi(step5 + 1) - d_phi(step5));               % change in phi
    velocity
end

step7 = 0;
total_d2theta_dt = 0;                                                  % creating an average d2theta/dt2
changing for the addition of each iteration
for step7 = 2:(length(pstotaltime) - 2)
    if isnan(d2_theta(step7))
        d2_theta(step7) = mean(d2_theta);
    end
    total_d2theta_dt(step7) = (total_d2theta_dt(step7-1) + d2_theta(step7));
    runavg_d2theta_dt(step7) = total_d2theta_dt(step7) / (step7);
end

step7 = 0;
total_d2phi_dt = 0;                                                  % creating an average d2phi/dt2
changing for the addition of each iteration
for step7 = 2:(length(pstotaltime) - 2)
    total_d2phi_dt(step7) = (total_d2phi_dt(step7-1) + d2_phi(step7));
    runavg_d2phi_dt(step7) = total_d2phi_dt(step7) / step7;
end

```

```

figure(f) % plotting phasespace derived body
rate acceleration vs time
plot(pstotaltimeelapsed(1:end - 2), (d2_theta.'), 'c')
hold on
plot(pstotaltimeelapsed(1:end - 2), (d2_phi.'), 'm')
plot(pstotaltimeelapsed(1:end - 2), (runavg_d2theta_dt.'), 'k')
plot(pstotaltimeelapsed(1:end - 2), (runavg_d2phi_dt.'), 'r')
pbaspect([2 1 1])
ylim([0 20])
title("PhaseSpace Derived Spherical Acceleration")
xlabel("Elapsed Time (Seconds)")
ylabel("Rotational Acceleration (degrees/second/second)")
legend("Theta (Within XY plane)", "Phi (Off XY Plane)", "Running Average
d2theta/dt2", "Running Average d2phi/dt2")
saveas(figure(f), [pwd '/60050/gain PhaseSpace Spherical Rotational Acceleration.pdf'])
f = f + 1; % step to next figure
disp("PhaseSpace acceleration plot complete")

```

### Cage Data

```

% time in elapsed seconds passed the Julian start time
% cagetimeinit = 2458384.57916667; % Julian Date start time - 2458384.57916667, time
in elapsed seconds
% cagetime = cageDetAcq(:, 1);
%
% cageBFieldx = cageDetAcq(:, 8); % x component, mag is
in milliGauss (mG)
% cageBFieldy = cageDetAcq(:, 9); % y component, mag is
in milliGauss (mG)
% cageBFieldz = cageDetAcq(:, 10); % z component, mag is
in milliGauss (mG)
% cageBField = [cageBFieldx, cageBFieldy, cageBFieldz]; % composite
[x, y, z] magntic field
% figure(2)
% plot(cagetime, cageBFieldx, '-.r')
% plot(cagetime, cageBFieldy, '-.g')
% plot(cagetime, cageBFieldz, '-.b')

```

### 3D Visualization

```

% figure out the number of points and then do the color change thing
centroidx = mean(ps_pos_x); % x component from
PhaseSpace

```

```

centroidy = mean(ps_pos_y);           % y component from
PhaseSpace
centroidz = mean(ps_pos_z);           % z component from
PhaseSpace

%figure stepping
N = 1;
C = numel(ps_pos_x);
figure(f)
scatter3(centroidx, centroidy, centroidz, 'k');           % plot centroid of the
rotation (centroid of the cameras, should always be the same)
hold on
scatter3(ps_pos_x, ps_pos_y, ps_pos_z, 'r')           % plot composite x, y, z
data points
title("PhaseSpace 3D Visualization")
legend("PhaseSpace Positional Centroid", "PhaseSpace Ridig Body Centroid Motion
[X,Y,Z]")
disp('Rotational plot complete')
f = f + 1;

```

### End of Script

```

a = 1;
disp('Complete')

```

---

*Published with MATLAB® R2020b*

## References

- [1] G. Wahba, "A Least Squares Estimate of Satellite Attitude," *SIAM Rev.*, 1965, doi: 10.1137/1007077.
- [2] C. E. Ananda and N. Bartel, "CaNOP 3U CubeSat Attitude Determination and Control Testing System: Helmholtz Cage Design," *Proc. Wisconsin Sp. Conf.*, 2018, doi: 10.17307/wsc.v1i1.222.
- [3] M. R. Brewer, "CUBESAT ATTITUDE DETERMINATION AND HELMHOLTZ CAGE DESIGN," *Air Force Inst. Technol.*, 2010.
- [4] M. Swartwout, "The first one hundred CubeSats : A statistical look," *J. Small Satell.*, 2013.
- [5] H. J. Kramer and A. P. Cracknell, "An overview of small satellites in remote sensing," *International Journal of Remote Sensing*. 2008, doi: 10.1080/01431160801914952.
- [6] CubeSat, "Cubesat design specification," 2014. doi: <http://dx.doi.org/10.1155/2015/681901>.
- [7] "Nanosats Database." <https://www.nanosats.eu/>.
- [8] Planet Labs, "PLANET IMAGERY PRODUCT SPECIFICATION: PLANETSCOPE & RAPIDEYE," 2016. [Online]. Available: [https://www.planet.com/products/satellite-imagery/files/1610.06\\_Spec\\_Sheet\\_Combined\\_Imagery\\_Product\\_Letter\\_ENGv1.pdf](https://www.planet.com/products/satellite-imagery/files/1610.06_Spec_Sheet_Combined_Imagery_Product_Letter_ENGv1.pdf).
- [9] Santana Ortiz, "AFRL TECHNOLOGY SET FOR LAUNCH TO INTERNATIONAL SPACE STATION." <https://afresearchlab.com/news/afrl-technology-set-for-launch-to-international-space-station/>.
- [10] A. H. (NASA), "Small Satellite Missions." [https://www.nasa.gov/mission\\_pages/smallsats/elana/index.html](https://www.nasa.gov/mission_pages/smallsats/elana/index.html).
- [11] R. Reesman and A. Rogers, "Getting in Your Space: Learning from Past Rendezvous and Proximity Operations," 2018. [Online]. Available: [www.aerospace.org/policy](http://www.aerospace.org/policy).
- [12] B. (NASA) Granath, "Gemini's First Docking Turns to Wild Ride in Orbit," 2016. <https://www.nasa.gov/feature/geminis-first-docking-turns-to-wild-ride-in-orbit>.
- [13] F. L. Markley and J. L. Crassidis, *Fundamentals of spacecraft attitude*

determination and control. 2014.

- [14] H. D. Black, "A passive system for determining the attitude of a satellite," AIAA J., 1964, doi: 10.2514/3.2555.
- [15] M. D. Shuster and S. D. Oh, "Three-axis attitude determination from vector observations," J. Guid. Control. Dyn., 1981, doi: 10.2514/3.19717.
- [16] Z. Meng, C. Fan, G. Zhang, and Z. You, "A brief survey of the deterministic solution for satellite attitude estimation," 2008, doi: 10.1117/12.807456.
- [17] P. B. Davenport, "A VECTOR APPROACH TO THE ALGEBRA OF ROTATIONS WITH APPLICATIONS," 1968.
- [18] E. J. Leffens, F. L. Markley, and M. D. Shuster, "Kalman filtering for spacecraft attitude estimation," J. Guid. Control. Dyn., 1982, doi: 10.2514/3.56190.
- [19] M. L. Psiaki, F. Martel, and P. K. Pal, "Three-axis attitude determination via kalman filtering of magnetometer data," J. Guid. Control. Dyn., 1990, doi: 10.2514/3.25364.
- [20] "Attitude Systems." <https://www.adcolemai.com/attitude-systems/>.
- [21] "Attitude Control Systems." <https://bluecanyontech.com/components>.
- [22] L. Federici, B. Benedikter, and A. Zavoli, "Machine Learning Techniques for Autonomous Spacecraft Guidance during Proximity Operations," 2021, doi: 10.2514/6.2021-0668.
- [23] R. Chai, A. Savvaris, A. Tsourdos, S. Chai, and Y. Xia, "A review of optimization techniques in spacecraft flight trajectory design," Progress in Aerospace Sciences. 2019, doi: 10.1016/j.paerosci.2019.05.003.
- [24] K. (NASA/Goddard) Aaron, "Earth's Magnetosphere." NASA, p. 1, 2017, [Online]. Available: [https://www.nasa.gov/mission\\_pages/sunearth/multimedia/magnetosphere.html](https://www.nasa.gov/mission_pages/sunearth/multimedia/magnetosphere.html).
- [25] M. K. Prinkey et al., "CubeSat attitude control testbed design: Merritt 4-Coil per axis helmholtz cage and spherical air bearing," 2013, doi: 10.2514/6.2013-4942.
- [26] J. L. Schwartz, M. A. Peck, and C. D. Hall, "Historical review of air-bearing spacecraft simulators," Journal of Guidance, Control, and Dynamics. 2003, doi: 10.2514/2.5085.
- [27] FME; CJW;, "MAI-401 Mini ADACS System Manual." Adcole Maryland Aerospace, Inc., Crofton, MD, p. 144.

- [28] Matt Baumgart, "GN&C Users Guide." Blue Canyon Technologies, Lafayette, CO, p. 117.
- [29] "Magnetic Field Calculators."  
<https://www.ngdc.noaa.gov/geomag/calculators/magcalc.shtml>.

**REPORT DOCUMENTATION PAGE**

*Form Approved*  
OMB No. 0704-0188

The public reporting burden for this collection of information is estimated to average 1 hour per response, including the time for reviewing instructions, searching existing data sources, gathering and maintaining the data needed, and completing and reviewing the collection of information. Send comments regarding this burden estimate or any other aspect of this collection of information, including suggestions for reducing the burden, to Department of Defense, Washington Headquarters Services, Directorate for Information Operations and Reports (0704-0188), 1215 Jefferson Davis Highway, Suite 1204, Arlington, VA 22202-4302. Respondents should be aware that notwithstanding any other provision of law, no person shall be subject to any penalty for failing to comply with a collection of information if it does not display a currently valid OMB control number.  
**PLEASE DO NOT RETURN YOUR FORM TO THE ABOVE ADDRESS.**

<b>1. REPORT DATE (DD-MM-YYYY)</b> 03/05/2021	<b>2. REPORT TYPE</b> Master's Thesis	<b>3. DATES COVERED (From - To)</b> Oct 2019 - Mar 2021
--	--	--

<b>4. TITLE AND SUBTITLE</b> CubeSat Attitude Determination and Control System (ADACS) Characterization and Testing for Rendezvous and Proximity Operations (RPO)	<table border="1" style="width:100%; border-collapse: collapse;"> <tr><td><b>5a. CONTRACT NUMBER</b></td></tr> <tr><td><b>5b. GRANT NUMBER</b></td></tr> <tr><td><b>5c. PROGRAM ELEMENT NUMBER</b></td></tr> </table>	<b>5a. CONTRACT NUMBER</b>	<b>5b. GRANT NUMBER</b>	<b>5c. PROGRAM ELEMENT NUMBER</b>
<b>5a. CONTRACT NUMBER</b>				
<b>5b. GRANT NUMBER</b>				
<b>5c. PROGRAM ELEMENT NUMBER</b>				

<b>6. AUTHOR(S)</b> Bednarski, Steven, T, Capt	<table border="1" style="width:100%; border-collapse: collapse;"> <tr><td><b>5d. PROJECT NUMBER</b></td></tr> <tr><td><b>5e. TASK NUMBER</b></td></tr> <tr><td><b>5f. WORK UNIT NUMBER</b></td></tr> </table>	<b>5d. PROJECT NUMBER</b>	<b>5e. TASK NUMBER</b>	<b>5f. WORK UNIT NUMBER</b>
<b>5d. PROJECT NUMBER</b>				
<b>5e. TASK NUMBER</b>				
<b>5f. WORK UNIT NUMBER</b>				

<b>7. PERFORMING ORGANIZATION NAME(S) AND ADDRESS(ES)</b> Air Force Institute of Technology Graduate School of Engineering and Management (AFIT/EN) 2950 Hobson Way Wright-Patterson AFB OH 45433-7765	<b>8. PERFORMING ORGANIZATION REPORT NUMBER</b> AFIT-ENY-MS-21-M-288
--	---

<b>9. SPONSORING/MONITORING AGENCY NAME(S) AND ADDRESS(ES)</b>	<b>10. SPONSOR/MONITOR'S ACRONYM(S)</b>
	<b>11. SPONSOR/MONITOR'S REPORT NUMBER(S)</b>

**12. DISTRIBUTION/AVAILABILITY STATEMENT**  
Distribution Statement A. Approved for Public Release; Distribution is Unlimited

**13. SUPPLEMENTARY NOTES**

**14. ABSTRACT**  
This research endeavors to evaluate and characterize the performance of CubeSat specific commercial-off-the-shelf (COTS) Attitude Determination and Control Systems (ADACS) for Mission suitability. To ensure COTS components are capable of meeting CubeSat mission requirements, deliberate performance testing of critical CubeSat subsystems in flight-like conditions is essential. This effort focuses on testing the MAI-401 ADACS subsystem as configured to support the Grissom-1 CubeSat mission, as mounted to an air bearing, residing within a 3-axis Helmholtz Cage, and subjected to a simulated magnetic environment of various orbital parameters.

**15. SUBJECT TERMS**  
attitude determination and control, helmholtz cage, flight-like testing, mission suitability

<b>16. SECURITY CLASSIFICATION OF:</b>			<b>17. LIMITATION OF ABSTRACT</b>	<b>18. NUMBER OF PAGES</b>	<b>19a. NAME OF RESPONSIBLE PERSON</b>
<b>a. REPORT</b>	<b>b. ABSTRACT</b>	<b>c. THIS PAGE</b>			Dr. Andrew Keys, AFIT/ENY
U	U	U	UU	161	<b>19b. TELEPHONE NUMBER (Include area code)</b> (937) 255-3636 x4747



## INSTRUCTIONS FOR COMPLETING SF 298

**1. REPORT DATE.** Full publication date, including day, month, if available. Must cite at least the year and be Year 2000 compliant, e.g. 30-06-1998; xx-06-1998; xx-xx-1998.

**2. REPORT TYPE.** State the type of report, such as final, technical, interim, memorandum, master's thesis, progress, quarterly, research, special, group study, etc.

**3. DATE COVERED.** Indicate the time during which the work was performed and the report was written, e.g., Jun 1997 - Jun 1998; 1-10 Jun 1996; May - Nov 1998; Nov 1998.

**4. TITLE.** Enter title and subtitle with volume number and part number, if applicable. On classified documents, enter the title classification in parentheses.

**5a. CONTRACT NUMBER.** Enter all contract numbers as they appear in the report, e.g. F33315-86-C-5169.

**5b. GRANT NUMBER.** Enter all grant numbers as they appear in the report. e.g. AFOSR-82-1234.

**5c. PROGRAM ELEMENT NUMBER.** Enter all program element numbers as they appear in the report, e.g. 61101A.

**5e. TASK NUMBER.** Enter all task numbers as they appear in the report, e.g. 05; RF0330201; T4112.

**5f. WORK UNIT NUMBER.** Enter all work unit numbers as they appear in the report, e.g. 001; AFAPL30480105.

**6. AUTHOR(S).** Enter name(s) of person(s) responsible for writing the report, performing the research, or credited with the content of the report. The form of entry is the last name, first name, middle initial, and additional qualifiers separated by commas, e.g. Smith, Richard, J, Jr.

**7. PERFORMING ORGANIZATION NAME(S) AND ADDRESS(ES).** Self-explanatory.

**8. PERFORMING ORGANIZATION REPORT NUMBER.** Enter all unique alphanumeric report numbers assigned by the performing organization, e.g. BRL-1234; AFWL-TR-85-4017-Vol-21-PT-2.

**9. SPONSORING/MONITORING AGENCY NAME(S) AND ADDRESS(ES).** Enter the name and address of the organization(s) financially responsible for and monitoring the work.

**10. SPONSOR/MONITOR'S ACRONYM(S).** Enter, if available, e.g. BRL, ARDEC, NADC.

**11. SPONSOR/MONITOR'S REPORT NUMBER(S).** Enter report number as assigned by the sponsoring/monitoring agency, if available, e.g. BRL-TR-829; -215.

**12. DISTRIBUTION/AVAILABILITY STATEMENT.** Use agency-mandated availability statements to indicate the public availability or distribution limitations of the report. If additional limitations/ restrictions or special markings are indicated, follow agency authorization procedures, e.g. RD/FRD, PROPIN, ITAR, etc. Include copyright information.

**13. SUPPLEMENTARY NOTES.** Enter information not included elsewhere such as: prepared in cooperation with; translation of; report supersedes; old edition number, etc.

**14. ABSTRACT.** A brief (approximately 200 words) factual summary of the most significant information.

**15. SUBJECT TERMS.** Key words or phrases identifying major concepts in the report.

**16. SECURITY CLASSIFICATION.** Enter security classification in accordance with security classification regulations, e.g. U, C, S, etc. If this form contains classified information, stamp classification level on the top and bottom of this page.

**17. LIMITATION OF ABSTRACT.** This block must be completed to assign a distribution limitation to the abstract. Enter UU (Unclassified Unlimited) or SAR (Same as Report). An entry in this block is necessary if the abstract is to be limited.